Bond and Development Length in Concrete Beams with Exposed Reinforcement

by

Alireza Masnavi

A thesis
presented to the University of Waterloo
in fulfillment of the
thesis requirement for the degree of
Master of Applied Science
in
Civil Engineering

Waterloo, Ontario, Canada, 2013

I hereby declare that I am the sole author of this thesis. This is a true copy of the thesis, including any required final revisions, as accepted by my examiners. I understand that my thesis may be made electronically available to the public.

Abstract

Corrosion of steel reinforcement in Ontario bridges is causing severe soffit spalling in many situations. These spalled areas are often located within the lap splices and curtailment zones of the primary reinforcement. This can lead to inadequate bar development lengths and the possibility of failures. In order to better predict the residual strength of these deteriorated bridges, a test program was designed, which involved mid-sized concrete beam specimens, with partially de-bonded reinforcement. The de-bonding was simulated in various beam locations, with various de-bonding patterns. The test program consisted of thirteen beams; ten under-reinforced and three over-reinforced. All beams had dimensions of 2100×150×100 mm. The span between simple supports was 1900 mm with a single point load applied at the midspan. Rebar strains and displacement at the midspan were recorded. The goal of this experimental study was to determine the correlation between the spatial location and surface area of de-bonding with the strength of the beams. This was achieved by testing beam specimens with different combinations of de-bonding patterns with respect to location and area. Four beams had de-bonded reinforcement in the flexural zones, seven were de-bonded in the anchorage and flexural zones, and two were fully bonded.

In a previous study, a so-called “modified area concept” was developed for rapid assessment of the remaining capacity of heavily spalled girders. This concept was integrated in a computer program, which assesses girder capacity, given a graphical spalling survey and a structural drawing of the girder. The developed program can be easily adapted for full bridge analysis, and to evaluate the effects of reinforcement cross section loss and bond deterioration. The research presented in the current thesis investigates several of the assumptions made in this previous study.

The current thesis includes the rationale for the design of the experimental program. In addition, the test results are presented and analyzed. By analyzing the failure modes, failure loads, and crack patterns, along with the load-displacement, load-stiffness, and load-strain behaviour of the various beams, it is concluded that: 1) reinforced concrete beams can carry a significant portion of their original capacity after losing cover over a significant portion of their flexural reinforcement, 2) predictions of the beam capacities and failure modes using the modified area concept are reasonably accurate and conservative in most cases, and 3) the flexural stiffness of the beams was seen to decrease with an increase in the length of the exposed area, in most cases.

Recommended areas of future research are identified, including: 1) tests of beams with splices in the flexural reinforcing along the span, 2) field investigation of the concrete strength in regions of the soffit immediately adjacent to the spalled regions, and 3) the development of a correction factor to account for the effects of violating the plane sections assumption.

Acknowledgments

I would like to express my deepest gratitude and appreciation to Dr. Walbridge and Dr. Polak for their invaluable advice, guidance, suggestions, and support since the beginning the research. Their support and valuable remarks were greatly useful and helpful to achieve valuable and beneficial results.

The experimental work was carried out at the University of Waterloo Structures Laboratory. The great help of the department to use all facilities is highly appreciated. I would like to thank the laboratory technical staff, Robert Sluban, Richard Morrison, and Doug Hirst for the laboratory assistance.

Sincere thanks to my sister, Engineer Mahnaz Masnavi, for her valuable support, assistance, and endless help. Thanks for sharing broad experience, and providing great inspiration. Undoubtedly without her support, patience and encouragement the completion of this research would not have been possible to me. Therefore, I embrace the opportunity to dedicate this thesis to her.

A special gratitude is owed to my friends Behrad Rezaie, Mohsen Shafiee, Mohsen Maghrori, Sina Jafari, Armin Omidi, Paulina Arczewska and Jeffrey Luckai, whom I always relied on as support throughout this work.

Table of Contents

List of Figures

Chapter 1 : Introduction

1.1 General

Countries all around the world are currently facing considerable challenges, due to the deterioration of their civil infrastructure, including roads, sewer systems, and bridges.

"The total cost of Canada's infrastructure is estimated between 3-5 trillion dollars, and because of lack of funding the related political decision leading to deferred maintenance, the current infrastructure deficit is well over $100 billion" according to Amleh,(2000).

The Federal Highway administration, the body in charge of overseeing transportation infrastructure in the United States, established that nearly a third of their 590,000 bridges are either structurally defective or operationally inadequate. In other words, they are incapable of responding to the ever-increasing traffic load and as such, must either be subjected to appropriate functional restrictions or decommission altogether, (Jeppsson and Thelandersson, 2002). In Russia, it is estimated that roughly 20,000 of their bridges are in detrimental condition, representing approximately one third of the total. The European Union put standards in place prior to 1999, requiring that all highways meet a carrying capacity of 44 tons. In this regard, the United Kingdom has all but failed, with over 40,000 bridges falling short of this benchmark, (Jeppsson and Thelandersson, 2002).

In the case of bridges, much of the observed deterioration consists of corrosion of the reinforcing steel in reinforced concrete (RC) structures exposed to harsh environments, pollution, and de-icing salt. This form of deterioration can lead to serious concerns regarding the structural capacity and remaining life of these structures. In many cases, the corrosion is so severe that the concrete covering the reinforcing steel has spalled off, exposing the steel directly to the environment, resulting in further acceleration of the corrosion process and a reduction in the bond between the steel and the concrete.

The bond between the steel and concrete in RC structures is critical from the point of view of structural capacity. The bond strength between concrete and steel depends on several factors such as surface friction between the steel and concrete, the reinforcement "lugs" interlocking with the surrounding concrete, cohesion, and adhesion. The reduction or complete loss of these

load transfer mechanisms results in a reduction in in structural capacity. The loss of contact between steel and concrete in RC structures has caused catastrophic failures in some specific cases, (Goyette et al, 2007).

Corrosion of steel reinforcement in Ontario bridges is causing severe spalling of the girder soffit (or underside) in many situations. This problem mainly occurs in overpass structures, where the underside of the bridge is within the splash zone of the vehicles passing underneath. These spalled areas are often located within the lap splices and curtailment zones of the primary flexural reinforcement. This can lead to inadequate bar development lengths and the possibility of failures.

Highway authorities confronted with large numbers of structures in this condition are in need of simple tools for rapidly assessing which structures are unsafe or in most urgent need of repair or replacement. In a previous study conducted at the University of Waterloo, a so-called "modified area concept" was developed for rapid assessment of the remaining capacity of heavily spalled girders. This concept was integrated in a computer program, which assesses girder capacity, given a graphical spalling survey and a structural drawing of the girder. The developed program can be easily adapted for full bridge analysis, and to evaluate the effects of reinforcement cross section loss and bond deterioration.

Certain assumptions were made in the development of the modified area concept, based on first principals of concrete mechanics, without extensive verification by testing. The research described in the current thesis was undertaken in order to further investigate these assumptions. This research consists mainly of an experimental study, involving the static strength testing of mid-sized reinforced concrete beam specimens, with partially de-bonded flexural reinforcement representing the spalled regions in a heavily deteriorated bridge girder with severe soffit spalling.

1.2 Objectives and Scope

The main objectives of the research presented in this thesis are as follows:

- to perform static tests of RC beams with flexural reinforcement de-bonded in various patterns, in order to improve our understanding of the effects of de-bonding on structural capacity,

- to relate various aspects of the RC beam specimen performance with parameters that are known, based on the beam design, or can be determined by visual inspection, including the reinforcing ratio and the length, shape, and location of the exposed reinforcement regions, and
- to assess the suitability of structural resistance models employing the modified area concept for predicting the residual capacity and failure modes of the de-bonded beams.

The experimental portion of the study presented in this thesis is limited to simply-supported mid-sized beams with a single point load applied at the midspan. The spalled or de-bonded regions of the beam specimens were simulated using Styrofoam blocks, which prevented the concrete from covering certain predetermined portions of the flexural reinforcing, during the fabrication of the specimens. The analytical portion of the study presented in this thesis is limited to the identification of trends in the test data and analysis of the test specimens using the modified area concept.

1.3 Structure of Thesis

This thesis consists of six chapters.

Chapter 2 presents a literature review of the mechanisms for transferring forces between rebar and concrete and the effect of bond deterioration on the structural capacity of RC beams.

Chapter 3 describes the experimental program, which consists primarily of static bending tests on concrete beams with de-bonded regions. In addition, it discusses the test setup, and specimen preparation, along with the concrete physical, chemical, and mechanical properties.

Chapter 4 presents the experimental results and elaborates on outputs such as the load versus displacement and strain data, as well as the observed crack patterns and failure modes.

Chapter 5 presents further analysis of the experimental results, including the identification of trends in the collected data and analysis of the test specimens using the modified area concept.

Chapter 6 presents the conclusions and recommendations for further research.

Chapter 2 : Literature Review

2.1 Overview

Bond behaviour is influenced by the interaction between concrete and steel interface. In this chapter, primary background information concerning bond behaviour is presented.

The load transfer between steel and concrete in reinforced concrete structures is referred to as "bond". Untrauer and Henry (1965) defined bond as the mechanism or mechanisms that causes hardened concrete to hold an embedded steel bar. Bond stress is defined in experiments as the mechanical friction that generates the shear stress at the steel-concrete interface, which results in the transfer of load between the steel and concrete (ACI Committee 408, 1966). Bond stress can be defined as the force per unit area of the steel surface being subjected to shear.

Throughout the past few decades, bond in reinforced concrete has been the subject of a myriad of studies. Tepfers (1979) analyzed the stress state in the concrete due to bond forces and used a concrete ring model to determine the cracking resistance of the concrete cover. The correlation between slip in reinforced concrete and its associated bond stress were at the centre of experiments conducted by Elignehausen et al (1982). Malvar (1991) investigated the effect of confinement on the bond stress-slip behaviour. Together, the foregoing studies have helped lay a foundation of solid research into bond behaviour in reinforced concrete.

2.2 Previous Structural Testing of Beams with Debonded Regions

Minkarah and Ringo (1981) were the first researchers to examine the debonding phenomenon more closely. Their study, "Behavior and Repair of Deteriorated Reinforced Concrete Beams" aimed at quantitatively assessing the effect of debonding on the strength of concrete beams and the efficacy of subsequent repairs subjected to these defective members.

A total of forty beams were constructed, each with a dimension of 12.7 × 25.4 × 290 cm, and reinforced with two #4 bars at the bottom of the cross-section. During the production of these beams, a section of 3.8 cm from the bottom were blocked out during the pouring of concrete, resulting in exposed bars. The latter was done in varying patterns and sizes in order to determine

a quantitative relationship between the position and size of debonding and the loss of strength in the beams. The size of debonded areas varied between 30 and 180 cm.

From these 40 beams, were left intact, while others were repaired before being subjected to any testing. All of them were subjected to loads at different points of the beams.

They concluded that repairing debonded beams was successful beyond expectations. More specifically, the laboratory tests were conclusive in affirming that strength recovery for when the bonding agent was not used and for when it was used, were 86% and 100%, respectively, setting a promising ground for later studies.

Other prominent researchers, such as Zhang et al (1994), picked up where their predecessors had left off, conducting experiments on partially exposed concrete beams. The primary purpose of their research was to present details of newly developed theory about the neutral axis location and critical stress along the span of the beams with exposed reinforcement.

Their study consisted of tests on a series of 124 small-scale (1.76 m length and 130 mm depth) and large scale (3 m length and 300 depth) beams. All test specimens were debonded in a symmetric pattern and were tested under two point loads. The test variables included in their experiments were: percentage of reinforcement; effective depth of the beam; and exposed length of reinforcement.

The testing of large scale beams (L=3000 mm) were conducted with specific parameters: there were two equal loads placed at a distance of 30 cm on either side of the midspan, and the supports were pinned-roller. The reinforcement yield strength was 460N/mm².

The Figure 2-1 shows the variations in the position and curvature of the neutral axis with respect to the range of exposure ($1200 \leq L_{exp} \leq 2400$ mm). It was concluded that by increasing the exposure length, the beginning of the neutral axis moved closer and closer to the support.

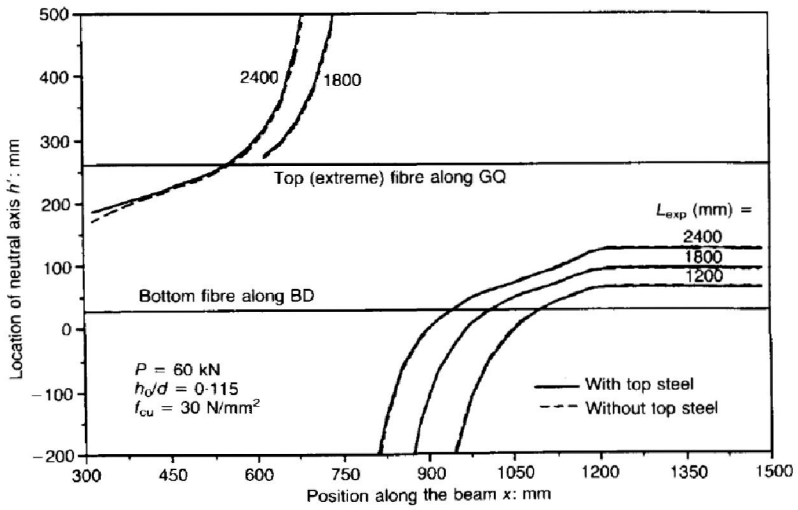

Figure 2-1: Predicted location of neutral axis over the region of the beam with exposed main reinforcement for various lever of exposure. (Zhang et al, 1994)

Furthermore, they acknowledged that the top reinforcement is critical in controlling cracks when exposed areas on the bottom reinforcement begin to develop. As shown in the figure above, the presence of nominal top steel has minimal influence on the location of the neural axis.

The Figure 2-2 presents numerical variations in the percentage loss of strength P/P0 with changes in the extent of exposed reinforcement L_{exp} (non- dimensionalized with respect to the total span L) for different range of concrete strength $20 \leq f_{cu} \leq 40$ N/mm².

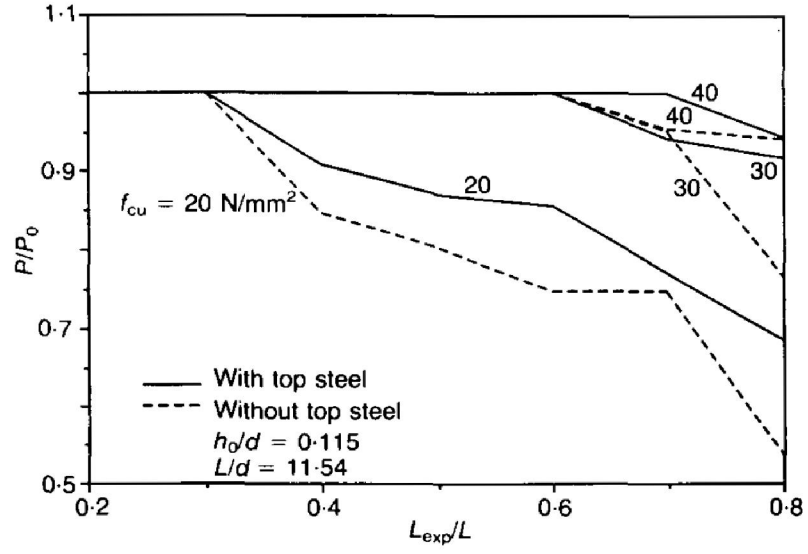

Figure 2-2: Variation of percentage strength loss P/P0 with change in the extent of exposed main reinforcement L_{exp}/L for a range of concrete cube strengths f_{cu}. (Zhang et al, 1994)

They found certain behaviours in simply supported reinforced concrete beams that experienced two point loading. There appeared to be no loss in strength for specimens debonded up to 30% of their entire spans. It was also observed that if the top reinforcement of the beam was used, the ultimate load of the beam would be considerably increased. It is suggested these results should be of interest to those involved with patch repairs of reinforced concrete beams.

Jeppsson et al (2002) conducted a study with the purpose of examining the effects of debonding along the reinforcement close to the supports on the strength of the beam. They obtained a series of results from beam specimens with absent bottom concrete by surrounding them with plastic tubes. Longitudinal reinforcements with 16 mm diameter at the bottom of the beams were used and the average yield strength was f_{st} = 530 MPa. They also used 10 mm diameter bars at the top of the sections and 6 mm stirrups with 180 mm spacing.

A total of six specimens were designed for testing. Of these, one was a reference beam – without stirrups and with full bond. The remaining beams all had stirrups and a certain length with no bond, differing by the length of one stirrup each – ranging from 0 – 720 mm.

All were subjected to point load at 850 mm from the tip of the beam using a displacement-controlled actuator set to a constant rate of 0.05 mm/s. This process was continued even after failure, in order to observe post-peak behaviour.

They concluded that the load carrying capacity was inversely proportional to the unbonded length. Their results have also shown that reducing 80% of the total bond length causes only 33% reduction in strength capacity. Furthermore, it was shown that decreases of the bond length caused a more brittle type of failure, and that stirrup reinforcement plays a critical role in structural strength.

Sulaimani et al (1990) examined the effects of reinforcement corrosion on the steel-concrete behaviour. They reported a loss of strength in simply supported beams with loss in steel section of about 4%-5% caused by corrosion. It was shown that specimens that were reinforced with 14 mm single bars suffered an 11% decrease in capacity when loss of steel section reached 4%.

Tests showed that the loss of local bond was not as significant as the loss of anchorage capacity. Minimal evidence is present to suggest that conventional calculations and procedures for shear and flexural strength are insufficient, acknowledging that consideration is given to reductions in

beam section. Nevertheless, evidence still exists showing that a correlation may exist between loss of bond and corrosion damage in structures, especially when plain round bars are used. No research has been conducted for the effects of corrosion/debonding on anchorage capacity of hooks or bends.

In beams with uniform corrosion, up to 0.5 % corrosion can be withstood without having any adverse effect on the beam strength. After that point, an increase in corrosion corresponds with a decrease in strength. However, every specimen that was tested was insensitive to loss of bond between two supports, and bonding force in anchorage zone would have improved by lateral pressure at supports.

Luckai (2011) developed a new methodology and a computer program for the rapid assessment of heavily spalled RC bridge girders and multi-girder bridges. The project was supported by the Ministry of Transportation of Ontario (MTO) and conducted at the University of Waterloo.

He proposed a modified strength concept to evaluate the residual strength due to development deficiencies resulting from spalling. The concept was founded on the following basic assumptions:

- The spalled areas are fully debonded with no remaining force transfer.
- Full concrete and bond strength is assumed in the unspalled areas.
- The reinforcing steel is at full strength and has no change in strength or ductility due to corrosion.
- The bond strength is linearly proportional to the available development length.

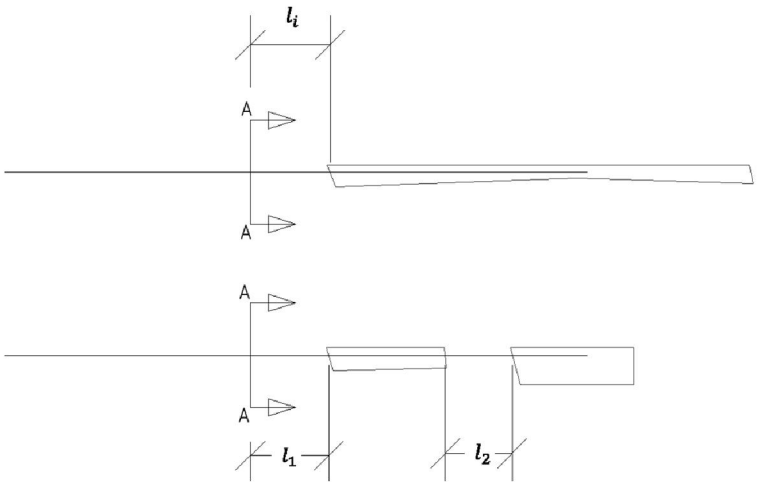

Figure 2-3: Modified concept area, Luckai (2011)

As shown in the figure above, this concept states that the value of the overall bond can be obtained by adding together the values for all the small bonds. If the overall bond value is greater than the minimum anchorage length (concrete code) then, it will be assumed that the overall bond value is the same as the minimum anchorage length.

$$l_i = \sum_{k=1}^{n} l_k \tag{2-1}$$

If the intact length is less than the required development length $l_i < l_d$ then the proposed method proportionally modifies the bar's cross-sectional area as follows:

$$A_d^{'} = A_d\left(\frac{l_i}{l_d}\right) \tag{2-2}$$

Where:

$A_d^{'}$ = modified bar cross sectional are

A_d = actual steel cross section area

l_i = intact (remaining) length

l_d = minimum anchorage length

Based on the proposed method, Luckai suggested a modification to the Moment Capacity formula (concrete code), from which he derived a second formula as:

$$M_r^{'} = A_d^{'} \cdot \phi_s \cdot f_y (d - \frac{a}{2}) \qquad (2\text{-}3)$$

ϕ_s = resistance factor for non-prestressed reinforcing bars

f_y = yield strength of steel

d = distance from extreme compression fibre to centroid of longitudinal tension reinforcement

a = depth of equivalent rectangular stress block

He went further, as to do the same with the Shear Resistance formula. All of the work he conducted based on this central concept, culminated into a computer program. The program developed herein allows the user to evaluate the resistance of a single girder at a specified number of points along its length. The program was developed in three steps corresponding with: modified area, moment resistance and shear resistance computations.

The computer program facilitates the analysis of the single girder model, the multiple girder model, and the probabilistic analysis. The program generates plots to graphically describe the deteriorated moment resistance. For instance, the Figure 2-4 shows the moment evaluation for one of the Girders in the bridge.

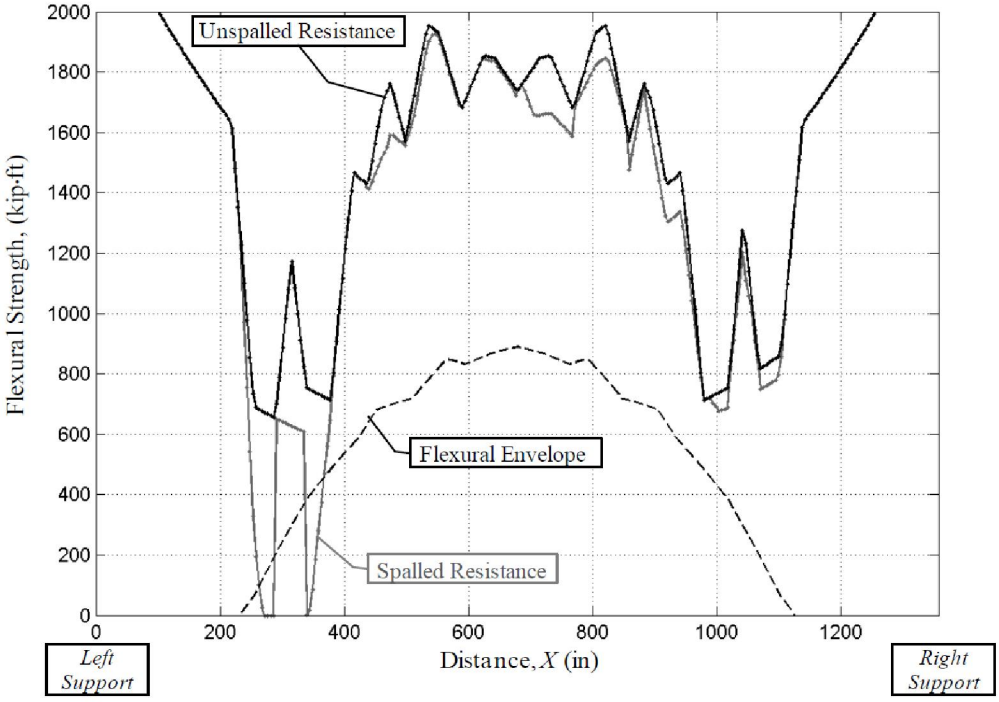

Figure 2-4: Flexural evaluation of single girder (Luckai, 2011)

The dashed line indicated the envelope of the maximum moment due to the CL-625-ONT truck (CAN/CSA S6-06) located at any position along the bridge span. The remaining curves in this figure represent the factored unspalled and spalled moment resistances, as indicated. The curved shape of both resistant curves is a result of the change in cross-section along the span (i.e. the girder arch). The impact that exposing longitudinal reinforcement has on the member's strength is clearly visible. It is immediately evident that spalling has the greatest effect on the strength of this girder near the general splice locations. Locations where the resistance drops below the moment envelope are obvious areas of concern.

Luckai used of this computer program to conduct a full-structure or multi-girder analysis. The program also generates plots for the entire bridge. A combination of all moment resistance plots is shows in the following figure.

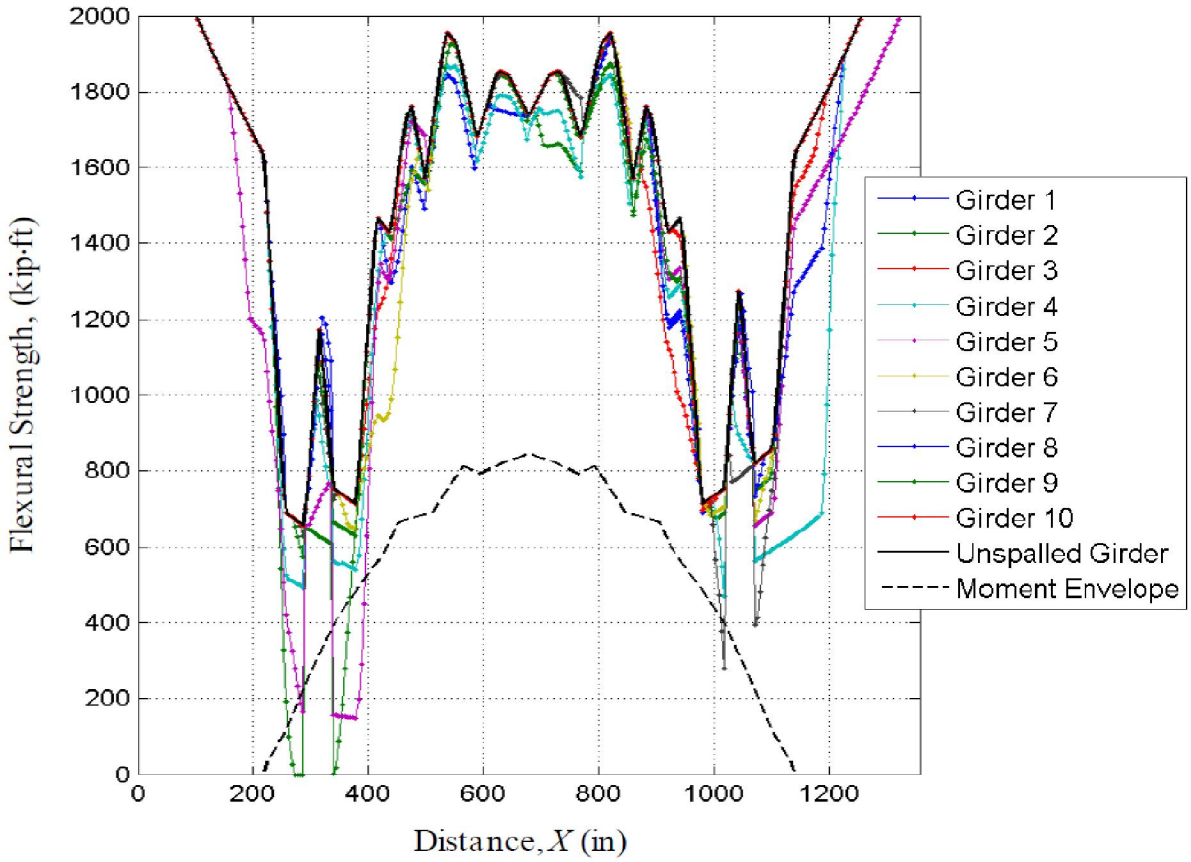

Figure 2-5: Spalled moment resistance for each girder in the bridge. (Luckai, 2011)

These plots describe the minimum girder resistance and show the weakest girder points and can be used as a quick check to determine if any girders in the entire bridge are insufficient and if further analysis is required.

He also initiated a pilot laboratory study to determine if proposed modified area concept could predict the behaviour of spalled concrete beams with exposed reinforcement.

The test program included the fabrication of 12 specimens with different patterns of debonding, which were separated into two groups. The first group was used to test the strength of spalled concrete while the second was used to determine the effectiveness of a mortar patch (as currently utilized in industry) in restoring bond and strength.

Of the specimens Luckai tested, 11 had a dimension of 1400 × 100 × 150 mm, while the remaining one had a dimension of 1700 × 100 × 150 mm. All of them were reinforced at the bottom with two 10M bars.

All 12 specimens were subjected to a point load at mid-span and compared the experimental results with the values hypothesized prior to beginning the lab tests. All ratios were found to be between 0.87 – 1.28. Arch action was demonstrated by fully anchoring longitudinal bars past the supports.

Technically the current research is built on the previous research conducted previously by the University of Waterloo, and continued with complimentary lab tests to verify the correlations between proposed model and reality; however this research is more focused on beams which are affected by flexural loads.

2.3 Mechanisms of Bond Transfer

There are three mechanisms through which forces are transmitted between the concrete and the reinforcement in RC concrete structures:

1- adhesion between the concrete and the bar,
2- friction between the concrete and bar surface, and
3- bearing of the ribs against the concrete.

These mechanisms vary in significance at various stages of loading. Initially, before a certain point is reached where the forces at play break the adhesion bond, adhesion and friction provide support. After this breaking point, the effect of friction begins to wane as the mechanical bearing of the ribs against the concrete becomes the primary mechanism for load transfer.

The adhesion bond is only effective once. More specifically, it only comes into play until the initial time the loads induce adhesion breaking, after which it becomes an irrelevant factor. Friction forces are negligible in contrast to the adhesion and bearing influences. In addition, they lose efficiency when a load is imposed on the concrete reinforcement, causing it to stretch out and thin, according to the Poisson effect.

Two force components: longitudinal and radial, account for the force transferred from the reinforcement to the concrete. The latter causes circumferential tensile stresses in the concrete around the bar. Eventually, the concrete will split parallel to the bar, and the resulting crack will propagate out to the surface of the beam. The splitting cracks follow the reinforcing bars along the bottom or side surfaces of the beam.

When investigating splitting-induced effects on bonds, the simultaneous and combined interaction of these two components with the structure presents researchers with a difficult task. This challenge arises from the fact that it must be determined which component acts when and to what degree – so as to consequently establish the degree of involvement of both in the failure of a structure. As such, numerous studies have been dedicated to address this point, resulting in novel test procedures and results that will be further discussed in the following sections.

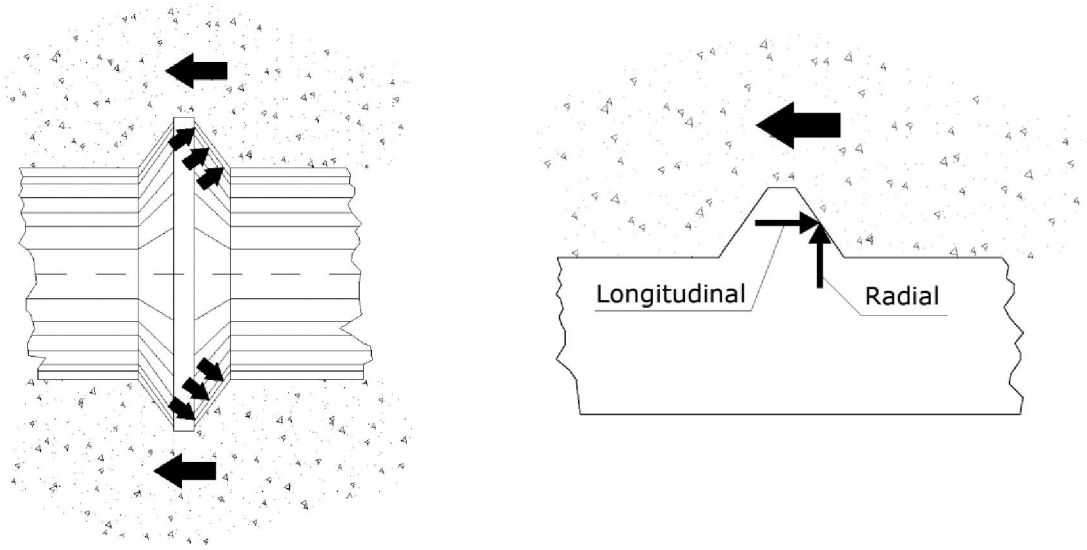

Figure 2-6: Components of force on concrete

As shown in Figure 2-6, reinforcement must be provided to hinder and halt the opening of the cracks, as once these develop, bond transfer drops rapidly. A concrete structure displays splitting failure after the load surpasses a certain point. This critical load is a function of:

1- The smallest distance from a given bar to the next or to the surface of the – this distance is directly proportional to the splitting load;

2- The ability and strength of the concrete;

3- The average bond stress – the greater the bond stress, the greater the wedging forces, which load to a splitting failure.

An external force implemented on reinforcement in the process of pull-out entails certain characteristic phases during its dissociation from concrete:

Stable Phase: for low bond stress values (Equation 2-4), the applied force does not overcome the chemical adhesion in play. Hence, no bar slips ensues, but lugs surfaces experience a high degree of stresses. (Task Group, 2000)

$$\tau \leq \tau_1 = (0.2 - 0.8)\, f_{ct} \qquad (2\text{-}4)$$

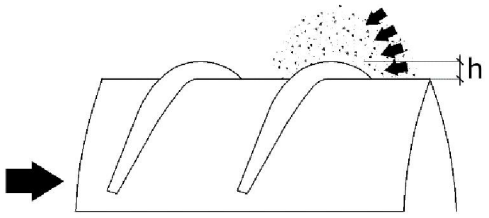

Figure 2-7: Initial bond stress on lug for low bond stress value

When examined on a microscopic scale, forces other than chemical adhesion, such as micromechanical interactions, are in question. The latter are due to the intrinsic rough surface of steel. However, on a larger scale, both these chemical and physical forces lose relevance, as demonstrated by the low bond performance characteristic of plain bars.

1- Initial cracking: for greater bond stress values, ($\tau > \tau_u$), the chemical adhesion and physical forces are overcome. At this point, the increasing bearing stresses between the lugs and the concrete instigate the development of transverse micro-cracks, which in turn cause the lugs to begin slipping. In contrast, the wedging action driven between the lugs and the surface of the bar – as shown in the Figure 2-8 – acts against the aforementioned slipping action. Thus, although there is some minor transverse fracturing in the concrete, no substantial splitting occurs.

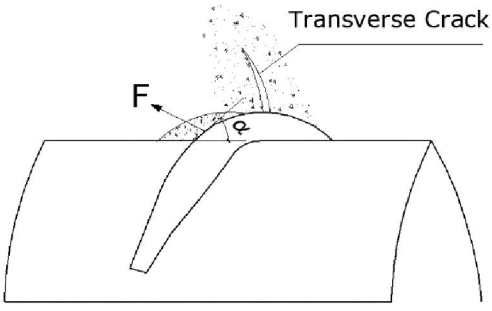

Figure 2-8: Crack initiation

2- Splitting cracks: for even greater bond stress values $\tau > \tau_1 (1-3)\, f_{ct}$ (Equation 2-5), the longitudinal micro-cracks begin to spread radially due to the resistance of the wedging action to slippage. This results in significant cracks, as depicted in Figure 2-9.

$$\tau > \tau_1 (1-3)\, f_{ct} \tag{2-5}$$

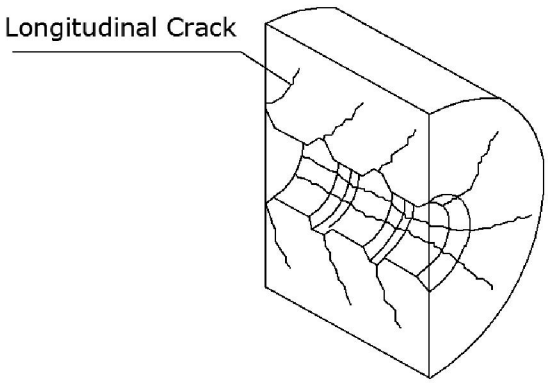

Figure 2-9: Crack initiation in 3D (Task Group, 2000)

It is also important to note that in this stage, according to Tepfers model, the pull-out force is counteracted by the hoop stresses in the surrounding concrete, as shown in Figure 2-10, (Tepfers, 1979). This will be further discussed in Section 2.10.1.

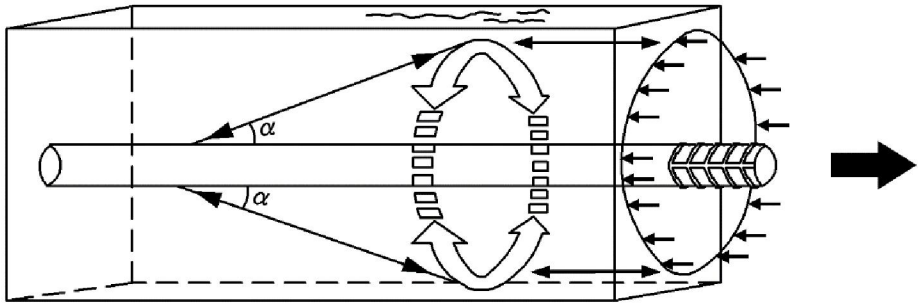

Figure 2-10: Schematic of internal forces within reinforcement concrete specimen (Tepfers, 1979).

3- Failure stage: the concrete collapses at various stages depending on the size and type of reinforcement, which has been broken down into three categories and further explained below.

i- In plain reinforcements, stages 2 and 3 are omitted as the forces in play in those scenarios are a manifestation of the impact of lugs. In plain bars, the only remaining resistive forces are the adhesive bonds and micromechanical interactions. Thus, when those are overcome in stage 1, it results in immediate failure. As such, other forces such as friction, transverse pressure, and bar roughness strongly influence the bond stress transfer.

Although stages 2 and 3 are skipped, the stress withstood by the bar before succumbing to failure is still relatively high. Before reaching stage 4, significant slipping between the bar and the concrete occurs, which can be confirmed by the ratio formula (Equation 2-6).

$$\frac{\tau_b}{f_c} = 0.15 - 0.30 \text{ (Gambarova and Karakoc, 1982)} \quad (2\text{-}6)$$

ii- In light to medium reinforcements, the longitudinal cracks spread through the concrete section and between the bars, resulting in the abrupt failure of the structure. Nevertheless, should stirrups be incorporated into the design, concrete splitting will not immediately result in failure by virtue of the confinement action involved.

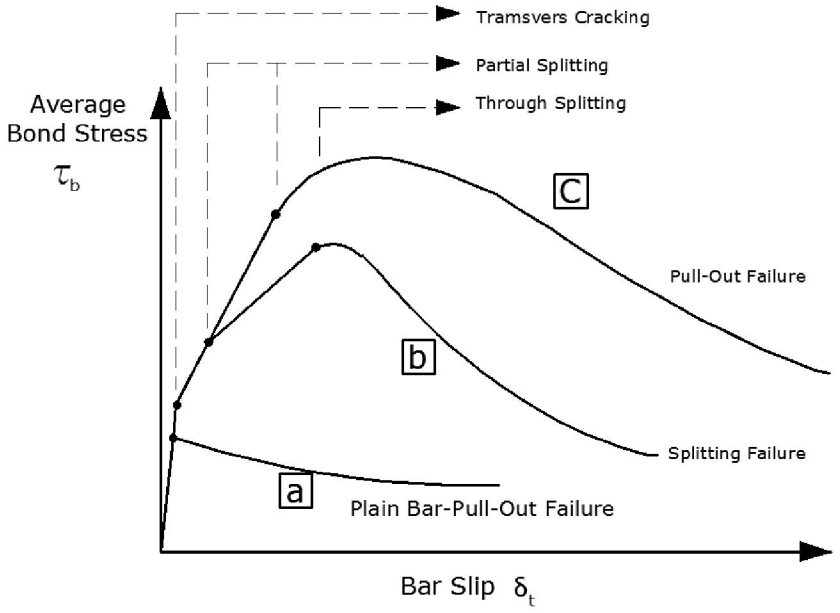

Figure 2-11: Local bond stress-slip law for different levels and type of reinforcing, (Task Group, 2000)

In heavy reinforcements confined by stirrups, the resulting radial longitudinal cracks are counterbalanced by the existing confinement forces. As a result, the eventual failure of a structure is not due to cracks, but rather to a complete pullout of the reinforcement.

2.4 Factors Affecting Bond Performance

The sum of the interactions between a myriad of factors and parameters influence bond behaviour. These include, but are not limited to: the material composition and type of the bars and stirrups, the connection wires used between these two components, and the type and strength of the concrete. However, the impact of various technical aspects should not be overlooked, such as: concrete cover; the spacing between bars; direction of casting in relation to bar direction; and bar alignment.

There are also less apparent factors which demand consideration, such as the Poisson ratio, size of the bars, and load time history.

2.4.1 Geometry and Stress Level

The principal factor influencing bond behaviour, and ensuring a high degree of bond resistance is the configuration and physical makeup of the bars.

The best bond performance of bonding depends on an optimal combination of various physical parameters of bars. The latter includes rib height (h), rib spacing (S_R), and bar diameter (d_b).

The commonly named "bond index" (f_R), is a coefficient that can be written as a function of the three above-mentioned factors (Equation 2-7).

$$f_R = \frac{A_R}{\pi . d_b . s_R} \quad \text{(Task Group, 2000)} \tag{2-7}$$

From a cross-sectional view, A_R is the area of the protrusion of two lugs, which form a single rib.

f_R value of 0.05 to 0.10 is generally regarded as acceptable and indicative of good service load performance, signifying that bond strength is at a maximum, splitting ability is at a minimum, and all industrial requirements are met.

The correlation between bond stress and slip is influenced by a myriad of factors. For instance, the softening of the steel at the points of yielding and the softening of the surrounding concrete have both primary and secondary effects in respect to the behaviour of the structure. In detail, yielding causes alteration of the shape of the ribs, reducing the surface area of the ribs and the projection of the lugs.

From various researches concluded that, bond stress will change in various bar geometries. It has been proven that when load is applied on top of supports, plain reinforcement is more effective than reinforcements with lugs.

Maslehuddin et al (1990) conducted their research on measuring different conditions of steel bar on bond strength, and evaluated different degrees of rusted steel on concrete surfaces, and its relations to bonding. Different specimens were tested with varying bar diameters, and they were subject to environmental exposure. Results showed that specimens with 16 mm diameter bars didn't lose any significant bond strength, and specimens with 22 mm diameter bar showed minimal increase of bond. In smaller bar diameters, rust acted as filler between reinforcement lugs, this is why there was no noticeable change in bond. But, in bigger diameter bars, rust increased the roughness of the surface increasing bond strength.

2.4.2 Concrete Cover and Bar Spacing

By increasing concrete cover thickness and bar spacing, bond strength will increase (ACI Committee 408, 1996). Tepfers (1979) and Eligehausen et al (1982) observed that a type of bond failure was correlated with concrete cover and bar spacing. For example, minimal concrete cover causes splitting tensile failure and lots of concrete cover causes pull-out failure. Commonly, in structures, splitting failure occurs between two reinforcements, or reinforcement and cover, or both. This is under the condition that "pullout failure can occur with some splitting if the member has significant transverse reinforcement to confine the anchored steel" (ACI Committee 408, 1996).

2.4.3 Transverse Reinforcement

The ratio of the steel in cross-sections influences the type of bond failure (Orangun et al, 1977). The increase in steel ratio will result in an increase in bond strength due to confinement action,

and will produce pull-out failure rather than splitting failure. For changing the mode of failure from splitting to pull-out, additional transverse reinforcement is needed.

2.4.4 Bar Size

The relationship between bond strength and the size of the bar never formulates because of the following reasons: 1- as bar size is increased, development lengths will increase; 2- thicker bars will achieve higher bond strength than thinner bars in certain developed lengths, (ACI Committee 408, 1996).

Therefore, it is more proficient to use a series of small bars with appropriate spacing, rather than large bars. Size of longitudinal bars is important in the contribution that stirrups have in maintaining bond strength. When bar slipping increases, higher stresses transfer to the stirrups, so concrete provides better confinement. Thus, stirrups have the same amount of influence on bond strength as longitudinal reinforcement (ACI Committee 408, 1996).

2.4.5 Concrete Quality

The quality of the concrete is of premier relevance in a bond, referring not only to concrete strength, but also to specific technological features related to concrete casting. These technological features are generally of greater importance than the strength itself.

Considering that bond action is an outcome of localized pressure residing underneath the ribs and is directly in relation to the shear in interface forces, the effectiveness of the bond is reliant on both concrete multi-axial behaviour in compression f_c, and tension strength (f_{ct}). These factors also play a primary role in pull out and splitting failures individually.

Bond action is also effected by a stress state in a concrete surrounded bar. The behaviour of both splitting anchorages and reinforcement covers are aggravated by the effects of transverse tensile forces. This can even cause a pull-out failure to turn into a splitting failure. Both these cases suggest a worse situation, as the presence of more tensile forces is caused by temperature and shrinking effects (Task Group, 2000).

2.4.6 Steel Strength

The amount of stress within the bond is a function of the amount of force in the reinforcement. When the force in reinforcement is more than the amount of yielding stress, lugs won't interlock with concrete in the same fashion as before and the mechanisms of friction will alter. The result of these conditions is the decrease of stress in bond (Task Group, 2000). Based on the research of ACI Committee 408, the amount of stress in bond is lower in reinforcements with high steel strength.

Researches that have been conducted in the past show those specimens without transverse reinforcement, only 2% of them failed because of yielding steel, and the rest failed due to bond. 10% of the specimen bars had yielded after bond failure when transverse reinforcement was present, (Zuo and Darwin, 2000).

2.5 Failure Modes

Based on the different types of load transfer between the concrete and the bar, two kinds of bond failure have been recognized: pull-out and splitting failure. Pull-out failures often occur because no contact between concrete and reinforcement exists, except the contact between lugs and surrounding concrete which causes the "shearing-off "effect on the lugs as shown in Figure 2-12. The failure is documented when anchorage zone has been breached (Crains and Abdullah, 1995).

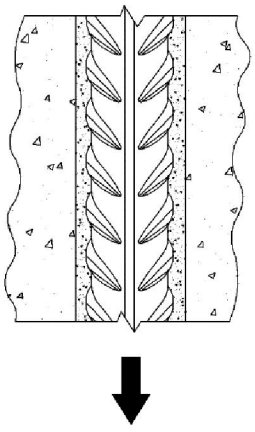

Figure 2-12: Pull-out failure

In the case of splitting failure, debonding originates from the longitudinal splitting and reinforcement exposure surrounding the bar as shown in Figures 2-13, and in this phase the bond

strength disappears when the radial cracks reach the outer surface of the structure. This is one of the primary factors for the start of structural collapses.

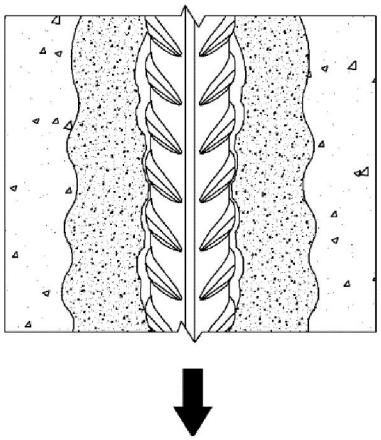

Figure 2-13: Splitting failure

2.6 Crack Analysis

Based on lots of conducted research, crack diagnosis was one of the major criterions for the estimation of the life of a structure. Despite longitudinal cracks, the beam can still save a major portion of its strength capacity. The formation of these longitudinal cracks does not necessarily translate into insufficient residual structural capacity.

Bond strength will decrease significantly before large losses in sections occur. Andrade et al (1993) proposes that a longitudinal crack as wide as 0.3mm-0.4mm means the end of service life. This proposition is from code limitations on width of flexural cracks, for visual and resident comfort, it does not mean the potential loss of strength in the beam. However in Andrade's research, the negative effect of longitudinal cracks on bond strength is not taken into consideration.

Cracking does not result a sudden loss of tensile strength in concrete, and steel has the ability to transmit shear and tensile forces through fine cracks. Philips and Binsheng, (1993) show that tensile strength will decrease rapidly after peak load is reached. This is because tensile strength releases in cracks as wide as 0.10mm-0.15mm. Other studies show that limitations in concrete cover will be irrelevant once longitudinal cracks surpass 0.15mm in width. Furthermore it is widely assumed that bond strength is directly related to splitting resistance. Therefore when longitudinal cracks reach a width of 0.15mm, bond strength will reach a negligible value.

2.7 Parameters that Affect Bond Response

One way to measure bond strength is to analyze the cracks that have been created on the surface of the concrete. Bond can be a function of these cracks, and the overall concrete strength. When localized crushing occurs, it has a great influence on bonding and the deformation of structures, and it is reasonable to obtain a correlation between shear strength of concrete and bond strength from the effects of crushing.

"Since both of these quantities typically are approximated as being proportional to the square root of the concrete compressive strength, bond strength (t_{bond}) also may be defined by the square root of concrete compressive strength". Eligehausen and Bertero (1982) suggest the following relationship:

$$t_{bond} \propto (f_c)^{\beta} \tag{2-8}$$

While Tepfers suggest simply $\beta=\frac{1}{2}$, the bond strength is normalized with respect to the square root of the concrete compressive strength:

$$t_{bond} \propto (f_c)^{\frac{1}{2}} \tag{2-9}$$

The model presented by Eligehausen shows the influence of bar size on bond strength; and since bond strength is reducing as bar size is increased, it suggests more chances of concrete crushing in larger sized beams.

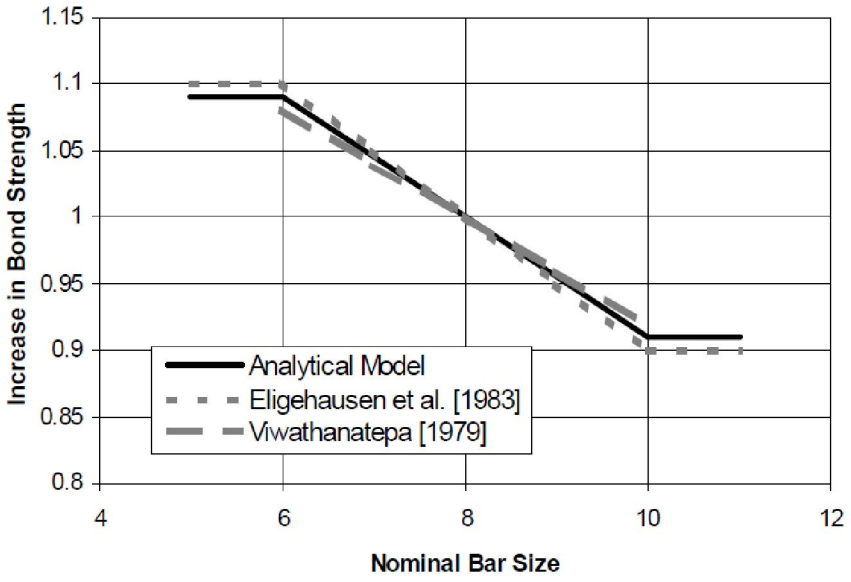

Figure 2-14: Influence of bar size on maximum bond strength, Lowes (2000)

2.8 Bond Modelling for Transversely Cracked Concrete

Based on previous research conducted on this subject, bond strength is lower in concrete under tension than concrete under influence of compression. This also affects the bond slip rate and crack width with the same relevancy of tension and compression effects on concrete; however the bond slip displacement can be expressed by a nonlinear relationship with the same form of equation shown below. The values τ_1 and S_1 in pull-out failures are much higher in concrete under tension (Equation 2-10).

$$\tau = \tau_1 \cdot (\frac{S}{S_1})^{\alpha} \text{ (Eligehausen, 1982)} \qquad (2\text{-}10)$$

The values S, S_1, τ, τ_1 and α are observed from experimental tests, shown in the Figure 2-15.

When $S < S_1$ the equation of the bond stress will obey a nonlinear function, under the formula $\tau_1 \cdot (\frac{S}{S_1})^{\alpha}$ Following that, the function $\tau = \tau_1$ represents the bar displacement for $S_1 \le S \le S_2$.

After that, for $S \ge S_2$, τ declines gradually and linearly to reach S_3. When this phase is reached, the assumption is made that the bar has been shifted an equivalent distance of one lug.

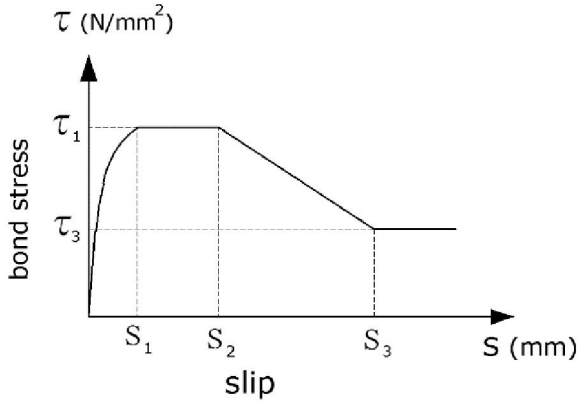

Figure 2-15 Analytical model for local bond stress-slip relationship

A bond reinforcement that is under influence of tensile forces is resisted by the surrounding concrete and steel members, because of the bond action which is responsible for the transfer of load from reinforcement to concrete and vice versa. However, there is an exception in the case of cracks in which load exerts pressure directly to the reinforcement. This exception justifies that in all levels of stress, the strains in the bar fixed in concrete is at lower rates than strains in those of a naked bar. The reduction in steel strain caused by concrete can be noted as a stiffness increase of the reinforcement, in comparison to a naked bar. Thus, this phenomenon is named "tension-stiffening".

The overall stretching of the de-bonded bar is: $\Delta l_0 = \varepsilon_{s0} \cdot l$

The overall stretching of a bar implanted in a concrete member subject to tension forces is:

$$l = 2\int_0^{\frac{l}{2}} \varepsilon_s dx \tag{2-11}$$

By applying the above noted analytical model, Δl has the following expression (Equation 2-12),

$$\Delta l = \frac{\xi \cdot \varepsilon_{so} \cdot l + 2 \cdot \varepsilon_o}{1+\xi} \text{ (Gaetano and Romano, 1992)} \tag{2-12}$$

$$\xi = \frac{n\rho}{\psi} \tag{2-13}$$

ε_{so} =Steel strain in general, and at x=0

ψ = Concrete stress Ratio= $\dfrac{\int A_c \sigma(x,r)dA_c}{A_c \cdot \sigma_c}$

(2-14)

σ_c = tensile concrete stress adjacent to the steel-concrete interface

$\sigma(x,r)$ = concrete tensile stress and r is distance from centroid of the bar

$\rho = \dfrac{A_s}{A_c}$ (A_s : reinforcing-bar area, A_c : concrete cross-sectional area)

$n = \dfrac{E_s}{E_c}$

The overall equivalent shortening of the bar due to concrete restraining action (Δl_c) is:

$$\Delta L_c = \Delta L_0 - \Delta L \tag{2-15}$$

Thus, the relative influence of the concrete to the overall stiffness of the member can be defined as Equation 2-15 (Breslea and Bertero, 1968):

$$\lambda = \frac{\Delta l_c}{\Delta l_0} \tag{2-16}$$

The parameter λ is an index of tension-stiffening effectiveness. The rate at which λ increases; the amount of stress that is carried by concrete is increased.

$$\lambda = \frac{1}{1+\xi} \cdot (1 - \frac{2S_0}{\varepsilon_{so}.l}) \tag{2-17}$$

The contribution of concrete to the strength in bonding reinforcement is displayed in the Figure 2-16, with comparison to naked bar strength. With further analysis the average resistance which caused by load about two contiguous cracks can be calculated. Where ε_{sm} is the average steel strain of the embedded reinforcement and ε_{scr} is the steel stress in a section when a primary crack form (first cracks).

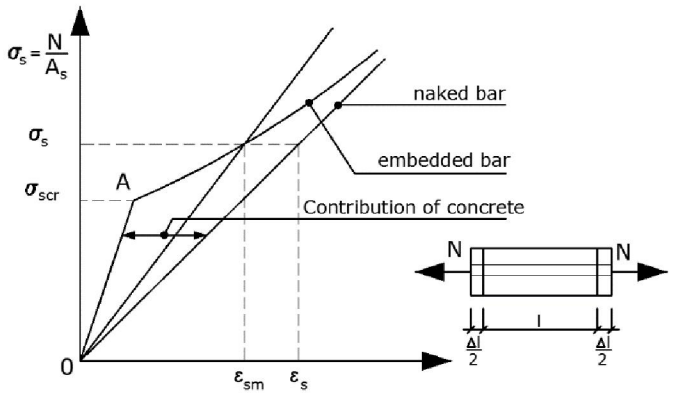

Figure 2-16: Tension stiffening: tensile stress versus tensile strain, (Task Group, 2000)

A relationship can be shown to compare the steel stress stability and the average strain strength of the fixed reinforcement ε_{sm} (that is equal to the average strain in the member ε_{cm}), as:

$$\sigma_s = E_{sef} \cdot \varepsilon_{sm} \tag{2-18}$$

Where E_{sef} is the effective modulus of elasticity of the steel bar.

Several methods can be used to determine ε_{sm}. The Euro code (1991) gives:

$$\varepsilon_{sm} = \frac{\sigma_s}{E_s} \cdot [1 - \beta_1 \cdot \beta_2 \cdot (\frac{\sigma_{scr}}{\sigma_s})^2] \tag{2-19}$$

$$E_{sef} = \frac{E_s}{1 - \beta_1 \cdot \beta_2 \cdot (\frac{\sigma_{scr}}{\sigma_s})^2} \tag{2-20}$$

Where β_1 and β_2 account for the bond reinforcement features (β_1=1 for ribbed bars, β_1= 0.5 for smooth bars) and the nature of the loads (β_2=1 for short-term loads, β_2=0.5 for long-term or repeated loads.

2.9 Anchorage Capacity after Cover Splitting

In stirrup reinforcement, a linear increase in bond capacity was observed by different researchers .They also gained different results while analyzing the effectiveness of corner and inner stirrup on member sections. The stirrups can have less effectiveness in restricting the inner bars, as observed by Warren (1969).

Thus, a correct implementation of stirrup bars increases its effectiveness on bond capacity as linked with concrete splitting. By taking this into account, a linear correlation of bond capacity on stirrup ratio was concluded by Darwin et al (1996). He discovered that because of concrete confinement, bonding capacity will increase linearly between the bars and surrounding concrete.

A study done by Maeda (1995) have explained stirrup reinforcement properties with spring features, showing that the confining action and bond stress have a linear relationship prior to cracking. This relation converts to nonlinear function after cracking occurs. It is assumed that these "springs" have fixed rigid support from one side as shown in the Figure 2-17.

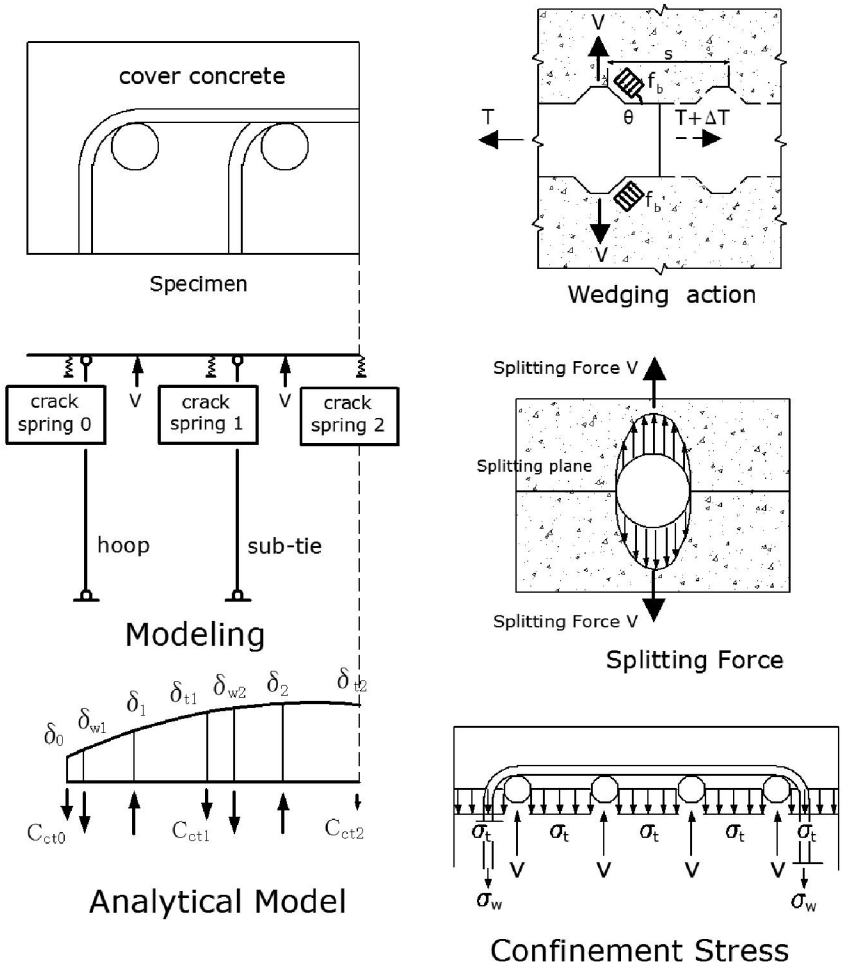

Figure 2-17 Definition of force and deformation Maeda (1995)

2.9.1 Splitting cracks control

Splitting grows longitudinally beside development lengths, therefore extended section of the bar can get visible to the environment exposing it to the risk of corrosion. With a result of a loss of bond, the strength of flexural and shear of the members will decrease, which is in contradiction of the structural code.

In order to properly analyze and asses the durability of a structure, the width of the splitting crack must be taken into consideration. A connection between the maximum crack opening (W_S) and the flexural crack width (W_f) which has been made from previous researches done by Giuriani and Plizzari (1998) is centered on the slip rate (s) of the bonding zone (shown in Figure 2-18). Moreover, Giuriani and Plizzari (1998), found a solution that simplifies the expression for W_S as a function of W_f. This was achieved by accounting only the linearly dependant terms on W_S and Ω in Equations 2-20.

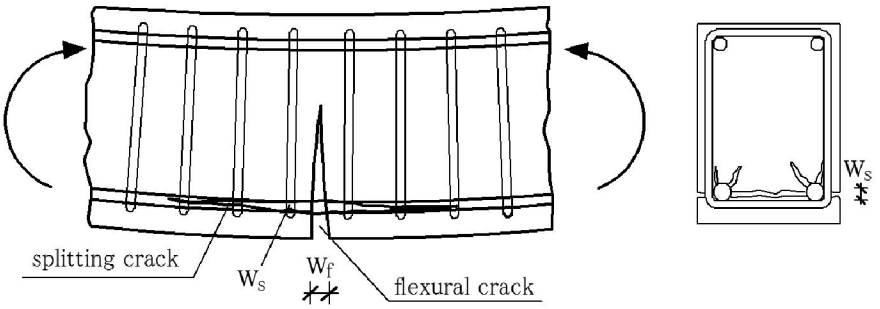

Figure 2-18: Flexural and splitting cracks in RC elements (Giuriani and Plizzari, 1998)

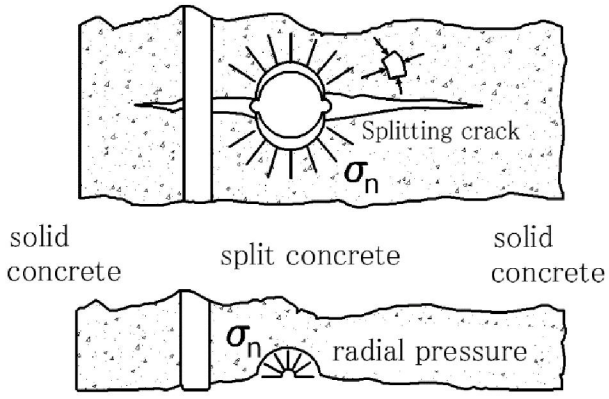

Figure 2-19: Splitting crack and confining action around ribbed bar (Giuriani and Plizzari, 1998)

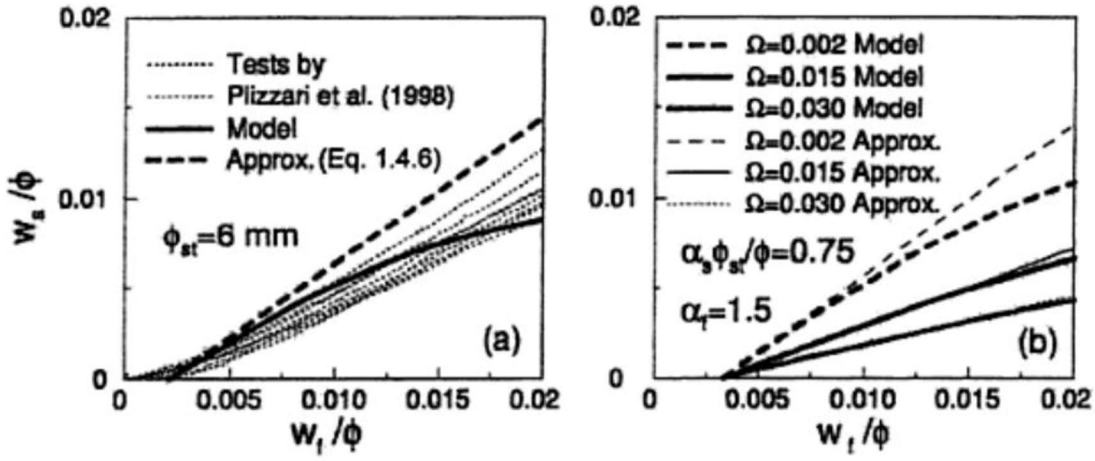

Figure 2-20: (a) Fitting of test results obtained by Plizzari (b) influence of stirrup index of confinement; splitting crack width (W_s) versus flexural crack width (W_f)

$$\frac{W_s}{\phi} = \frac{\frac{1}{\alpha_f}\frac{W_f}{\phi} - 0.0022 + 0.0034\Omega}{59.78\Omega + 0.6703} \tag{2-21}$$

Ω: refers to the stirrup index of confinement, defined by the relation between the sum of the total area of the cross-sections A_{st} of the stirrup legs, and the area assigned to the main bar in the splitting plane.

ϕ: nominal diameter of the main reinforcement.

From the Figure 2-20 the relationship between load and flexural crack openings based on earlier conducted research. By acknowledging this fact, a relationship between split crack openings W_s and flexural crack openings W_f can be established.

During the designing process, splitting cracks can be calculated based on the relation with the flexural cracks. This will help the designer to establish the basis in which corrosion can be prevented for any stirrup ratio (Represented by Ω =stirrup index of confinement). It is also important to mention that for minimal values of Ω, the splitting crack width is almost half of the flexural crack width.

Research indicates that longitudinal cracks parallel to the reinforcement will have far more damaging effects than of flexural or tension cracks. These cracks cause a reduction in bonding adhesion and deflections in the structure.

2.10 A Model of Bond Behaviour

2.10.1 Tepfers model:

Many previous researches has been conducted around the relationship between the effect of bond forces and the forces that cause concrete spalling (radial forces) in reinforced concrete members. As depicted in the Figure 2-21, Tepfers (1979) has proposed a model which measures maximum bond force when the concrete covers crack.

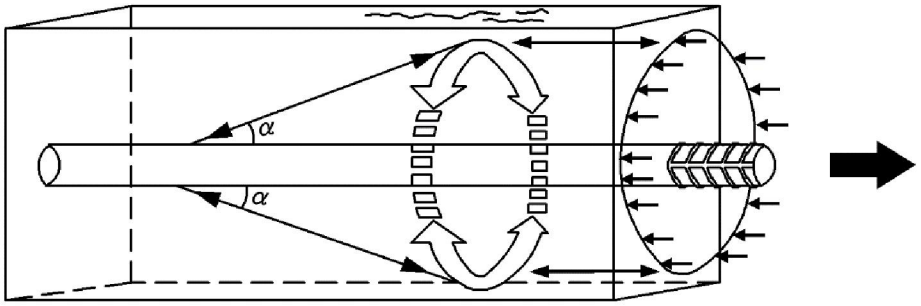

Figure 2-21: Schematic of Internal forces within reinforcement concrete specimen (Tepfers, 1979)

Maximum bond stress was assumed for the three different phases of applied force; an elastic phase, a plastic phase, and a moderately cracked elastic phase. In the first phase, force is assumed to be exerted like a cylindrical shape to the surrounding concrete. It is also assumed that in both compression and tensile forces the angle in which the force is being transferred is at a 45° angle.

Prior to the formation of any concrete cover cracks, it is theorized that concrete strength (f_t) and the applied load have the same magnitude. The level of bond strength during the failure stage in which concrete spalling occurs is calculated by Equation 2-21.

$$\tau_u = f_t \cdot \frac{[c + \frac{D}{2}]^2 - [\frac{D}{2}]^2}{[c + \frac{D}{2}]^2 + [\frac{D}{2}]^2} \quad (2\text{-}22)$$

D = diameter of the concrete cylinder;

c = amount of cover on the rebar;

f_t = tensile strength of the concrete;

τ_u = maximum bond stress;

In real life application, the sensitivity of the peak stress experienced during the debonding failure can cause the collapse of structures. This is because the prediction of bond behaviour relies on the non-uniform distribution of stress forces along the entire interface, specifically the maximum bond strength.

In the "plastic" phase of bond failure the maximum peak resistance is reached, however it is still complying under the concrete ring model. In this phase theory dictates that the concrete only begins to crack when the distributed hoop stress σ_t throughout the cylinder has extended to the maximum tensile capacity of the concrete. The Equation 2-22 is used:

$$\tau_u = f_t \cdot \frac{2 \cdot c}{D} \quad (2\text{-}23)$$

In the moderately cracked elastic stage, a crack will be formed in the inner surface of the cylinder. This occurs when the compressive bond stress exceeds the concrete tensile strength. This model implies that the cracks can spread out throughout the cylinder and still be stable. The maximum bond resistance is reached only when the cracks have breached to the outside of the cylinder. The following formula can be used to calculate bond stress in this phase.

$$\tau_u = f_t \cdot \frac{c + \frac{D}{2}}{1.664D} \quad (2\text{-}24)$$

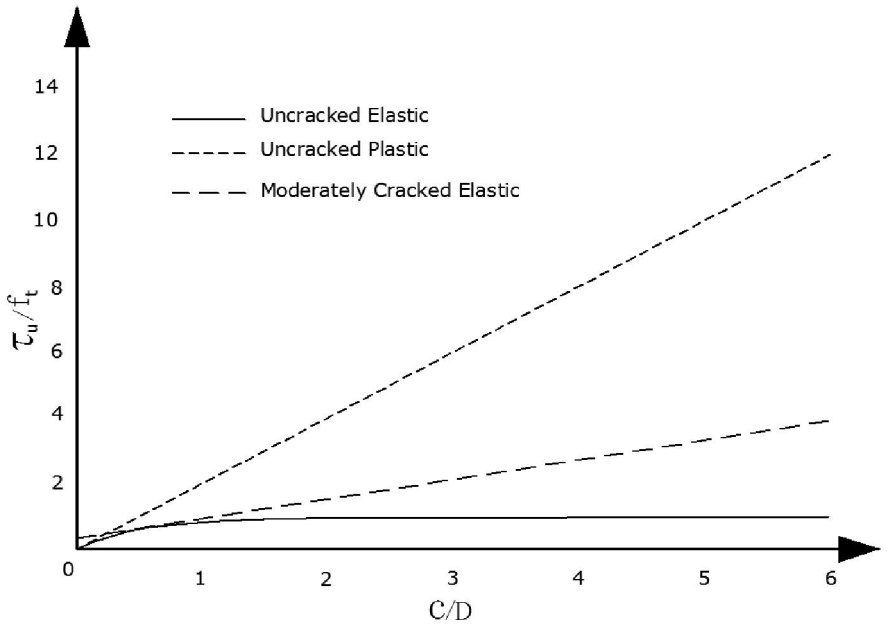

Figure 2-22: Displays the maximum peak stress of a cylinder in consideration of the three stages

The average of the un-cracked elastic and plastic phases can be a great relation in measuring the maximum bond stress in concrete members during the splitting failure. The moderately cracked stage records failure stress lower than the average of the other two phases.

Tepfers confirmed that the majority of the data lies between the un-cracked plastic stage and the moderately cracked elastic stage. Tepfers centred this around the comparison which was made between the model and the obtained peak bond stress in experimentations.

This simple model which was founded on clear norms, does not take into account some of the key features of splitting failure. Crack cohesion, the quantity of the cracks, the space between the reinforcement and the "ring", and the effects of external forces are some of the features of splitting failure that have not been accounted for.

2.11 Effects of Bond Loss on Structural Capacity

Figure 2-23 illustrates the possible impacts of reinforcement corrosion on residual bond strength which ends with the reduction in total load carrying capacity as a result of spalling and losing concrete cover, or through different types of cracking. In the case of general corrosion, bond needs more attention than loss of longitudinal reinforcement, since losing bond strength is more probable than the other factors. Thus, corrosion is more likely to affect the structural capacity than tensile failure. In the Figure 2-23, focus is directed on general corrosion effects on bond

strength and on residual structural capacity. All the variables which are depicted in Figure 2-23 are lead to bond weakness, and it could be comparable with other factors which cause reduction in load carrying capacity.

As seen in Figure 2-23, cover cracking or "loss of integrity" of concrete cover commonly has more serious consequences than loss of area in bar cross sections.

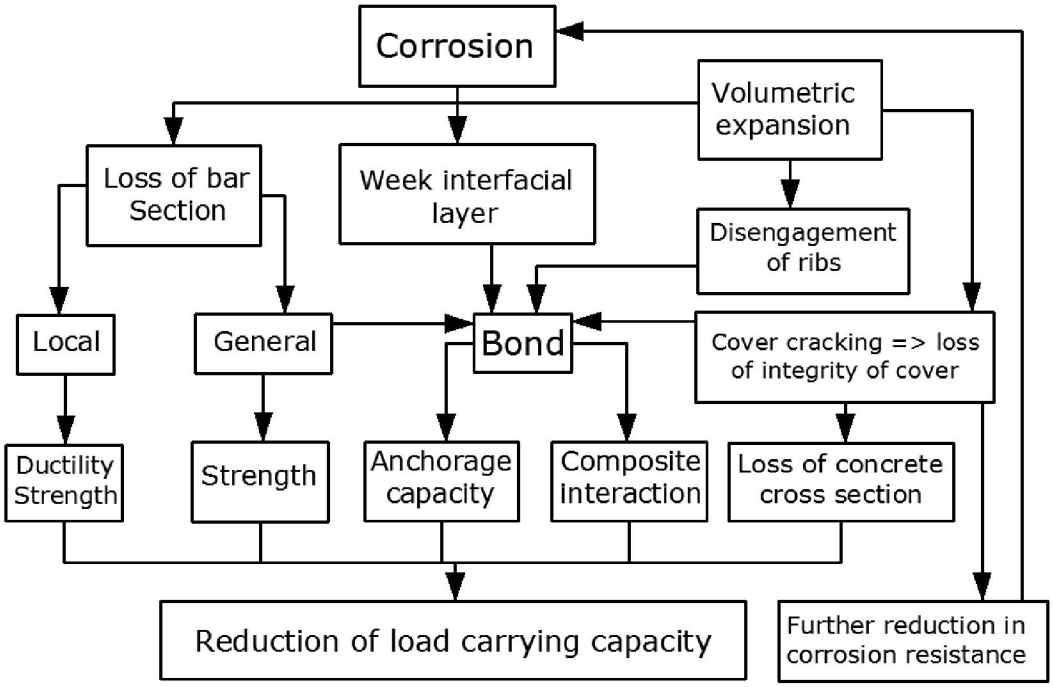

Figure 2-23: Effects of corrosion on residual strength. (Task Group, 2000)

Cairns & Zhao (1993) constructed a numerical model in which the complete loss of bond between reinforcement and remainder of the concrete section is accounted for. They analyzed stress strain graph that follows design codes, altering the shape of the beam form purely flexural beam and fully bonded, to tied arch action where no bonding effect exists.

The main objective of this paper is to further explain, in detail, the newly proposed theory in the field of concrete reinforcement. Focus is on the location of the neutral axis and critical stresses of beams with exposed reinforcement and how it varies in different load stages leading up to ultimate failure.

The behaviour as shown in Figures 2-24, 2-35 is concluded from numerical analysis that compares two beams, in which one bar is fully bonded and the other in which the bar is eliminated throughout the span. In the fully bonded model, the neutral axis remains mostly

horizontal except minor deformation existent on the side. This is due to the development of flexural cracking. In the eliminated bond specimen, higher compressive force is present on the top near the mid span and the neutral axis is drawn towards the bottom of the beam (arch action). The Increasing compression on top of the beam represents the reduction in flexural strength and ductility. The variation in the depth of the neutral axis shows an inclined formation of compressive force rather than horizontal which is present in fully the bonded beam.

The perpendicular load which travels in the member will not be resisted by shear, and instead by the vertical component of the inclined compressive portion. It is realized that in eliminating bond prevents shear failure. The Figure 2-25 illustrates results for a simply supported beam that increases in exposed area length. Each line on the graph represents variant steel ratio in the section. There is no significant loss of strength noted if bond is missing where shear is zero (the moment zone). The factors which effect the behaviour are:

- Debonding length
- Position of de-bonded portion
- Steel ratio in the section
- Strength of the bond, bar and concrete
- Method of loading
- Concrete area geometrics
- Presence of top reinforcement

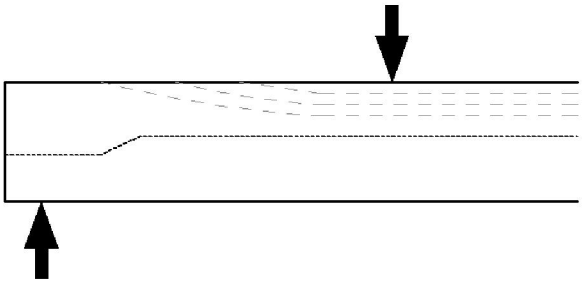

Figure 2-24 Fully bonded bars.

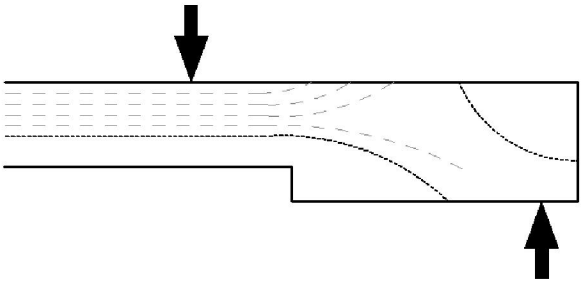

Figure 2-25 Exposed bars.

2.12 Analysis of Beams with Fully-bonded Flexural Reinforcement

The following sections introduce CAN/CSA A23.3-04 (2006) development, moment, and shear design concepts and use each to determine moment and shear capacities for any specimen.

Moment:

Based on CAN/CSA A23.3-04 for a conventionally reinforced rectangular cross section, as shown in Equation 2-24, the moment resistance is:

$$M_r = A_s \phi_s f_y (d - \frac{a}{2}) \quad (2\text{-}25)$$

Where:

A_s = total longitudinal steel in section

f_y = steel yield strength

ϕ_s = resistance factor for concreted

d = distance from extreme compression fibre to centroid of tensile reinforcement

a = depth of equivalent rectangular stress block

There are few assumptions worth taking note:

1. Sections perpendicular to the axis of bending that are plane prior to bending remain plane after bending.
2. The strain in the reinforcement is equal to the strain in the concrete at the same level.
3. The stresses in the concrete and reinforcement can be computed from the strains by using stress–strain curves for concrete and steel.
4. The maximum strain at extreme concrete compression fiber is assumed to be 0.0035.
5. The tensile strength of concrete is neglected in calculation of the factored flexural resistance of reinforced concrete members.

The design procedure relied on the assumption of an equivalent of stress block as shown in Figure 2-26:

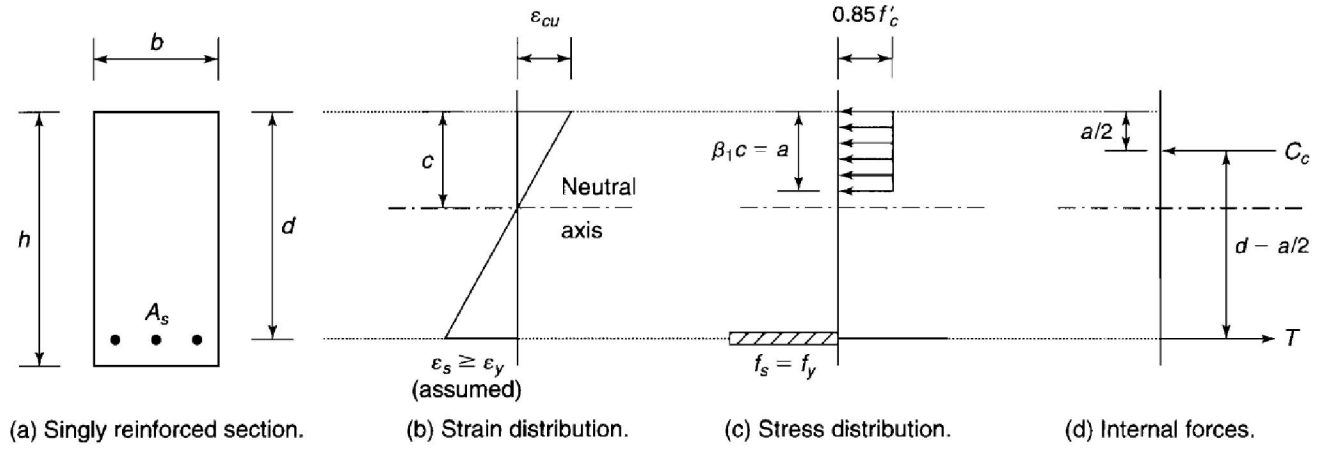

Figure 2-26: Rectangular stress block theory

Shear:

Based on CAN/CSA A23.3-04, the shear resistance is a combination of contributions from both concrete and steel, and the maximum resistance is the sum of these two:

$$V_c = 2.5\beta f_{cr} b_v d_v \tag{2-26}$$

$$V_s = \frac{\phi_c A_v f_y d_v \cot\theta}{s} \tag{2-27}$$

$$V_r = V_c + V_s \tag{2-28}$$

Defining each variables in the proposed formulas (Equation 2-24 to 2-26) is not limited to one method. Canadian concrete code defines two methods for computing the shear capacity of a reinforced concrete member: the general method and the simplified method.

General method: this method is based on compression field theory, and Canadian standards provide simple formula for computing the factor for shear resistance;

$$\beta = \frac{0.40}{(1+1500\varepsilon_x)} \cdot \frac{1300}{(1000+S_{ZE})} \tag{2-29}$$

The average longitudinal strain in a member at mid-depth of cross section can be estimated according to the (Equation 2-29):

$$\varepsilon_x = \frac{\frac{M_f}{d_v} + V_f}{2E_s A_s} \tag{2-30}$$

The angle of inclination of diagonal compressive stress is based on the strain effect as shown in Equation 2-30:

$$\theta = 29 + 7000\varepsilon_x \tag{2-31}$$

Simplified method: this method is an alternative method for calculating the shear force. If the section contains nor transvers reinforcement and the maximum nominal aggregate size of concrete in less than 20, β shall be taken as:

$$\beta = \frac{230}{(1000 + d_v)} \tag{2-32}$$

Both methods are practical and conservative. For the evaluation of the specimens' shear strength, both methods have been employed.

2.12.1 Response-2000

Predicting the behaviour of components of reinforced concrete is not an easy task. With increasing forces, other than the existing cracks new cracks may additionally develop. It can be assumed the force in all parts of the concrete structure is evenly distributed. This force will eventually reach the reinforcements embedded within the concrete structure. Vecchio and Collins (1986)

Stresses within the reinforcement's embedded within the concrete structure are found to have varying values at different locations. Moreover, the locations where a crack is detected on the concrete structure causes the reinforcements to experience the maximum stress. Formed cracks are found to transmit shear and compression at contact location. At times in presence of tensional stress, cracks are not found to withstand tension. However tensile stresses will exist in the concrete lying between the cracks. Vecchio and Collins (1986)

Modified compression field theory (MCF) is an analytical model capable of predicting the load-deformation response of reinforced concrete elements subjected to normal stresses. In the model, cracked concrete is defined as a new material with its own properties.

One of the important assumptions of compression filed theory is related to ignoring the presence of tension within the cracked spots. The model presented the presence of tensile stress found between cracks in concrete structures. This model employs experimentally verified average stress-average strain relationship for the cracked concrete.

In chapter 5 of this thesis, for the purpose of comparison between the laboratory results and the expected results, Response-2000 was used. The latter software is designed on the very presumptions explained above.

It is a user-friendly sectional analysis program that will calculate the strength and ductility of a reinforced concrete cross-section subjected to moment, shear and axial load. It is designed based on the latest studies on the MCF theory. The program was developed at the University of Toronto by Bentz (2000).

Response-2000 is able to calculate the strength of traditional beams and columns as well as or better than existing methods and, more importantly, is able to make predictions of the reinforcement stress for sections that cannot easily be modelled today.

With its fast input and output and user friendly interface and ample graphical output, it allows for easy checking of results. Moreover, Response-2000 allows the engineer to examine beam and column behaviour with a new level of confidence and accuracy.

Chapter 3 : Laboratory Test Description

3.1 Overview

The goal of this experimental study is to determine the correlation between the spatial location and surface area of de-bonding with the strength of the beams. In other words, the purpose of the current study is to investigate the behaviour and reduction of flexural capacity for the concrete beams with the de-bonding of reinforcements. A series of concrete beams with laboratory-induced loss of bond were examined. This is achieved by testing beam specimens with different combinations of de-bonding patterns with respect to location and area.

The results of the study can potentially be applied to existing bridges in Ontario, as most are affected by concrete cover spalling and reinforcement's exposure.

3.2 Specimen Geometry

A plan elevation of the test specimens are shown in Figure 3-1. The tests consist of 2100×150×100 mm beams. The span between simple supports is 1900 mm with a single point load applied at the mid-span. The test program contains mid-sized concrete beam prototypes, with partially de-bonded reinforcement. The de-bonding is simulated in various beam locations, with various de-bonding patterns.

The experimental specimens consisted of partially de-bonded beams pinned on one end and attached to a roller support on the other end. At the midpoint between these two extremities, each beam was subjected to a point load. The findings were analyzed through simple models based on force-equilibrium and bond-stress relation with the objective of gaining an understanding in regarding to mechanism of load transfer in beams.

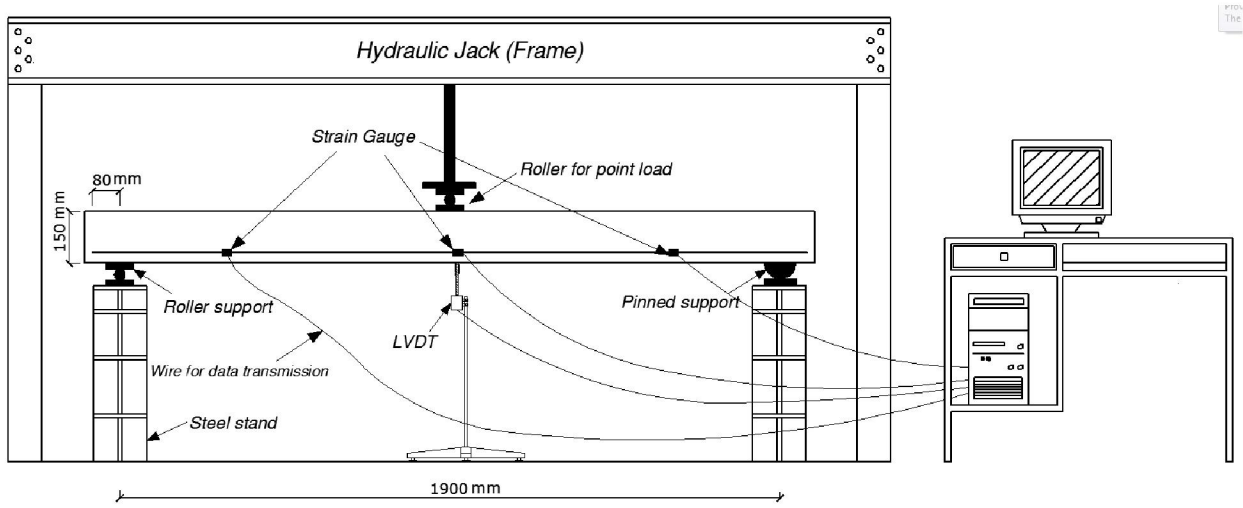

Figure 3-1: Overall test setup for control beam

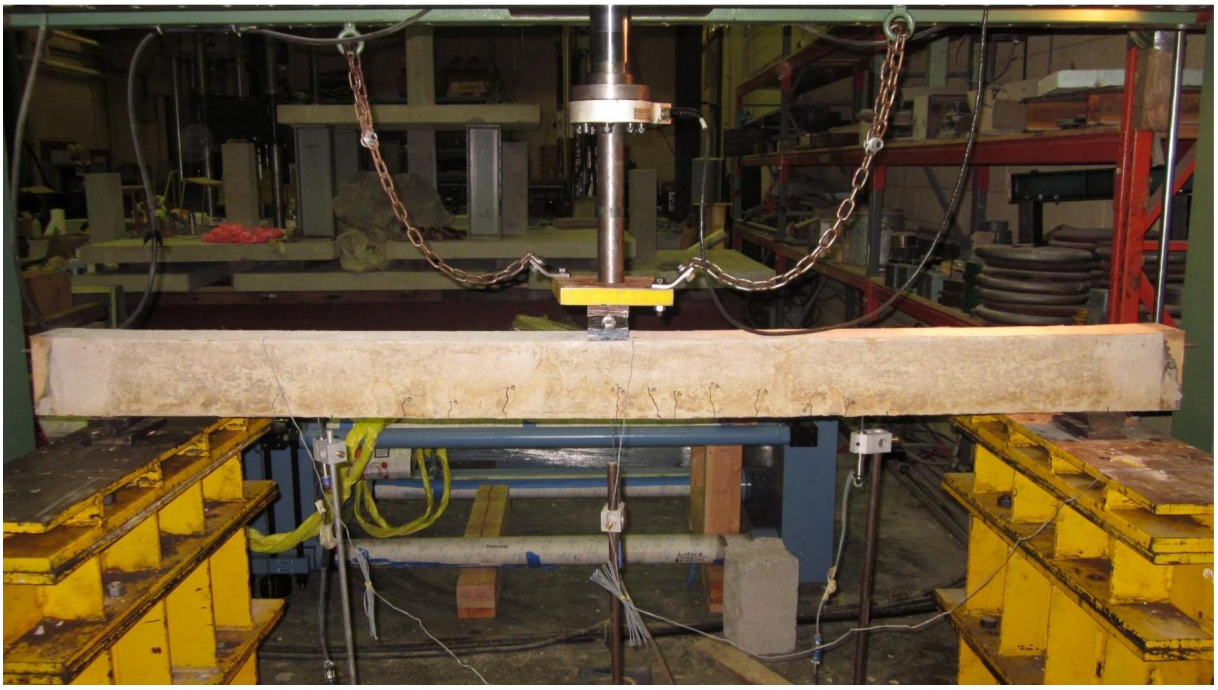

Figure 3-2: Plan elevation for control beam

3.3 Material Properties

Two different bar sizes (10M and 15M) with lengths of 2060 mm are used in this experiment. In an attempt to streamline the investigation, some variables are kept constant, such as: the steel

strength (470 MPa), concrete strength (34 MPa), and concrete specimen length of 2100 mm. Three different types of specimens have been designed. 1) Type 1: Four beams with de-bonded reinforcement in the flexural zones, 2) Type 2: seven specimens de-bonded in the anchorage and flexural zones, and 3) Type 3: two fully bonded specimen with different steel ratio.

The 10M and 15M size bars used in the tests were obtained locally, and they conformed to the Canadian standard association (CAN/CSA S6) standard to determine the mechanical properties of the reinforcing steel.

The concrete compressive strength $f_c^{'}$ was obtained from tests on 30 different standard cylinders, which were tested by compression testing concrete cylinders

3.3.1 Concrete Mix Parameters

The coarse aggregate had a maximum nominal size of 9 mm with 16cm slump; it was mixed with plasticizer and fine aggregate sand from HOGG Company and transferred to the lab by a concrete mixer. The temperature on the casting date was 22˚C inside the lab.

Figure 3-3: Mixer truck for concrete

3.4 Deboning Region Creation

Two layers of 2” Styrofoam were cut accurately in the machine shop and were attached from top to bottom to the longitudinal bars with electrical tape (Figure 3-6). Because of the presence of

stirrups, in some cases the Styrofoam's were cut in smaller parts in order to make them fit inside of the cage. It's noteworthy, that the Styrofoam was completely isolated by using electrical tape surrounding all areas to prevent any concrete penetration.

3.5 Specimens Preparation

Concrete is then removed by using Styrofoam around the areas where exposure is imitated. The Styrofoam was attached to each other by electrical tape, to ensure that there was no concrete penetration between Styrofoam and steel, during the casting process.

The concrete specimens were cast in a specially designed wooden mold. The formworks were constructed from 15 mm thick MDF (Medium Density Fibreboard). The formworks had two blocks at each end with two holes in each in order to allow steel bars to pass as shown in Figure 3-4. The top reinforcing bar was extended 30 mm outside at each end of the beam formwork.

Figure 3-4: Form work preparation

A wooden piece was installed on top of the mold; to prevent concrete losing the desired shape by using a steel wire to uplift cage, and to create a resistance against the clamp that held the frame in place. This piece was later removed after the concrete was fully formed into the beam.

Figure 3-5: Wooden support for hanging the cage in concrete casting

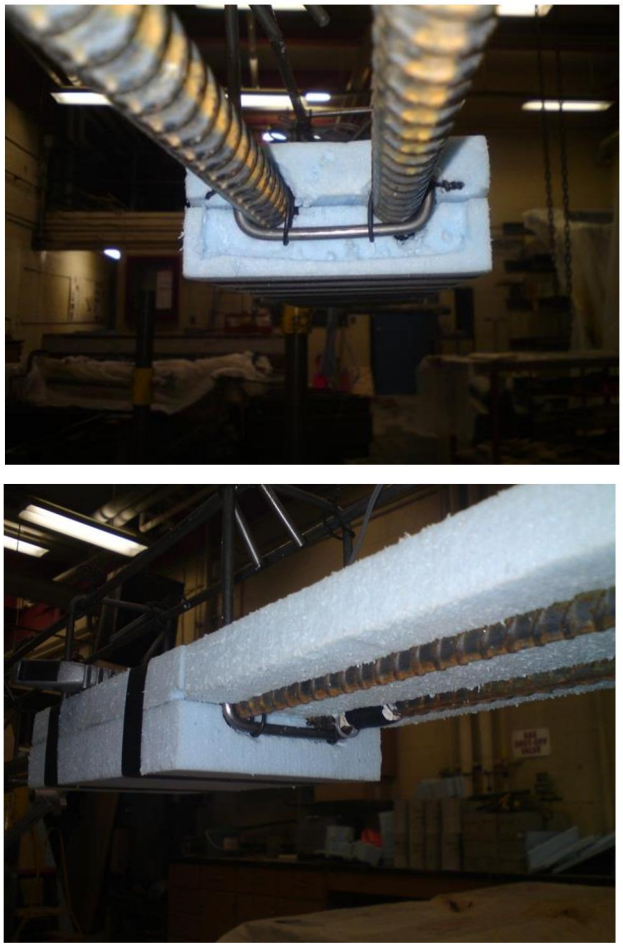

Figure 3-6: Installing the Styrofoam's before placing in formworks

Thirty concrete cylindrical specimens with 300mm×150mm diameter, were cast at the same time as the main specimens were cast.

Figure 3-7: Casting cylinders for concrete compression test

Figure 3-8: Slump test

Reinforcement of test specimens is smoothed in order to apply strain gauges, the application process is initiated by grindstone. After attaching the strain gauges with super glue (cyanoacrylate), and polishing them with a prime-coat, they were covered with ST tape and duct tape in an attempt to protect them from potential damage. It is important to note that while preparing the reinforcement for this installation, no lugs were removed in the process as smoothing took place on the side of the reinforcement (Figure 3-9).

Figure 3-9: Strain gauges installation

3.5.1 Placing of Concrete

Each specimen was cast in three layers, and each layer was vibrated well to ensure that concrete spreads evenly without any gaps of air. Concrete was mixed and filled to the surface of the formwork. Then, concrete was placed by hand and compacted with an internal vibrator. Finally, the surface was smoothed by using wooden and steel trowel, as seen in Figure 3-10:

Figure 3-10: Concrete of casting, vibration and smoothing the surface

About three hours after concrete was placed, the test specimens and control cylinders were covered with polyethylene sheets to avoid humidity escape. Moist curing continued for seven days. From then until the time of testing the specimens were placed in to the laboratory which had a fairly constant temperature of 20º C. All specimen and cylinders were cured in the same environment (humidity room) for 7 days and side formwork was stripped off after.

3.6 Experimental Tests

The experimental tests were designed to study the behaviour of beams with exposed reinforcement. Two different reinforcement ratios were used; 1.3% and 2.6%. Regular steel of 10M mm and 15M was used to reinforce the beams.in addition; a 135º hook closed stirrups was fashioned at each 190 mm to resist against of any shear force.

In the Figure 3-11 and 3-12, the geometrical and loading details for a simply supported reinforced concrete beam having a region of recess (i.e. fully exposed main reinforcement) within its tensile side where concrete cover and steel-concrete bond has been removed in a

symmetrical fashion about the mid-span by a total length L=700 mm, and a vertical gap exist between concrete and steel is shown. In addition to main tensile reinforcement, the beam also includes top steel and is further assumed to have been properly reinforced against shear failure so that the final mode of failure under the action of the symmetrical one-point loading is one of flexure (Thirteen beams with all shapes and dimensions are addressed in chapter 4).

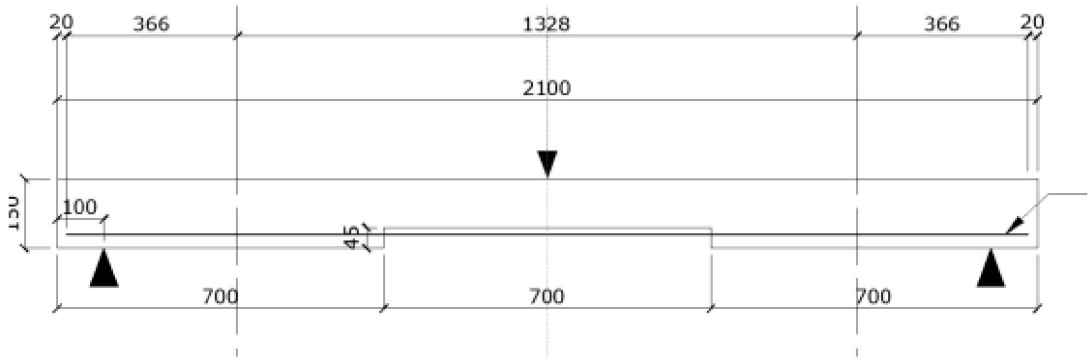

Figure 3-11: simply supported beam with symmetrical exposed area

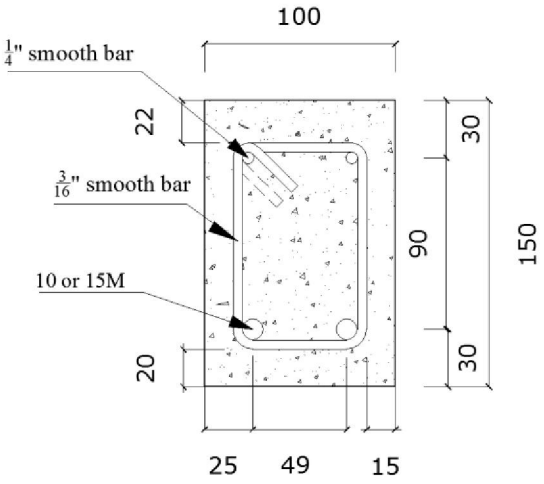

Figure 3-12: Cross section of beams

3.7 Test Specimens

Table 3-1 Specimen's specification

Specimen Type	Specimen ID	Specimen Layout	Development %	Span Spalled %	Anticipated Failuire
Type 3	1	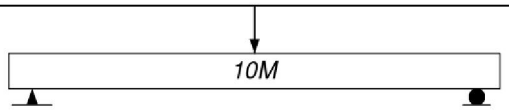	100	0	Flexural
Type 1	2	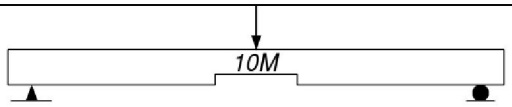	100	16.9	Flexural
Type 1	3	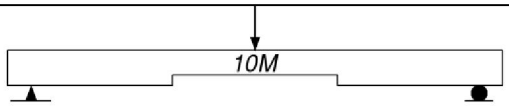	100	33.9	Flexural
Type 2	4	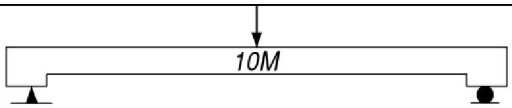	45	85.4	Bond
Type 1	5	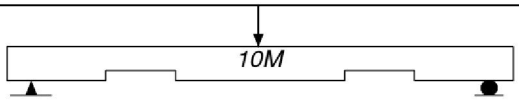	100	28.1	Flexural
Type 2	6	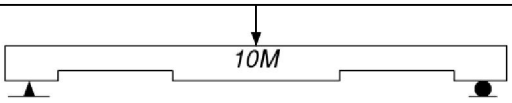	60	46.6	Bond
Type 2	7	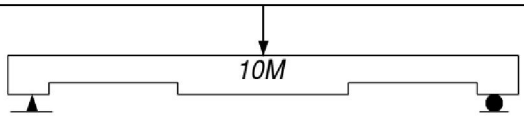	45	51.4	Bond
Type 2	8	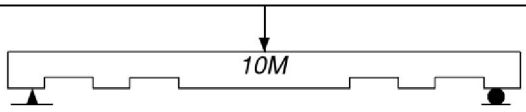	39	38.8	Bond
Type 2	9	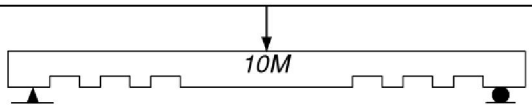	64	34.9	Bond
Type 2	10	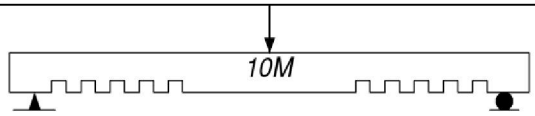	65	28.1	Bond

Specimen Type	Specimen ID	Specimen Layout	Development %	Span Spalled %	Anticipated Failuire
Type 2	11	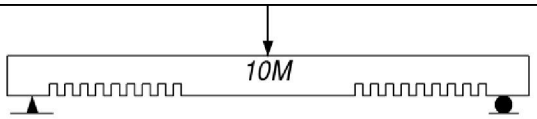	71	28.1	Bond
Type 3	12	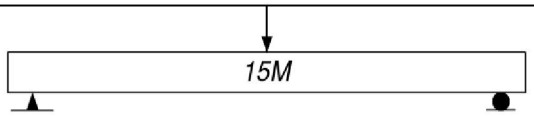	100	0	Flexural
Type 1	13	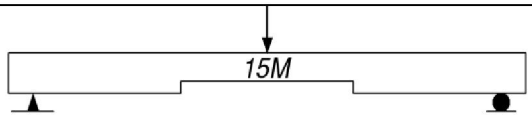	100	33.9	Flexural

3.7.1 Experimental Set-up

This specimens were tested in the civil engineering laboratory in the University of Waterloo. As depicted in Figure 3-14, the supports consisted of a pin and roller. Load force was exerted at the middle of the beam. The strain, load, deflection and crack patterns were recorded during these tests.

The hydraulic jack applied force vertical load in the middle of the beam. A displacement control was used in to be able to record post peak load behaviour. The cracks were traced over the concrete as soon as they reached the beam surface. The cracks were tagged every 5 kN to spot at what load force they were formed.

Figure 3-13: Specimens after curing period

The data acquired during the tests were documented in Microsoft excel and were used to provide information about all the relevant characteristics of the test. It included, the load-deformation and load-strain curves.

With the help of the installed strain gauges, the amount of strain existent in the reinforcement at each load level was documented. Number and location of strain gauges are depicted in chapter 4. The computer program in association with the hydraulic jack can document various variables, such as: displacement, time, load, and stress in reinforcement up to seven strain gauge channels to obtain a response every three seconds. In addition, for higher accuracy in determining deflection of the beam, a series of external LVDT's were installed.

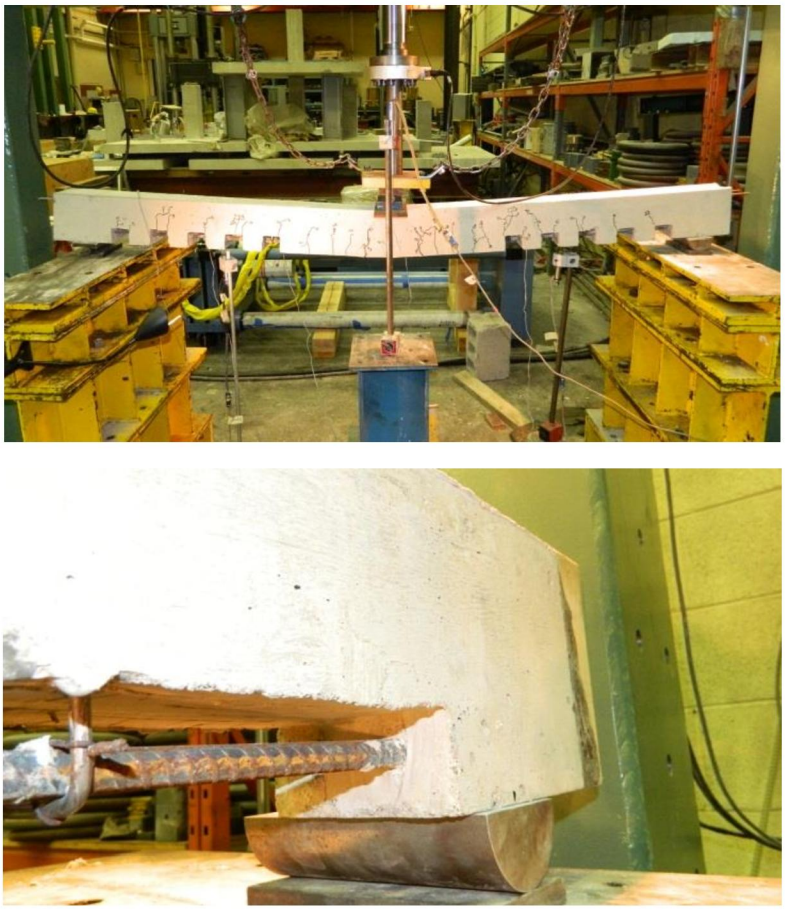

Figure 3-14: Testing specimens with point load

Figure 3-15: Testing specimens with hydraulic frame under point load

3.8 Concrete Compression Tests

Detail about concrete cylinder (compression tests) is presented in Table 3-1.

Table 3-1: Concrete compression test

Cylinder Test Result		
7 Day		
	Load kN	Load MPa
	117.568	22.608
	179.317	22.829
	177.729	22.629
	169.851	21.629
	165.465	21.071
	163.721	20.843
	188.493	24.001
	177.182	22.56
	169.055	21.526
Average	167.5979	22.18844

Cylinder Test Result		
43 Day		
	Load kN	Load MPa
	271.359	34.55
	249.327	31.744
	259.91	33.095
	272.378	34.681
Average	263.2435	33.5175

Cylinder Test Result		
46 Day		
	Load kN	Load MPa
	297.841	37.542
	275.839	35.122
	244.394	31.116
	259.883	33.088
Average	269.4893	34.217

Cylinder Test Result		
47 Day		
	Load kN	Load MPa
	246.894	31.433
	254.629	32.419
	244.554	31.137
	269.749	34.343
Average	253.9565	32.333

Cylinder Test Result		
48 Day		
	Load kN	Load MPa
	278.267	35.432
	276.074	35.15
	270.977	34.502
	290.709	37.011
Average	279.0068	35.52375

Cylinder Test Result		
49 Day		
	Load kN	Load MPa
	266.173	33.888
	273.672	34.846
	257.503	32.785
	272.449	34.688
Average	267.4493	34.05175

As seen in table 3-1 concrete cylinder compression tests were reported in 6 different days, the average strength after 7 days was 22.18 MPa. The calculated average for the rest (43, 46, 47, 48, 49 days) was around 34 MPa, which is later implemented in our numerical model.

Figure 3-16: Concrete compression test

3.9 Steel Tensile Test

Tensile tests measured the force required to break steel. The allowed to produce a stress-strain diagram, which is used to determine the maximum tensile strength and yielding point of reinforcement bars.

Before the tensile test, the specimens were cut to 45cm length. Then with computer controlled MTS machine, strain-strees tests were completed for three different 10M bars, and the average failure strength for those samples measured around 470MPa.

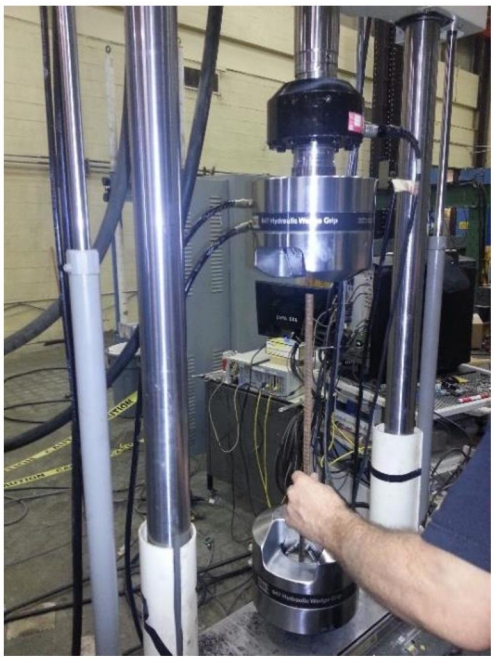

Figure 3-17: Specimen is clamped in the hydraulic grips

Table 3-2: Steel Tensile Test Results

	Steel Tensile Test	
	Axial Force kN	Strength MPa
	48.713612	487.13612
	46.50145	465.0145
	46.22546	462.2546
Average	47.14684067	471.4684067

Chapter 4 : Laboratory Test result

4.1 Overview

In this chapter the results of experimental investigation are summarized. The parameters in this series of tests were: the amount of exposure areas, location and shape of exposed area of reinforcement and longitudinal reinforcement ratio. The results are presented in terms of load versus deflection response, load-strain, crack width and crack spacing.

The modes of beam failure in this study are affected by the length of exposed reinforcement, concrete strength, concrete reinforcement strength, bar diameter, concrete cover, embedment length and bar spacing.

4.2 Load-Displacement Behaviour

The experimental result from the load-deflection response for both the bonded and the de-bonded specimens are summarised in Figure 4-1:

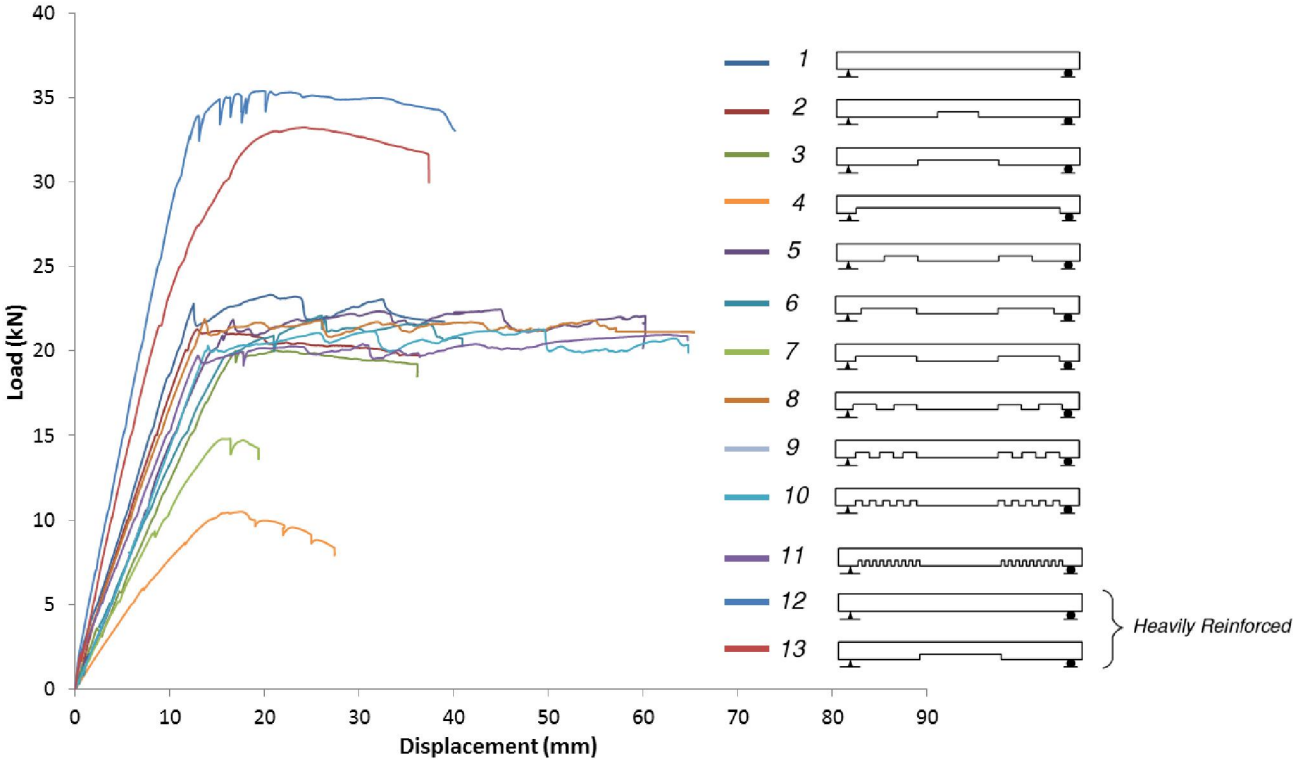

Figure 4-1: Load – Deflection graph for all specimens

It is worth to note that the concrete code suggests 335mm anchorage length for specimens with 10M reinforcement, while the 15M specimen's anchorage length is 474mm

4.2.1 Specimen 1

The total length of specimen 1 was 2100 mm, and it was reinforced with two fully-bonded 10M bars at the bottom. The length of the reinforcements was 2060 mm.

The load displacement curve increased almost linearly until the peak load of 22.8 kN. At this load, a displacement of 12.5 mm was recorded at the mid-span.

As shown in Figure 4-6, at a peak load of 22.8 kN, the bottom reinforcement began to yield.

There were no cracks until 10 kN loading. After increasing the load past 15 kN, flexural cracks started to propagate up the mid-span. The formations of the cracks in this phase was uniform. Figure 4-4 shows that the majority of the cracks were located in the mid-span.

Past the first peak load, a 12.9 mm central deflection was recorded at the mid-span, with the corresponding load dropping to 21.5 kN. As the displacement was further increased, the load increased again to 23.31 kN (which is more than the recorded initial strength of the beam). The displacement of the beam at this stage increased to 20.9 mm.

This trend (load increasing) was repeated one more time and the specimen experienced a 23.05 kN load with a 32.4 mm displacement. Finally, by further increasing the deflection, concrete crushing failure was observed in the compression zone, and the strength decreased rapidly, resulting in beam failure.

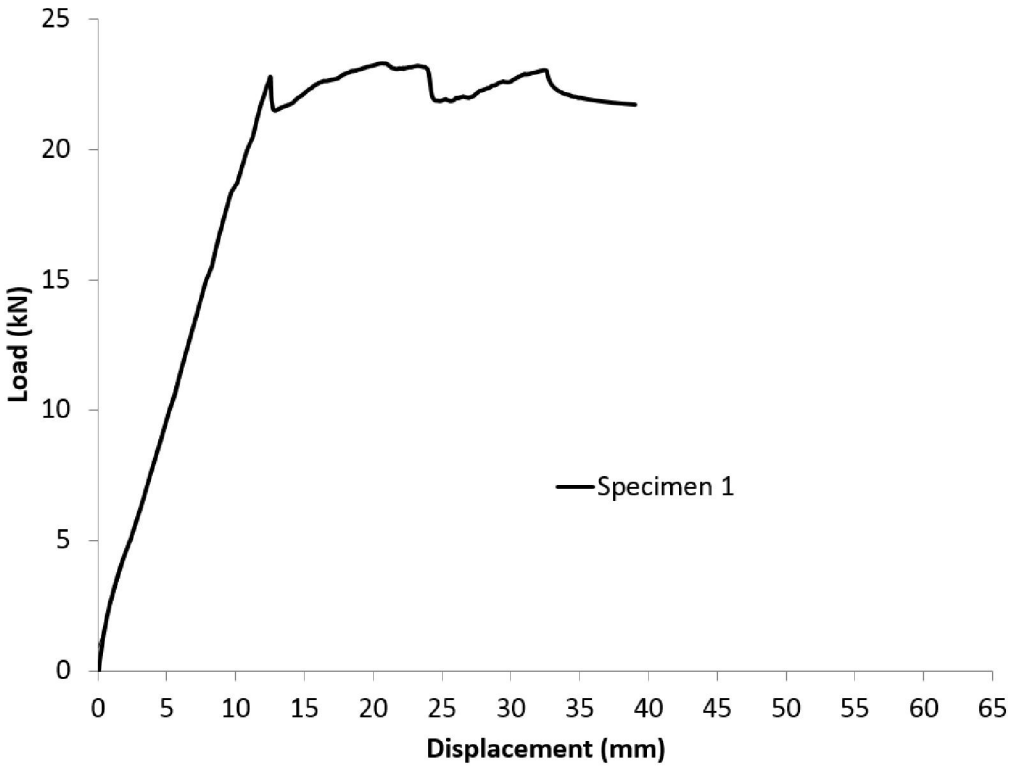

Figure 4-2: Load-displacement for specimen 1

Figure 4-3: Average crack width for specimen 1

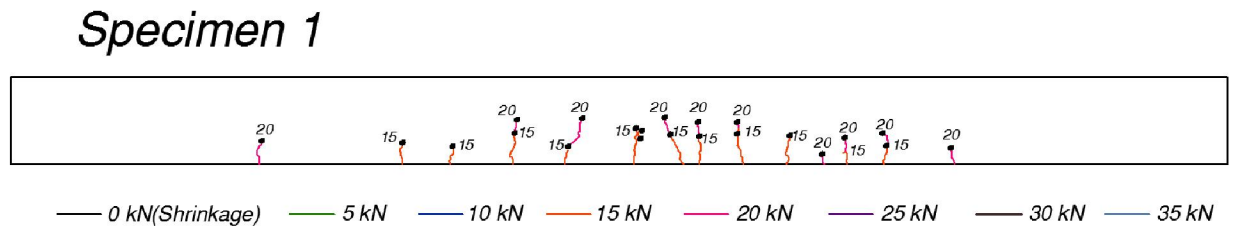

Figure 4-4: Details of crack pattern for specimen 1

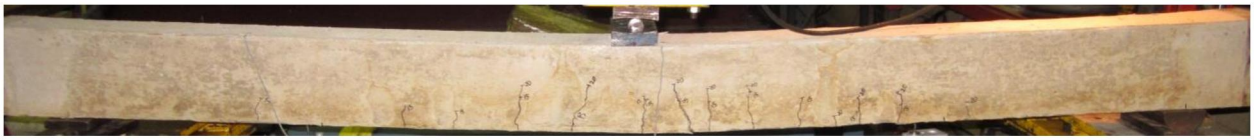

Figure 4-5: Crack pattern for specimen 1

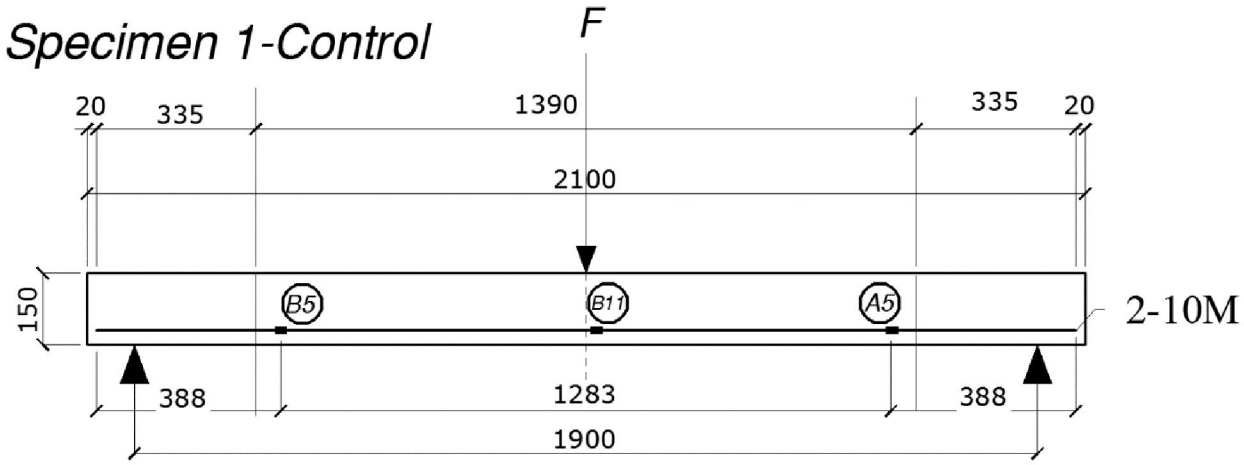

Figure 4-6: Specimen dimensions and strain gauges location

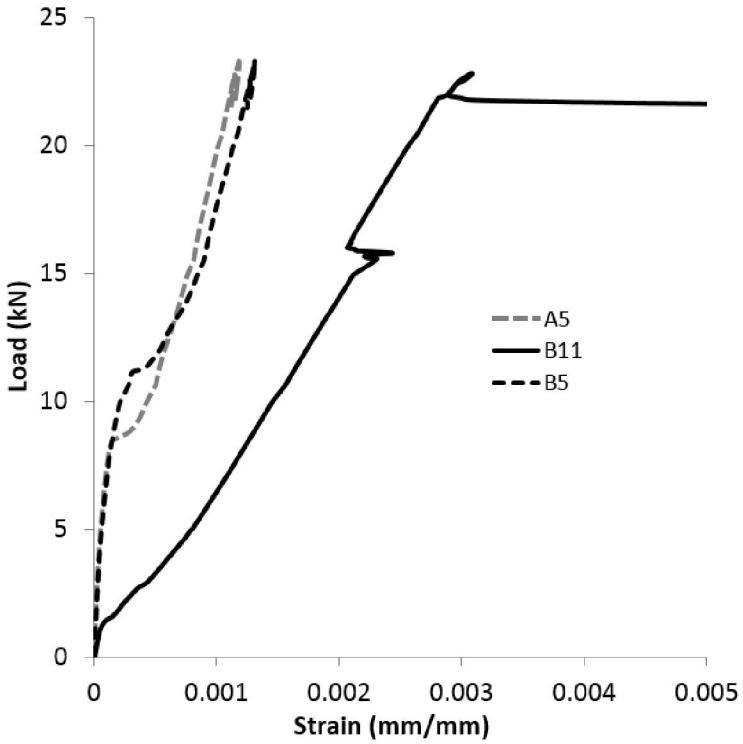

Figure 4-7: Load-strain diagram for specimen 1

4.2.2 Specimen 2

Specimen 2 was 2100 mm long and was also reinforced with two 10M bars at the bottom, each with a 350 mm exposed segment in the middle of the beam. As seen in Figure 4-8, the peak load of this beam was 21.3 kN at a displacement of 12.9 mm, which is slightly lower than the maximum load for the Specimen 1.

As it appears from Figure 4-13, at a peak load of 21.3kN, the bottom reinforcement started to yield.

At 10 kN load, first crack began to form in the middle of the exposed reinforcement section, as is illustrated in Figure 4-10. This crack continued spreading, becoming wider until it resulted in the failure of the section. There was also a crack (located at the left hand side of the exposed area) which was a result of the bond force. The remaining e cracks on the section are flexural cracks.

After experiencing the maximum load of 21.3kN in the first stage, the resistance of the beam began to decrease slowly. The beam failed due to flexural failure.

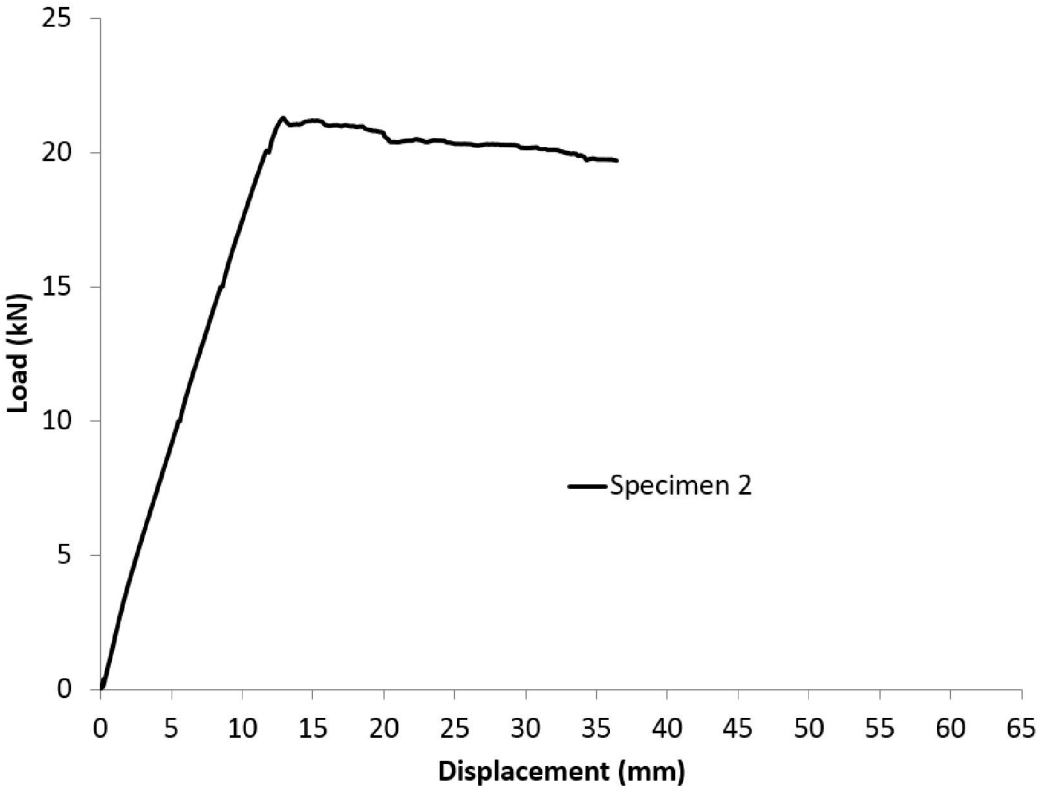

Figure 4-8: Load-displacement for specimen 2

Figure 4-9: Average crack wide for specimen 2

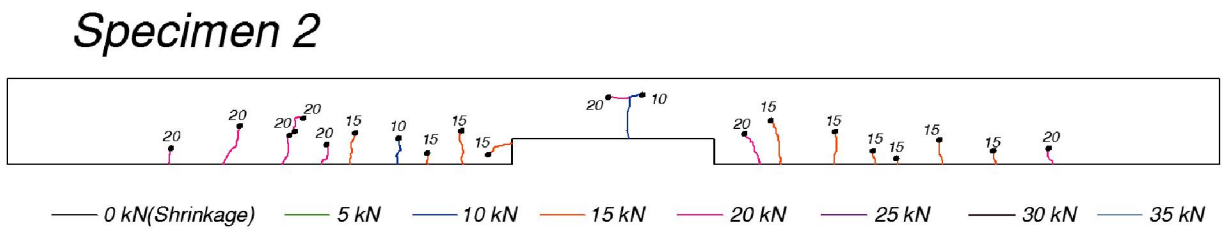

Figure 4-10: Details of crack pattern for specimen 2

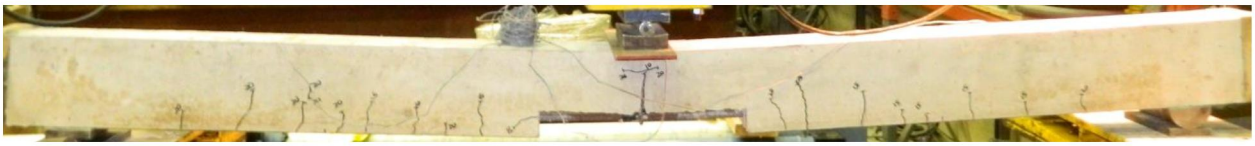

Figure 4-11: Crack pattern for specimen 2

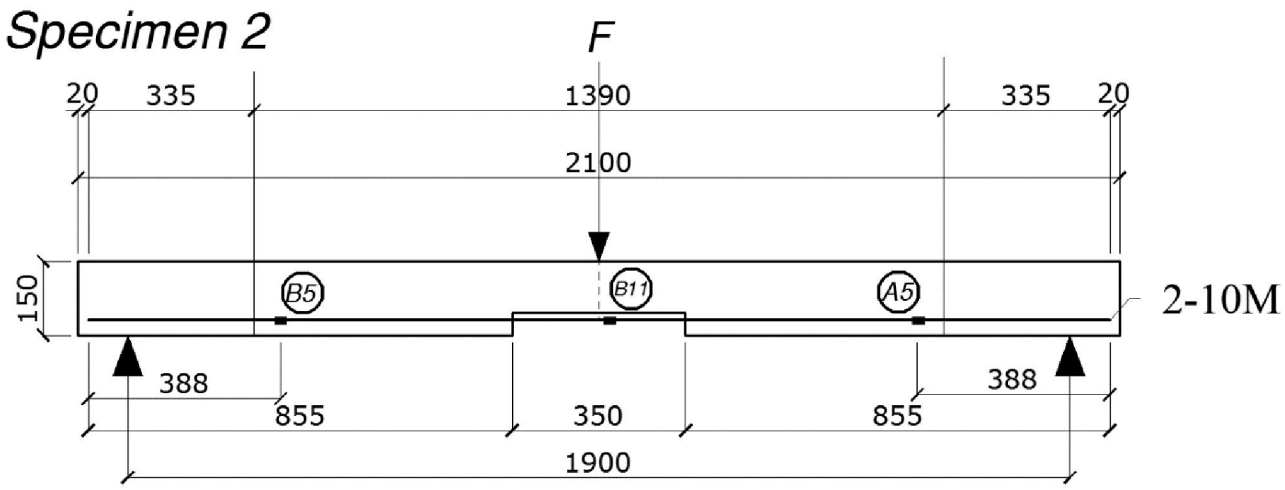

Figure 4-12: Specimen dimensions and strain gauges location

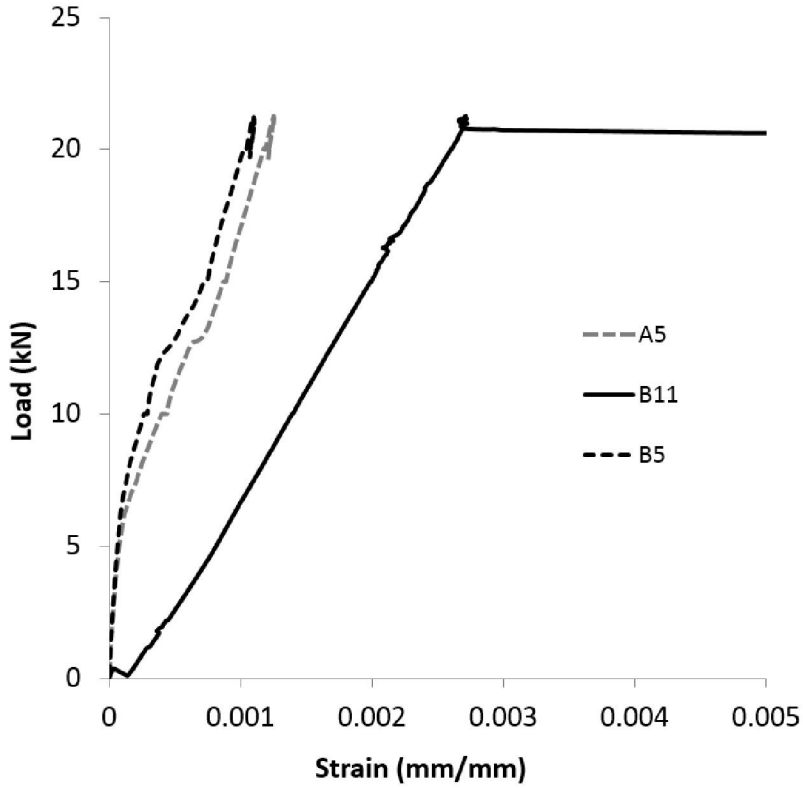

Figure 4-13: Load-strain diagram for specimen 2

4.2.3 Specimen 3

Specimen 3 measured 2100 mm in length and was reinforced with two 10M bars at the bottom, each with a 700 mm exposed span in the middle of the beam. As displayed in the Figure 4-14, the peak load of this beam was 20.0 kN at a displacement of 16.9 mm. At this point, a crack was found on the section during the curing process – formed due to shrinkage.

The specimen began to yield at a peak load of 20.0 kN, as shown in Figure 4-19. Longitudinal cracks on the right hand side of the exposed section were also formed at a maximum load. Subsequently, the strength began to slowly wane.

The first cracks formed at a load of 5 kN; at a lower value than less than the control specimen. In comparison to the control specimen, the maximum strength of this specimen is reduced by 3 kN (15%) which could be due to the bond effect or the reduced concrete section due to exposed reinforcement.

After experiencing the maximum load of 20.0 kN in the first stage, the resistance of the beam began to decrease slowly. The beam failed due to flexural failure.

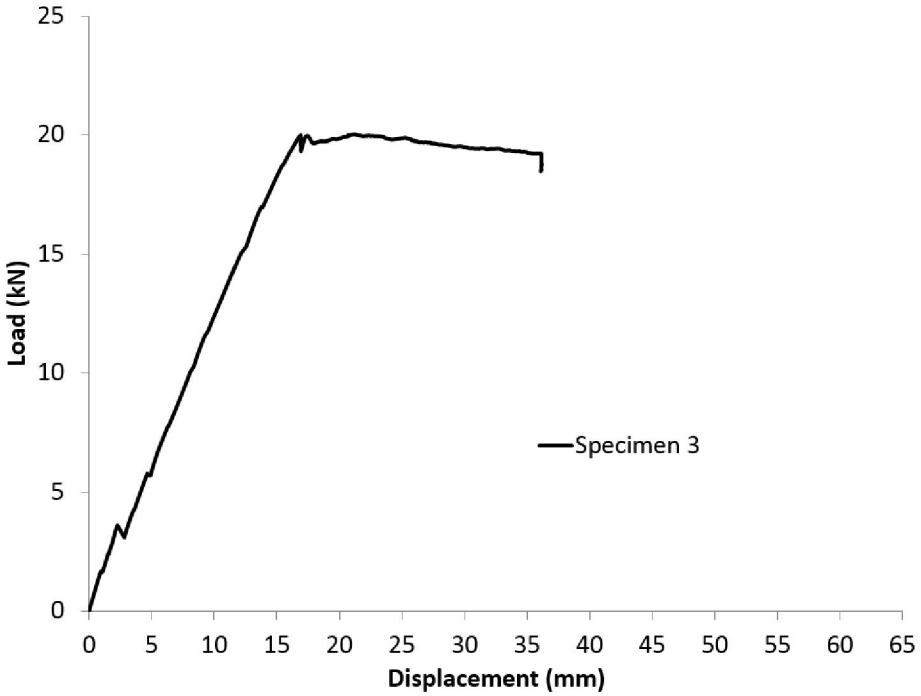

Figure 4-14: Load-displacement for specimen 3

Figure 4-15: Shrinkage crack for specimen 3

Figure 4-16: Average crack wide for specimen 3

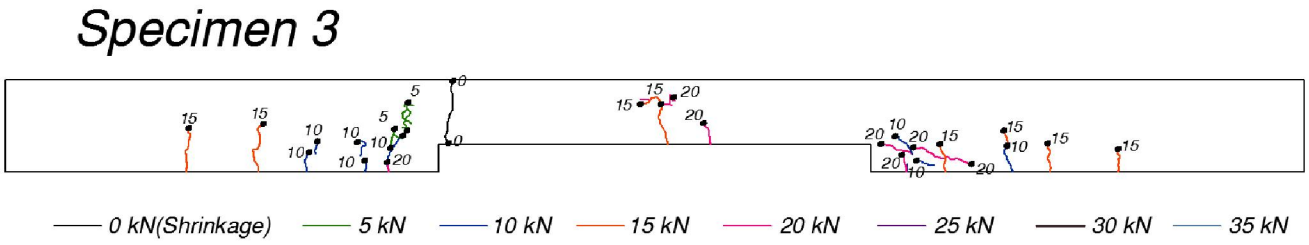

Figure 4-17: Details of crack pattern for specimen 3

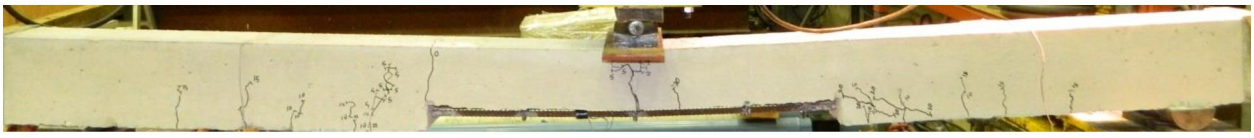

Figure 4-18: Crack pattern for specimen 3

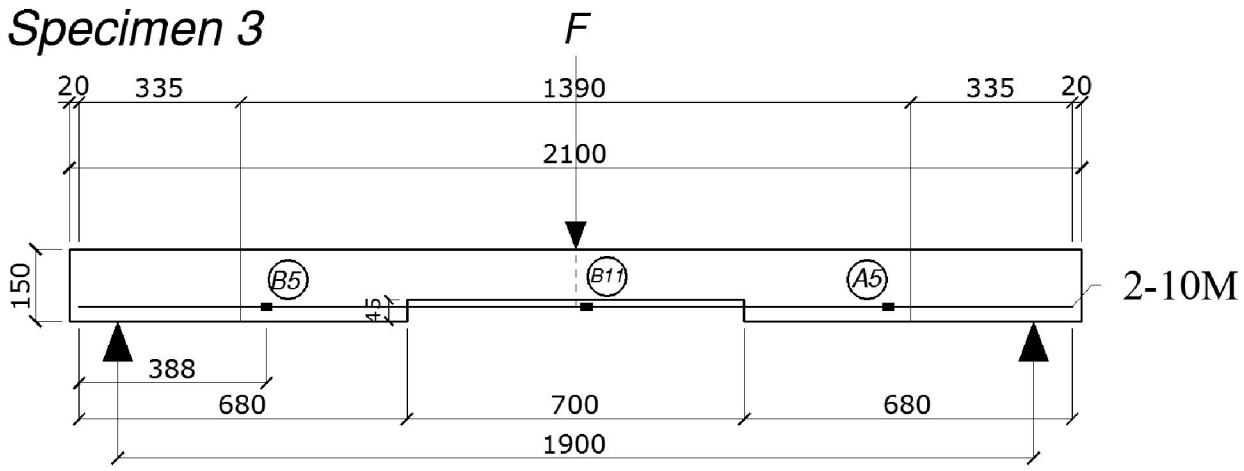

Figure 4-19: Specimen dimensions and strain gauges location

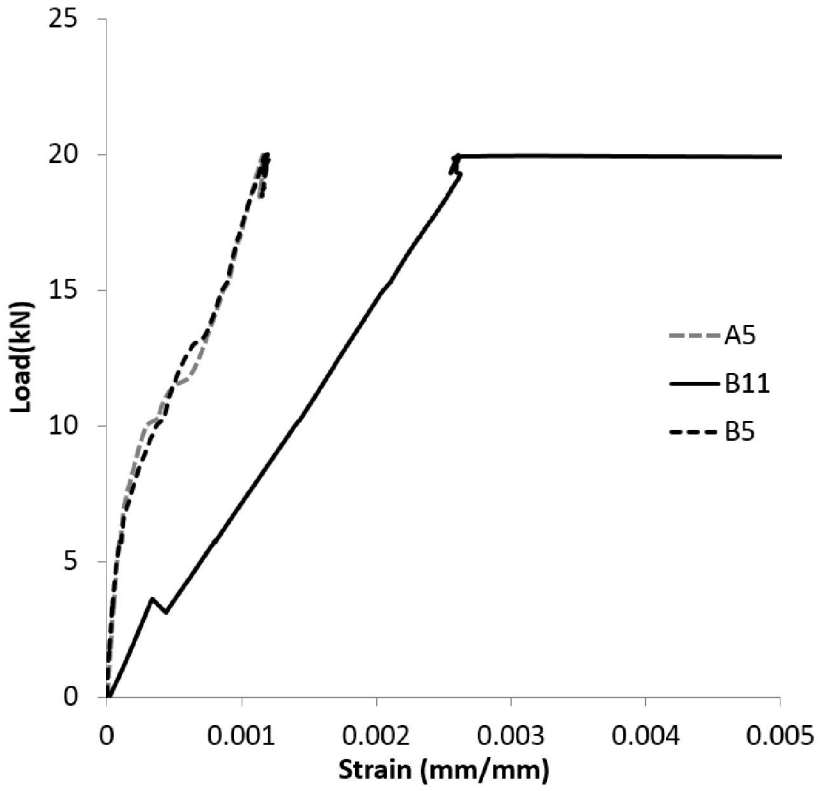

Figure 4-20: Load-strain diagram for specimen 3

4.2.4 Specimen 4

The total length of specimen 4 was 2100 mm and it was reinforced with two 10M bars at the bottom. 1760 mm of the total 1900 mm length of the reinforcement bars were exposed. As can

be seen from Figure 4-21, the maximum load of this specimen was 10.40 kN, at a displacement of 15.6 mm, the resistance of this beam was almost half that of the control beam.

As can be observed in Figure 4-26, at a peak load of 10.0 kN, the bottom reinforcement began to yield.

The first transverse crack was observed at a load of 5kN at the mid-span. It was formed as a result of shrinkage and was located beneath the point load prior to testing. It is important to note that this crack had no significant effect on beam failure.

Two major cracks formed on each side of the beam. The one on the right opened on the top surface of the beam. It is worth noting that the crack was circumferential and formed in the middle of the beam.

The post-peak behaviour of this beam was characterized by a drop in resistance after reaching the maximum load of 10.48 kN. Consequently, the beam failed due to pull-out failure.

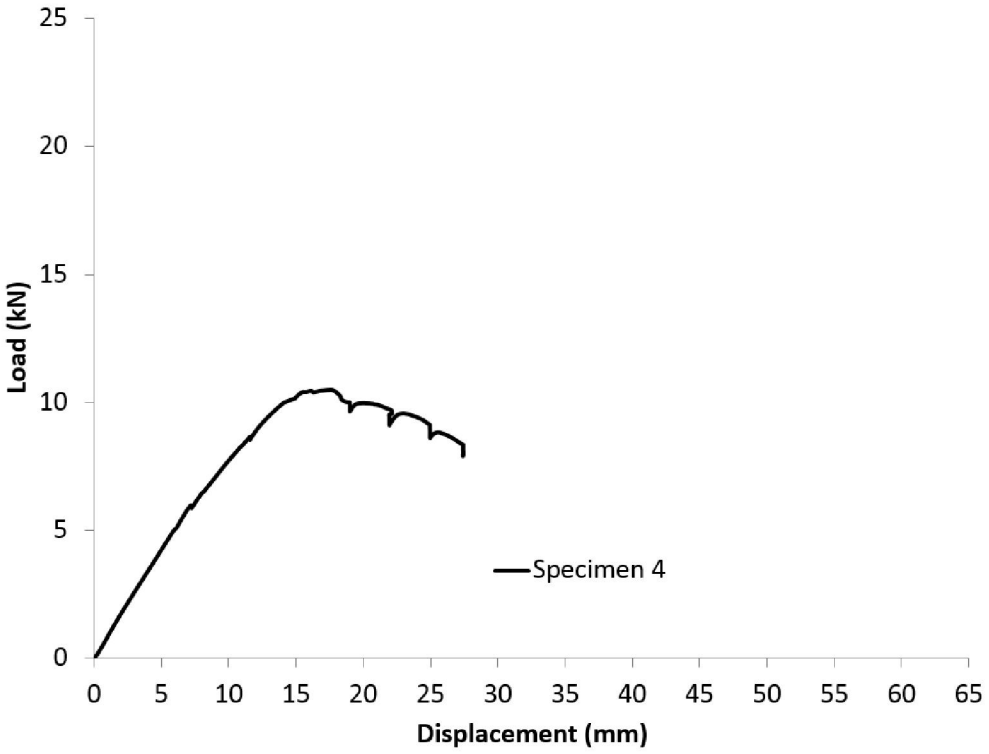

Figure 4-21: Load – Displacement for specimen 4

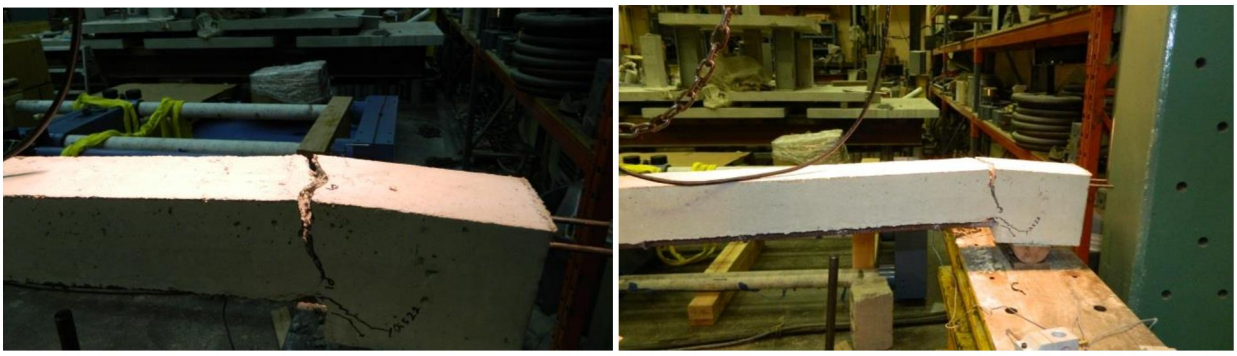

Figure 4-22: Crack pattern for specimen 4

Figure 4-23: Mid-span crack for specimen 4

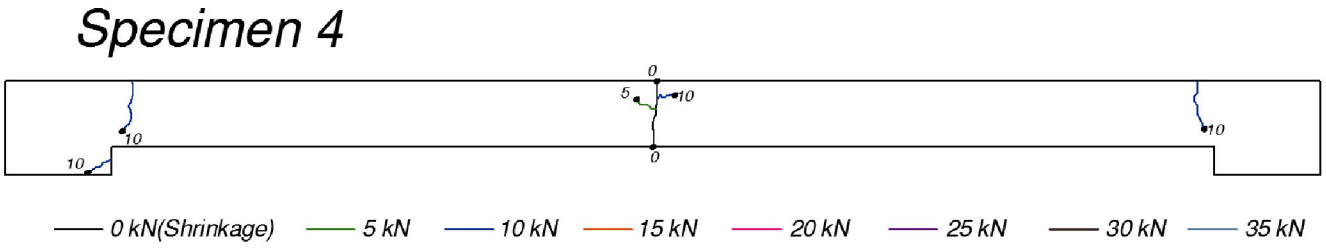

Figure 4-24: Details of crack pattern for specimen 4

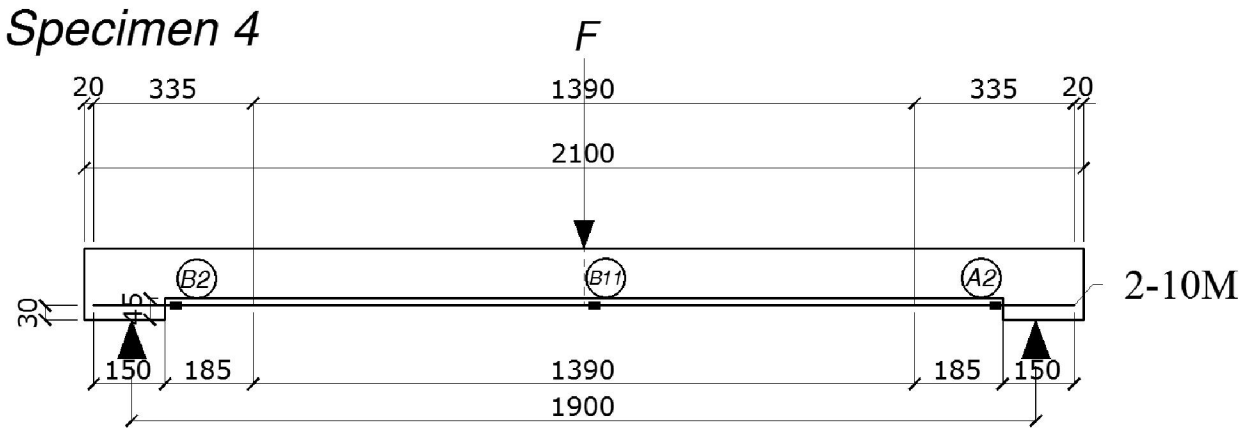

Figure 4-25: Specimen dimensions and strain gauges location

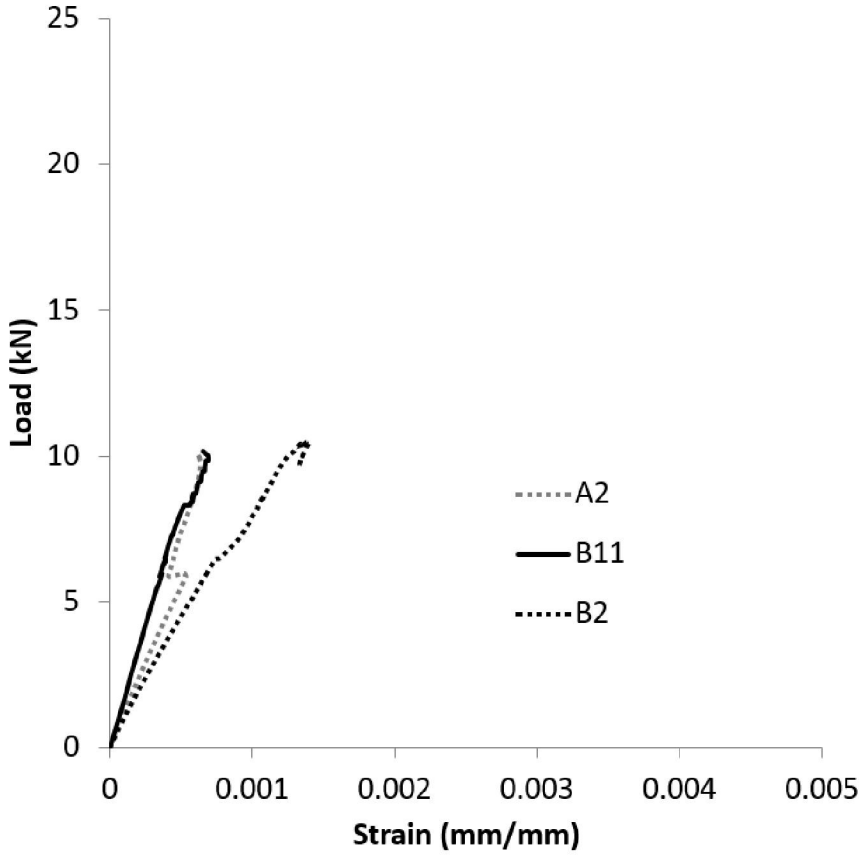

Figure 4-26: Load-strain diagram for specimen 4

4.2.5 Specimen 5

This specimen measured 2100 mm in length and was reinforced with two 10M bars at the bottom. The de-bonded zones in each of these bars were divided into two parts, both located in the anchorage zone. The total de-bonding area was 28% of the whole anchorage length.

In the first phase, the loading strength of the beam reached 21.84 kN with a 16.6mm deflection in the middle with almost 95% strength of the first beam (control beam). As displayed in Figure 4-34, the bottom reinforcement began to yield at a peak load of 21.84 kN.

As seen in the crack pattern diagram, both horizontal and vertical cracks were produced. Most of these cracks appeared from the 10 kN loading level.

As the crack patterns suggest, the main cause of failure was due to the flexural failure (Figure 4-31). The cracks shaped by pull-out did not have any notable effects on the strength of the beam. After a 60 mm deflection, the crack width on the bottom face of the beam reached about 3 mm.

Following the initial failure, the displacement of the beam corresponded with an increase in strength. With a 44.6 mm deflection, the beam strength reached 22.44 kN, almost 96% of the strength of the control beam in the same phase (23.31 kN). This displacement procedure was repeated two more times, and the strength of the beam increased accordingly, until the final failure at a displacement of 60 mm and a load of 22.06 kN.

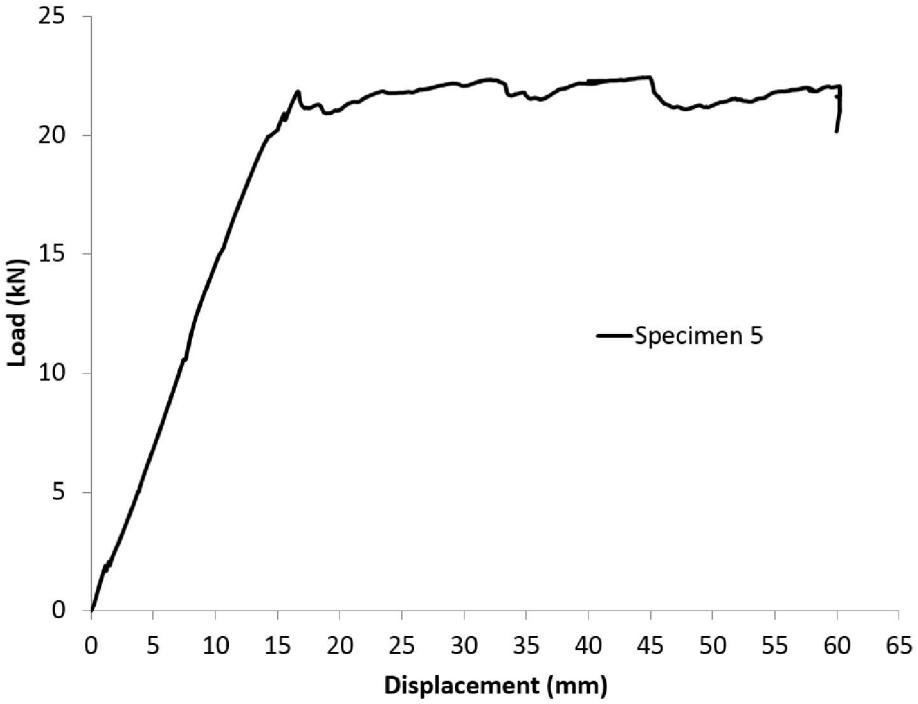

Figure 4-27: Load-displacement for specimen 5

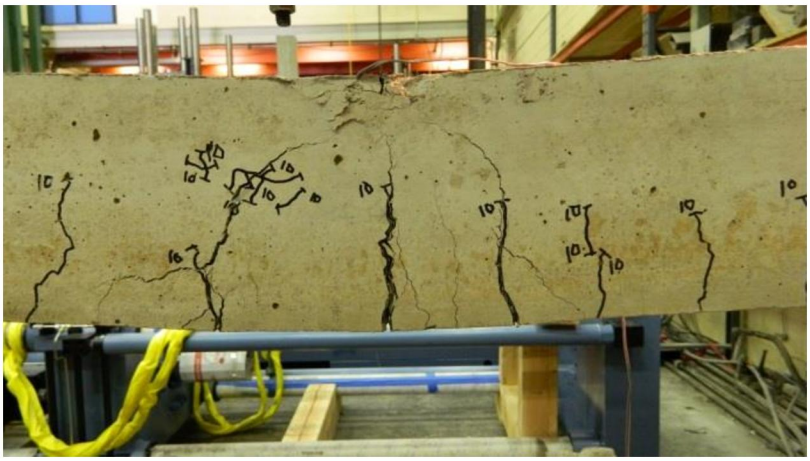

Figure 4-28: Flexural crack for specimen 5

Figure 4-29: Bottom crack pattern

Figure 4-30: Testing beam under single point load

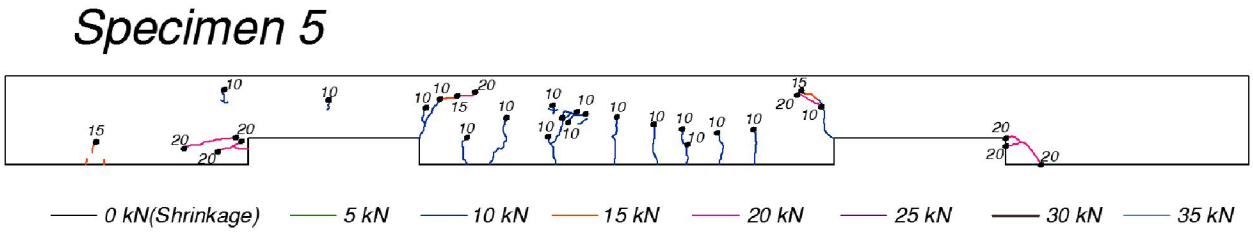

Figure 4-31: Details of crack pattern for specimen 5

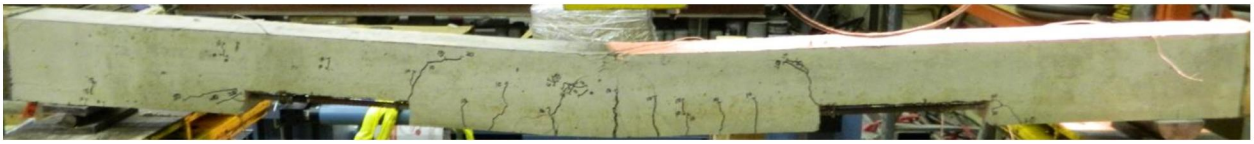

Figure 4-32: Crack pattern for specimen 5

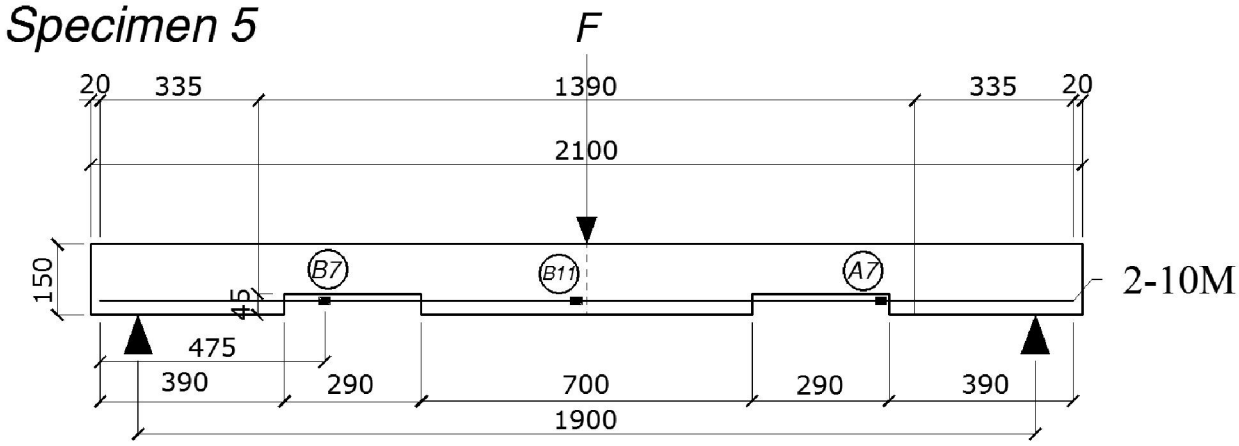

Figure 4-33: Specimen dimensions and strain gauges location

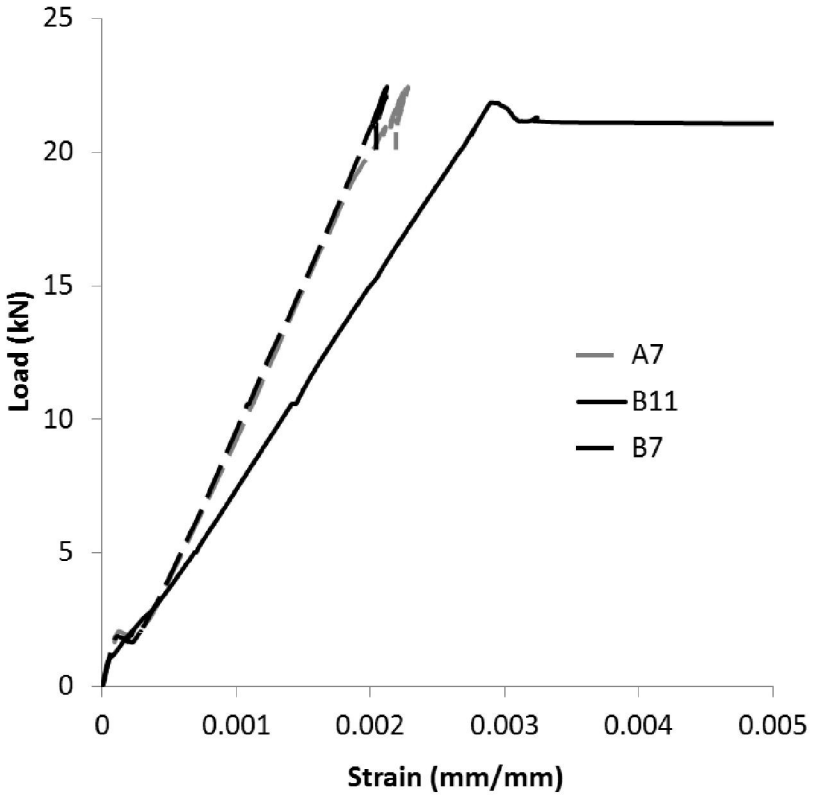

Figure 4-34: Load-strain diagram for specimen 5

4.2.6 Specimen 6

Specimen 6 was 2100 mm in long and was reinforced with two 10M bars at the bottom. The de-bonded zones in each of these bars were divided into two parts, both located in the anchorage zone. The total de-bonding area was 47% of the whole anchorage length.

The beam withstood a deflection of 15.7 mm prior to failing at a maximum load of 19.7 kN.

As shown in Figure 4-41, at a peak load of 19.7 kN, the bottom reinforcement began to yield.

In this specimen, more cracks formed in the middle versus the sides of the beam.

Cracks were mostly flexural in the centre of the beam. When the load reached 15 kN, a crack appeared on the top left face of the beam. At the 20 kN mark, an identical crack appeared on the top right face of the beam as shown in Figure 4-36. In addition, there were some minimal cracks damaging the support section of the beam (Figure 4-36).

The initial stages of failure began when a load of 20 kN was reached, but the beam still showed resistance up to a load of 22.1 kN with 26mm deflection. Following these stages, the strength starts to reduce gradually, ending up with a flexural failure. Maximum strength of this beam is almost 94% of the maximum strength of control beam (specimen 1).

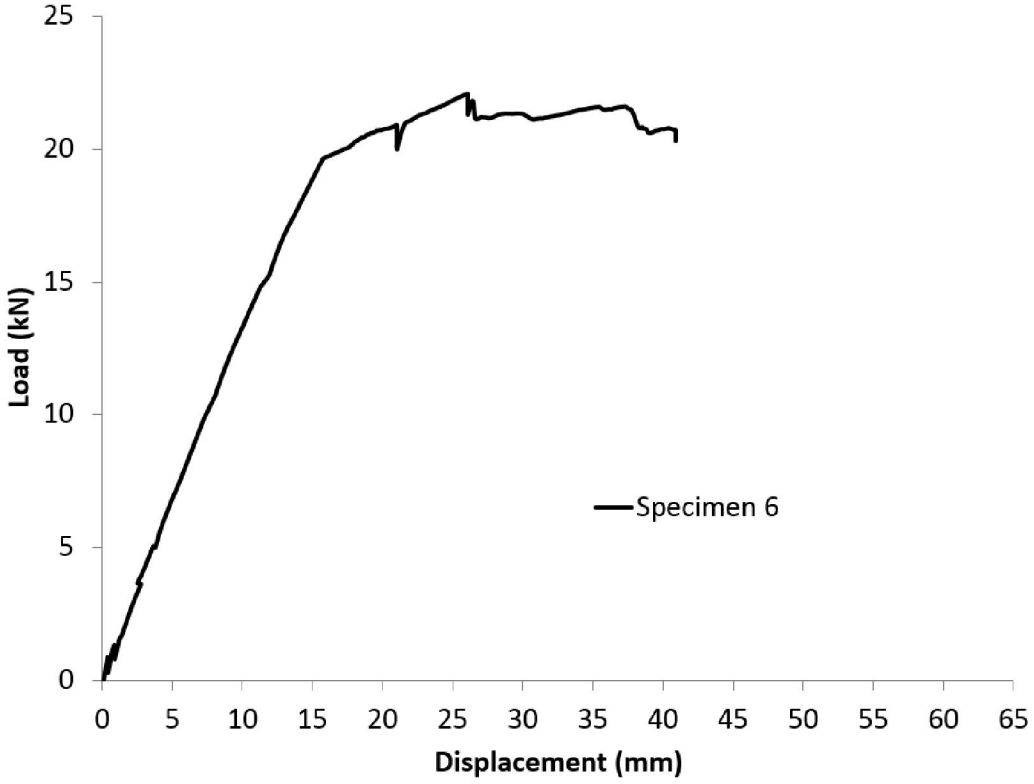

Figure 4-35: Load-displacement for specimen 6

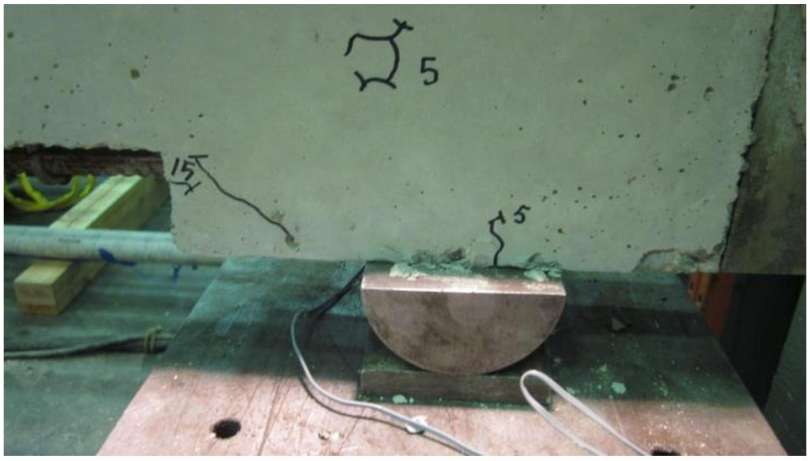

Figure 4-36: Beam support in specimen 6

Figure 4-37: Crack on top face for specimen 6

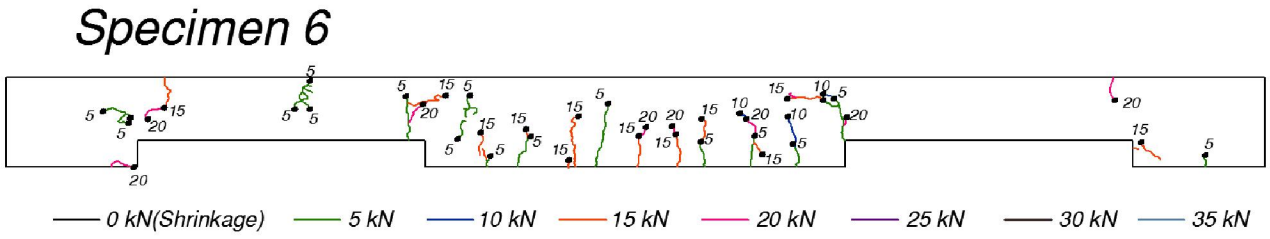

Figure 4-38: Details of crack pattern for specimen 6

Figure 4-39: Crack pattern for specimen 6

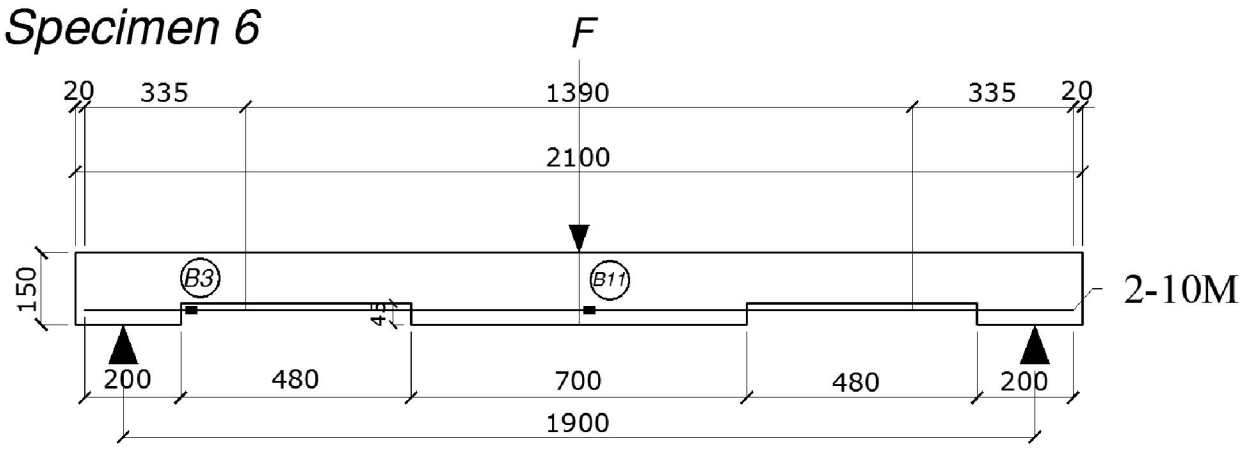

Figure 4-40: Specimen dimensions and strain gauges location

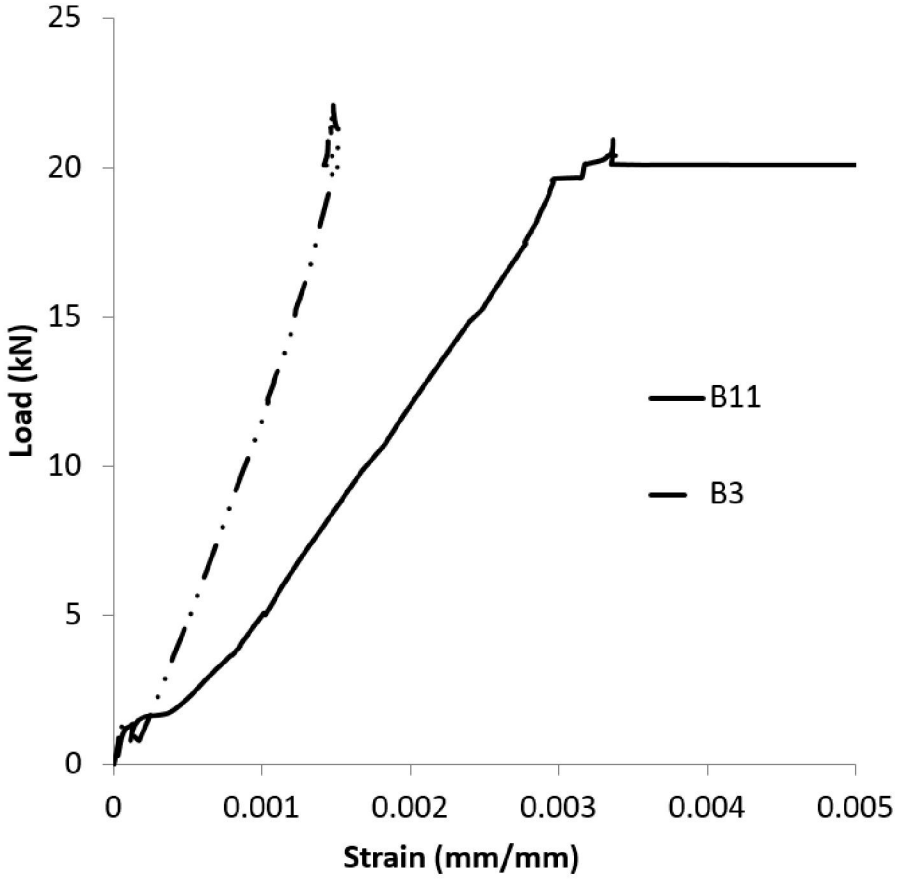

Figure 4-41: Load-strain diagram for specimen 6

4.2.7 Specimen 7

In this 2100 mm specimen, two 10M bars were used as reinforcement, both with two de-bonded areas, each divided again into two parts. As illustrated in Figure 4-47, there was a de-bonded

area on either side of the beam, each measuring 530 mm in length, 180 mm of which was in the anchorage zone. As seen in Figure 4-42, this beam had a peak load of 14.8 kN, with a deflection of 15.6 mm in the centre. Given the strength gauges installed in the middle were damaged as a result of the extreme load, we could not draw conclusive results from the behaviour of this specimen.

The majority of the cracks in this specimen were formed in the middle section of the beam. However, two cracks on the left hand sides of the beam were formed under a load of 10 kN. As the reinforcement was anchored only at the ends, the beam tilted up, and a wide crack formed on the top surface of the beam (Figure 4-43).

Another two cracks positioned in the exposed area nearest to the point load (Figure 4-45) were a result of shrinkage prior to testing (0 kN). These cracks had no significant effect on the resistance of the beam. At the last stage of testing, the maximum resistance of this beam was 64% of the resistance recorded in the control beam.

The only difference between sample 7 and sample 6 is that sample 7 has exposure areas that are 50mm larger and closer to the supports.

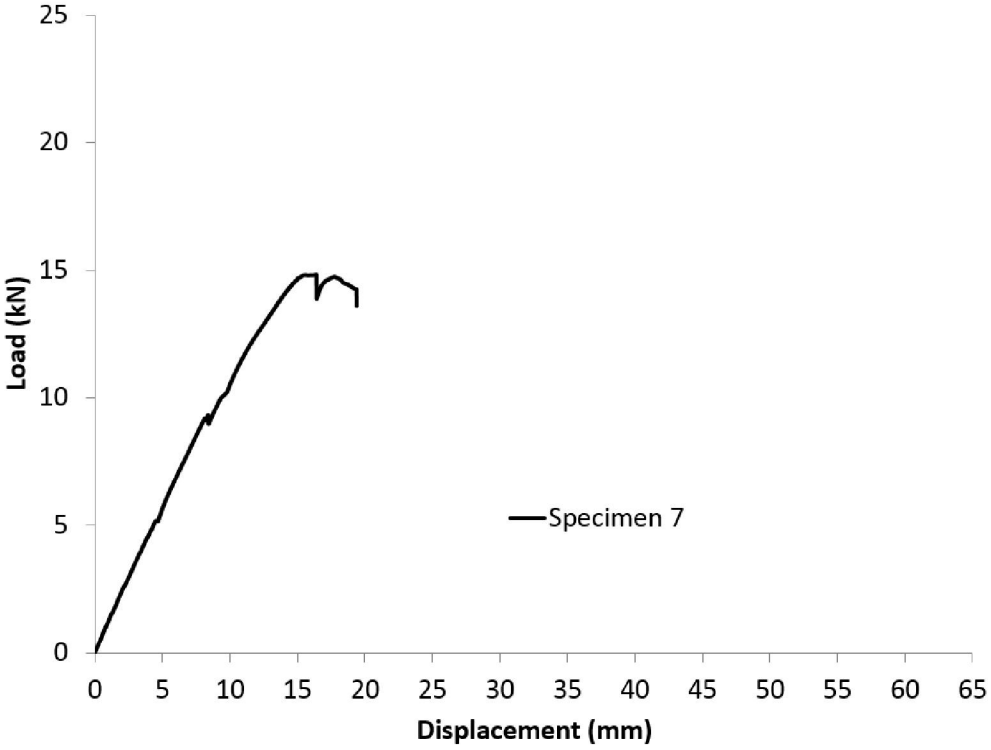

Figure 4-42: Load-displacement for specimen 7

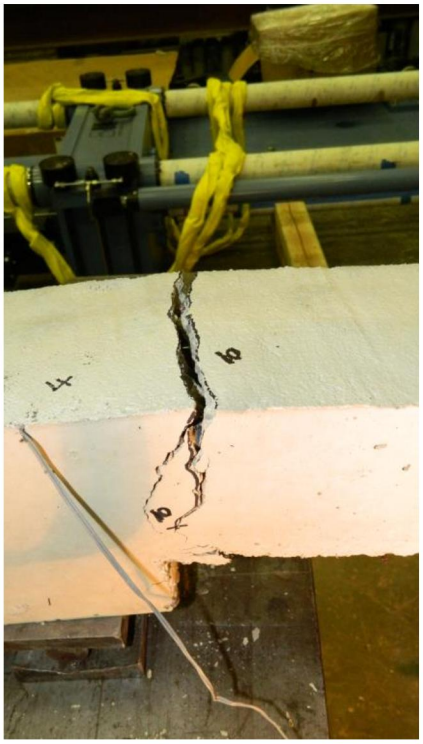

Figure 4-43: Crack at the end of the beam

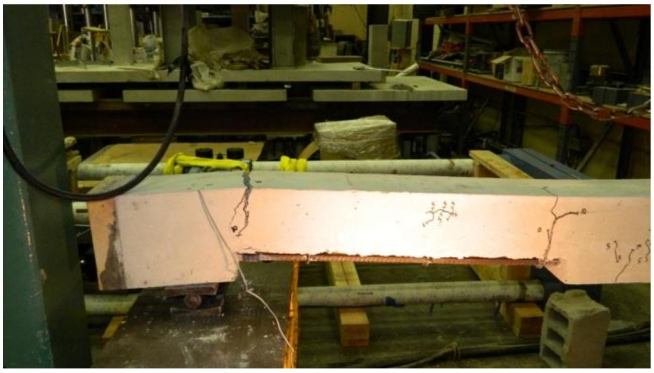

Figure 4-44: Wide crack on the top of the support

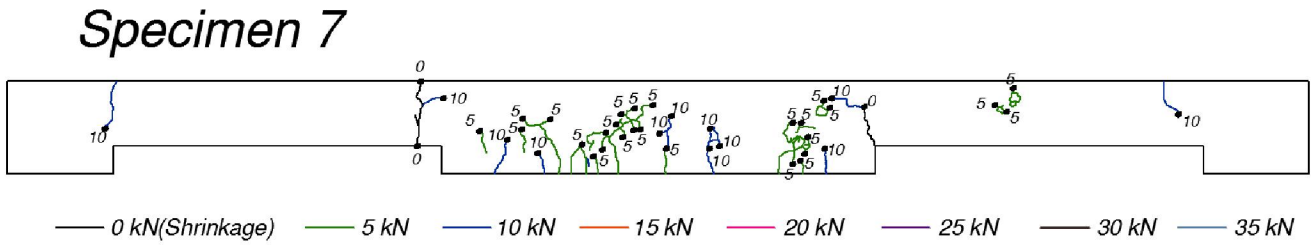

Figure 4-45: Details of rack pattern for specimen 7

Figure 4-46: Crack pattern for specimen 7

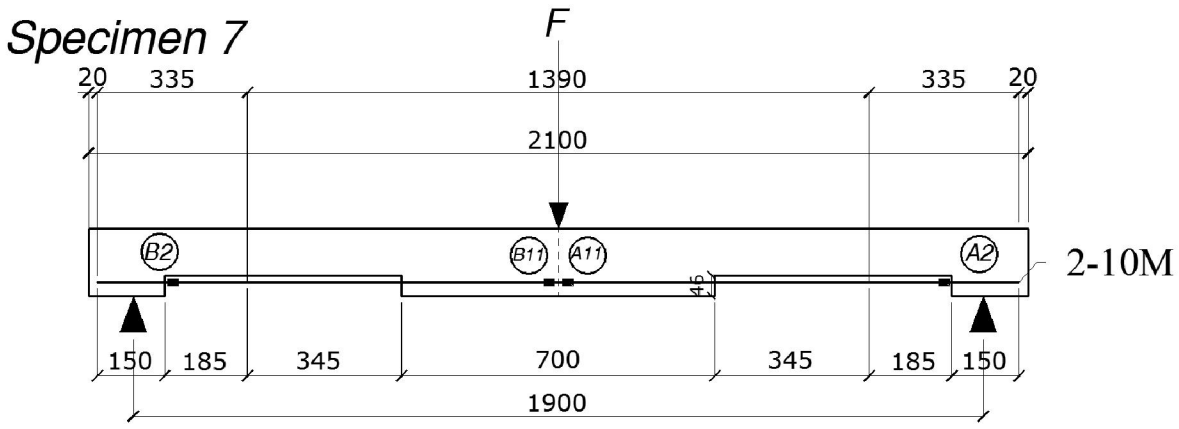

Figure 4-47: Specimen dimensions and strain gauges location

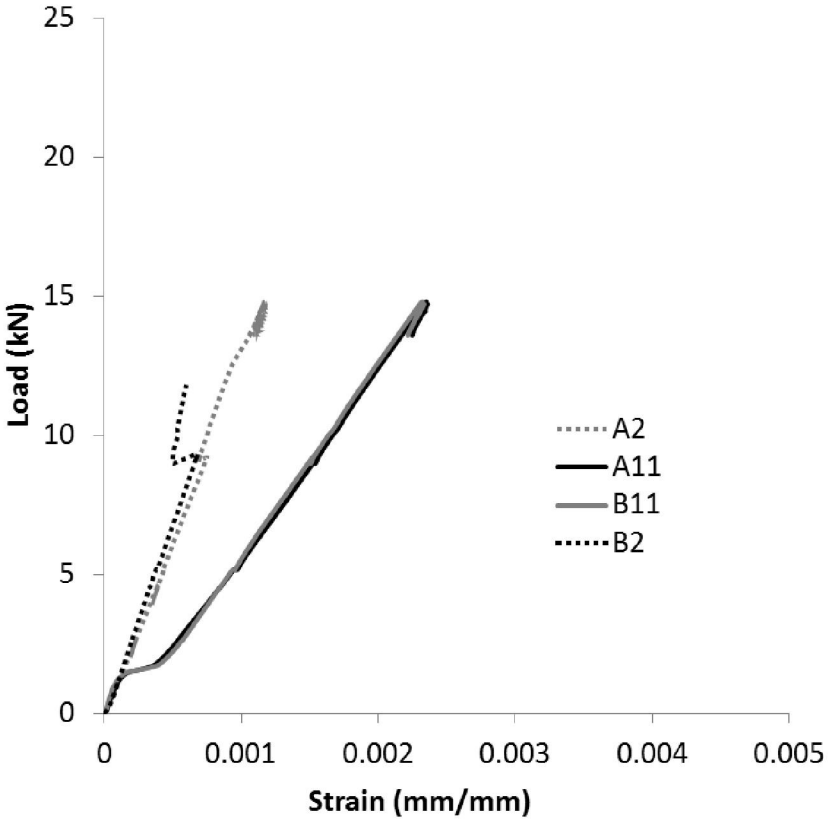

Figure 4-48: Load-strain diagram for specimen 7

4.2.8 Specimen 8

The total length of specimen 8 was 2100 mm and was reinforced with two 10M bars at the bottom. As can be seen in Figure 4-54, this specimen had four de-bonded areas, two on either

side of the beam. All four measured 200 mm and each pair was separated by 150 mm. The two de-bonded areas at either extremity of the beam were in the anchorage zone. The total de-bonding length in this specimen was 800 mm (39% of total length of rebar).

As shown in Figure 4-49, at a peak load of 21.9 kN, equivalent to 96% of the strength of specimen 1 (control beam), and a deflection of 14.2 mm, the bottom reinforcements began to yield (Figure 4-55).

The majority of the cracks appeared in the middle section of the beam. However, none resulted in bonding failure.

As the displacement reached 50 mm, cracks measuring 3 mm in width were formed on the bottom face of the beam. Some cracks also extended from the side of the beam to reach the inner teeth of each de-bonded area (as shown in Figure 4-50), all occurring in the 5 kN load stage. There were no pull-out failures since no horizontal cracks were formed.

There was minor fluctuation in the graph, representing the resistance of the beam after its initial failure at 21.9 kN. Even at a displacement of 25.9 mm, the beam still tolerated a load of 21.8 kN.

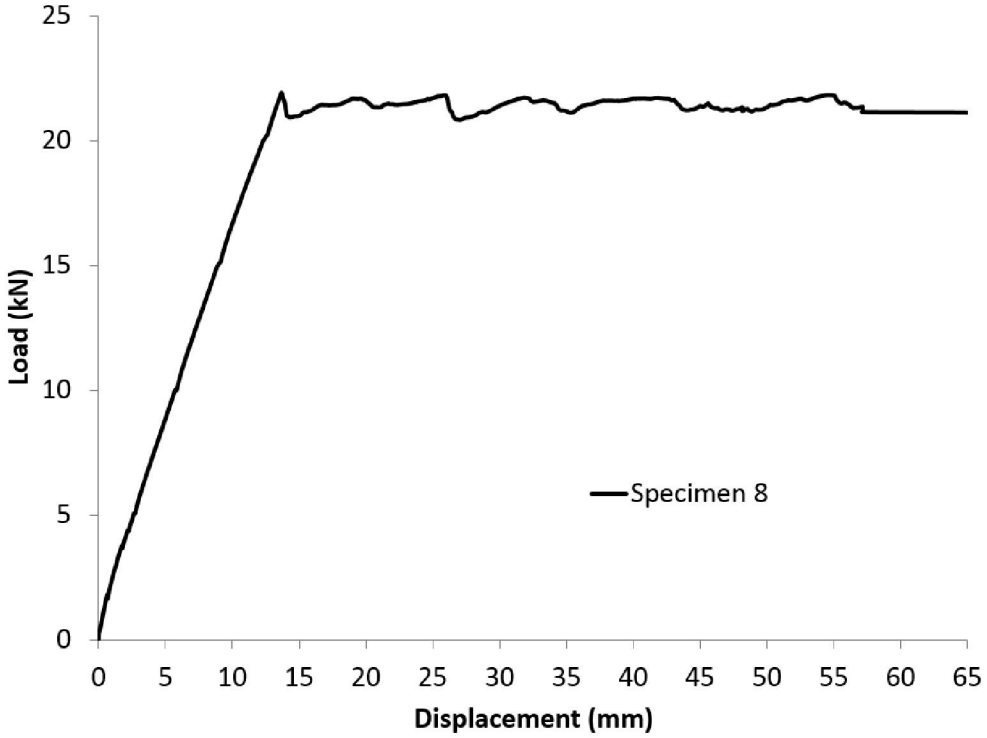

Figure 4-49: Load-displacement for specimen 8

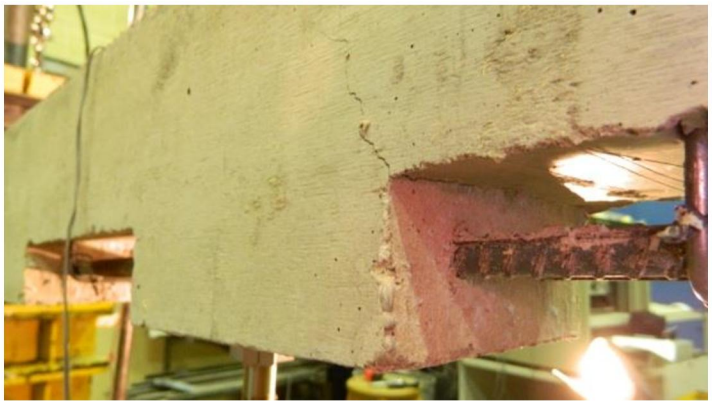

Figure 4-50: Corner crack, specimen 8

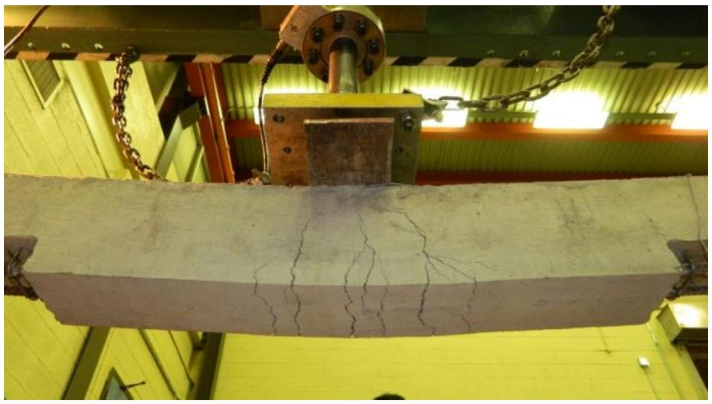

Figure 4-51: Bottom crack for specimen 8

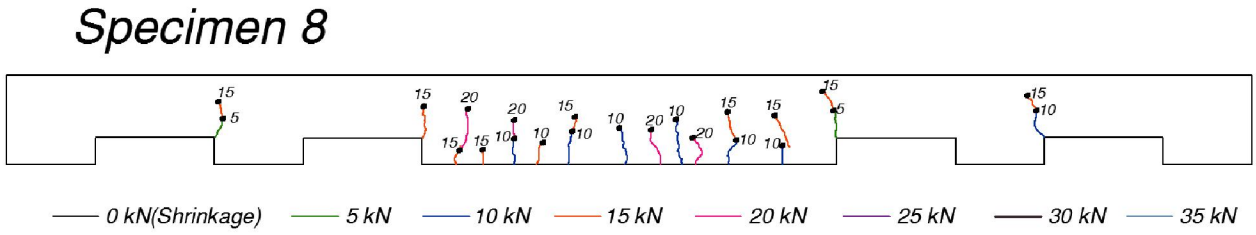

Figure 4-52: Details of crack pattern for specimen 8

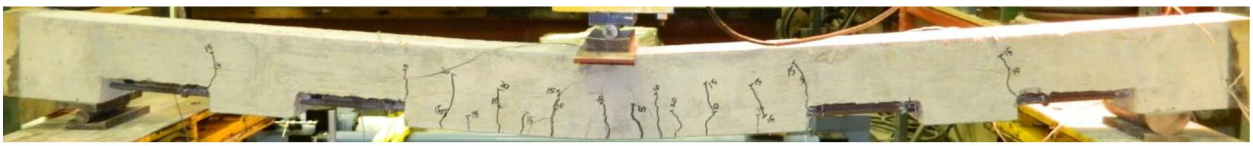

Figure 4-53: Crack pattern for specimen 8

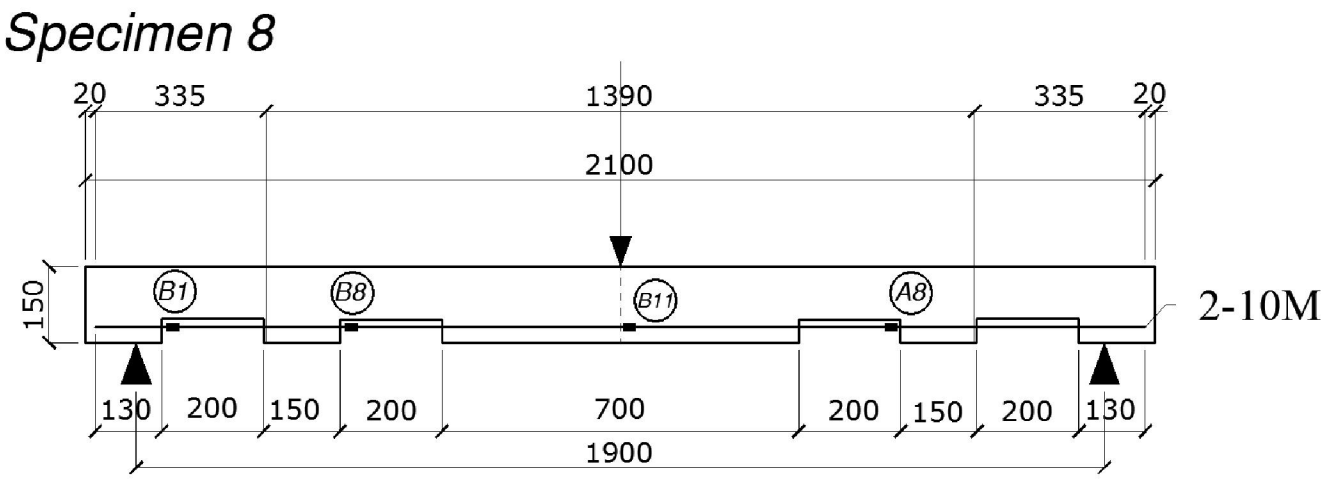

Figure 4-54: Specimen dimensions and strain gauges location

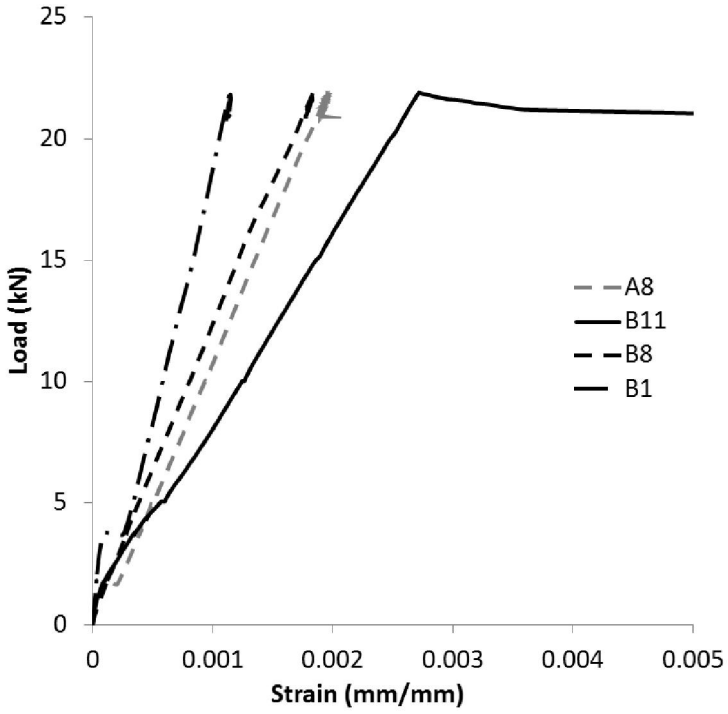

Figure 4-55: Load-strain diagram for specimen 8

4.2.9 Specimen 9

Specimen 9 was 2100 mm in length and was reinforced with two 10M bars at the bottom. In this specimen, there were a total of six de-bonded areas, three on each side of the mid-span. All measured 120 mm in length and each set of three were separated by two 85 mm bonded lengths;

creating “rectangular-patterned” cutouts or “tooth-shaped” areas of de-bonded reinforcement. The de-bonded areas at either extremity of the beam were in the anchorage zone.

The maximum load of the beam in elastic range was recorded at 19.9 kN with a bending displacement of 12.6 mm.

In this specimen, as can be seen in Figure 4-62, the yield load and maximum load were the same; the bottom reinforcements began to yield at a load value of 19.9 kN.

During the test, cracks formed on each corner of the exposed “teeth” in closer proximity to the mid-span (and in accordance, to the point load) at varying load forces (refer to Figure 4-59). When maximum strength is reached, the cracks under the loading point expanded 5mm in width.

As seen in the Figure 4-56, even following initial failure of the beam at a load of 19.9 kN and a displacement of 12.6 mm, its strength continued to augment. For instance, as the load was increased to 22.08 mm, the beam showed a displacement of 18.5 mm without collapsing. This was again seen at a load of 22.83 kN and a displacement of 42.2 mm.

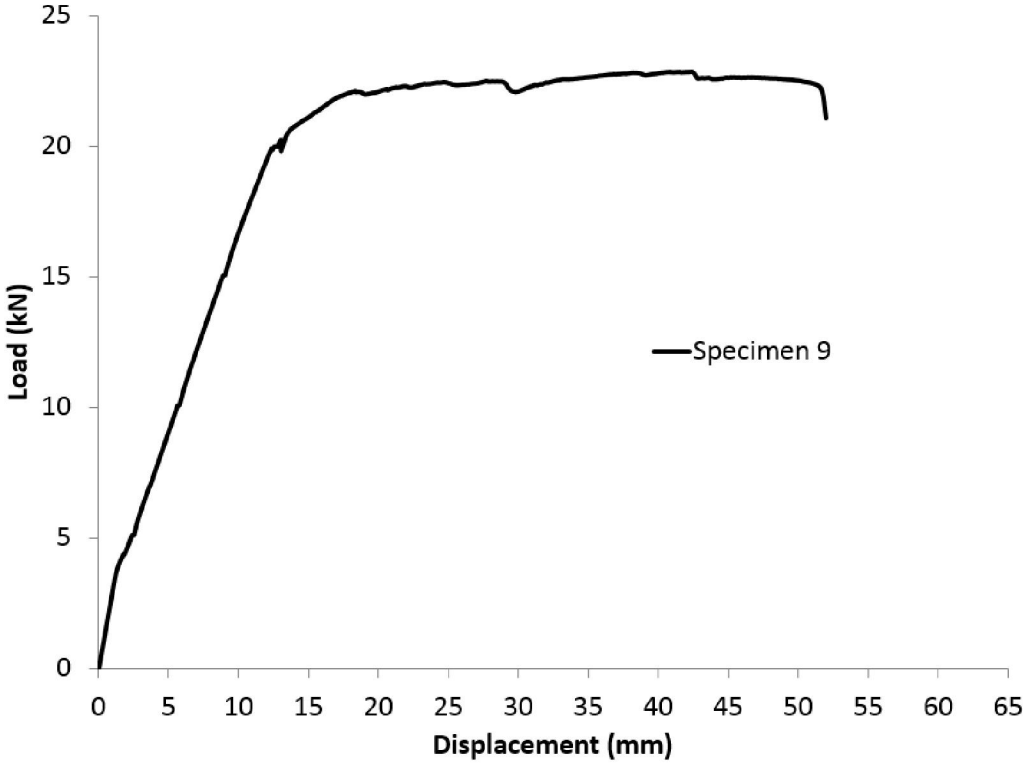

Figure 4-56: Load-displacement for specimen 9

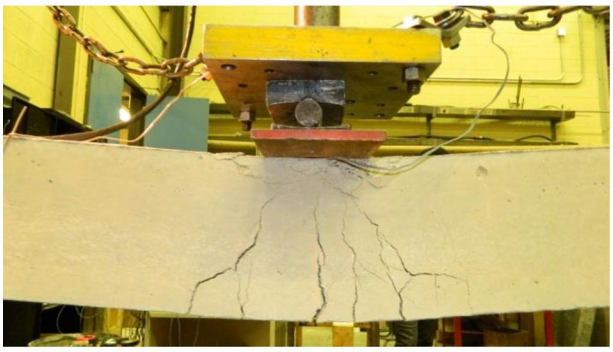

Figure 4-57: Pull out crack specimen 9

Figure 4-58: Flexural crack in specimen 9

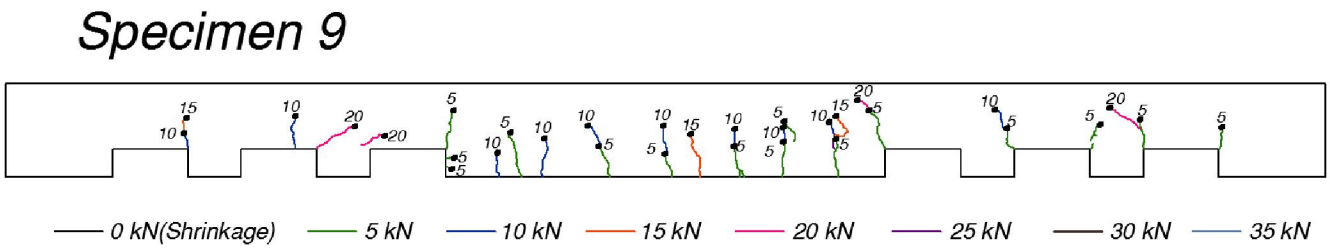

Figure 4-59: Details of crack pattern for specimen 9

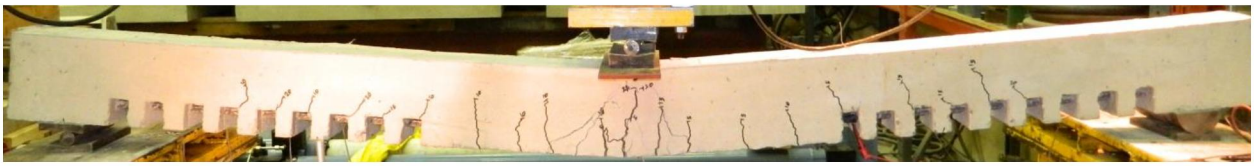

Figure 4-60: Crack pattern for specimen 9

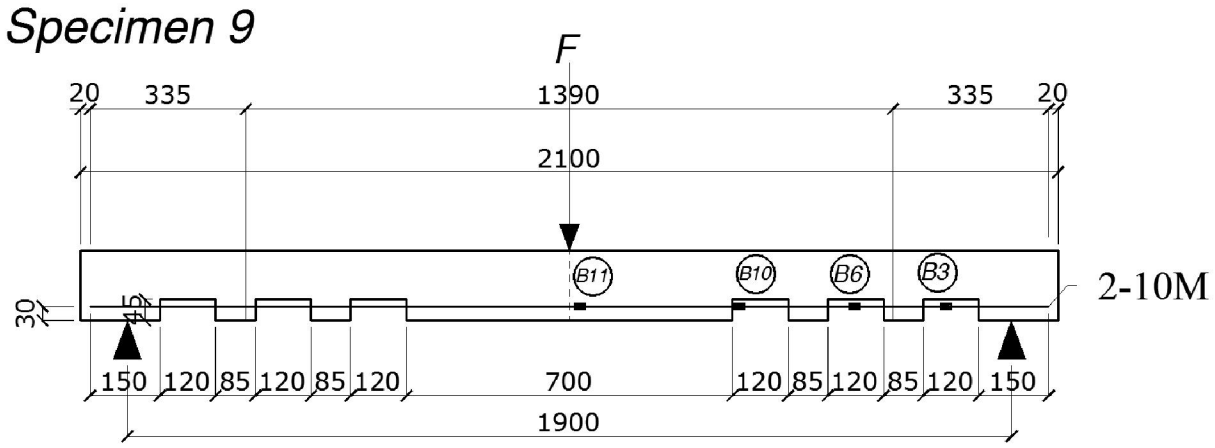

Figure 4-61: Specimen dimensions and strain gauges location

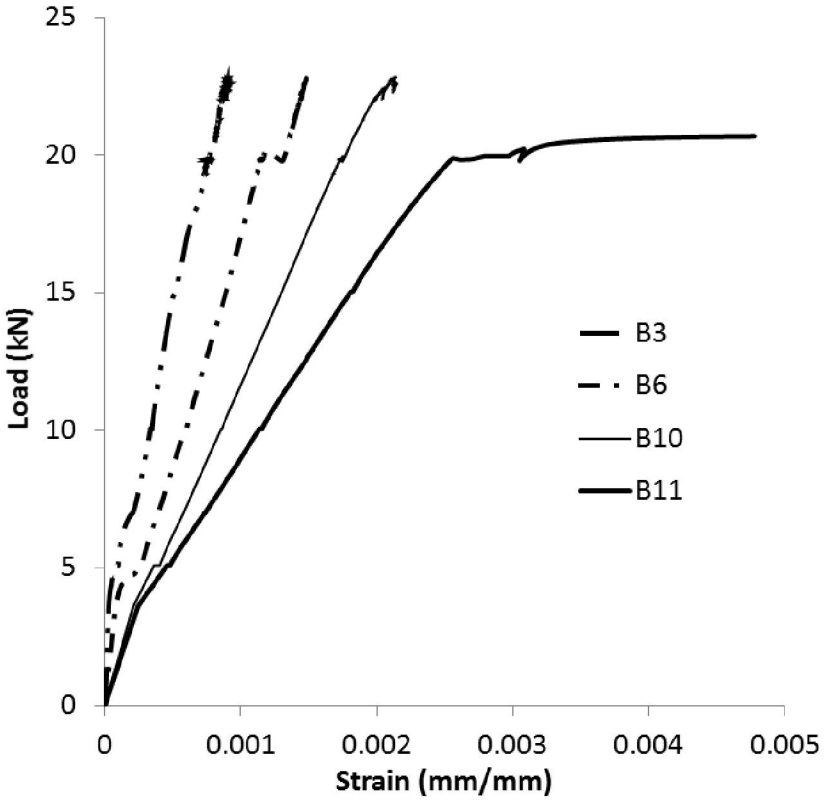

Figure 4-62: Load-strain diagram for specimen 9

4.2.10 Specimen 10

The total length of specimen 10 was 2100 mm and was reinforced with two 10M bars at the bottom. There were a total of ten de-bonded areas; five on each side of the mid-span, as can be seen in Figure 4-68. The de-bonded regions at either extremity of the bar measured 58 mm each and were in the anchorage zone.

The maximum strength in this specimen was recorded at the elastic stage, at a load of 20.1 kN with an elastic deflection of 13.9 mm. The specimen began to yield at this same load value. In comparison to specimen 9, the decrease in the size of each tooth had a negative effect on the total resistance of the beam. This is because the force is distributed among each tooth (proven by the cracks formed at the corners of the exposed areas as opposed to the previous specimen having cracks near the point load).

The cracks that were formed near the point load were deep and wide in the bottom. Eventually, the failure of this beam was caused by flexural forces.

The failure was recorded at a displacement of 64.7 mm.

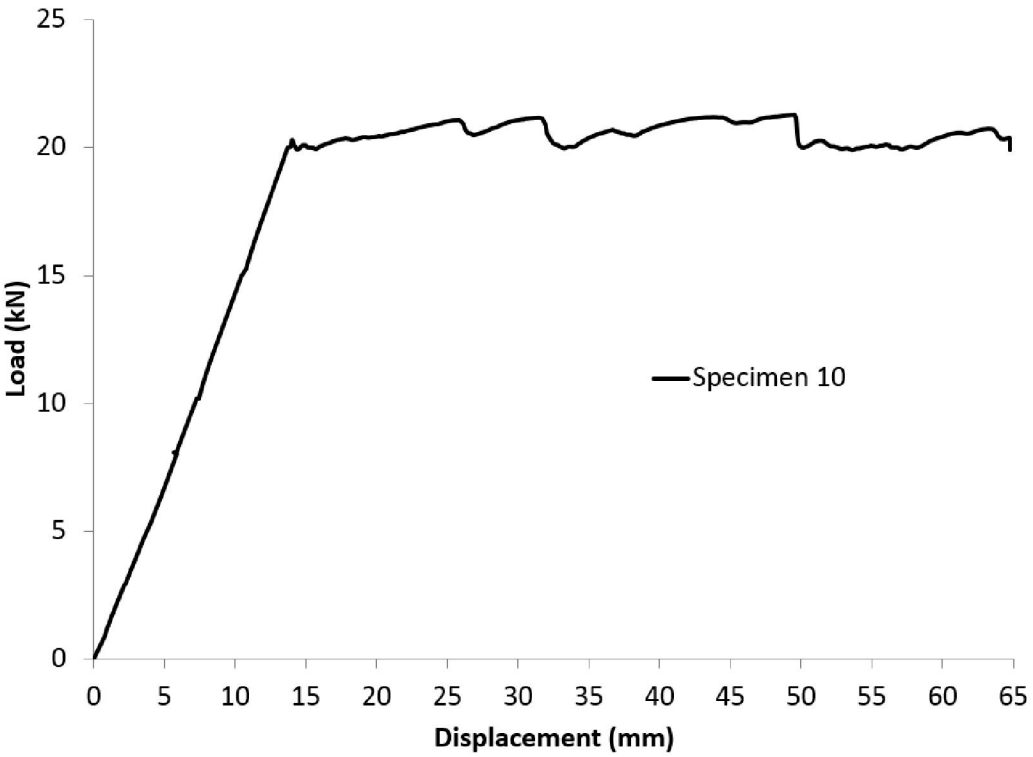

Figure 4-63: Load-displacement for specimen 10

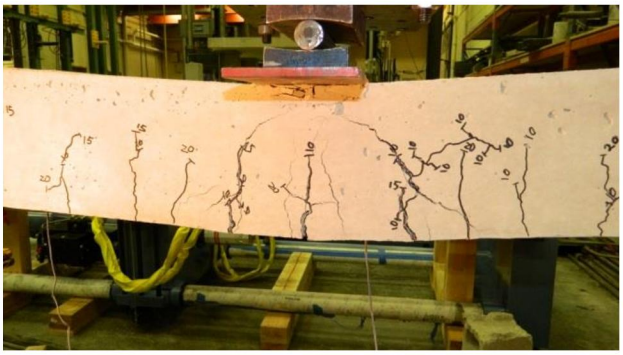

Figure 4-64: Flexural crack in specimen 10

Figure 4-65: Bottom crack in specimen 10

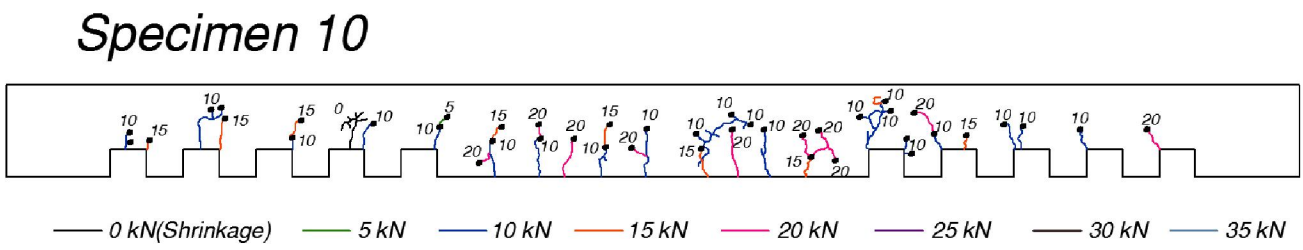

Figure 4-66: Details of Crack pattern for specimen 10

Figure 4-67: Crack pattern for specimen 10

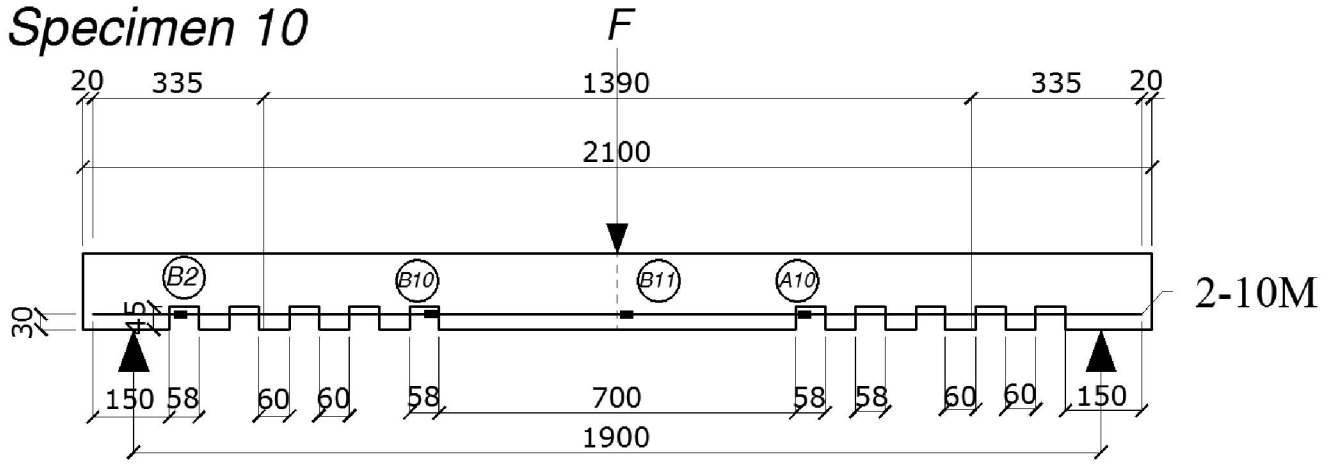

Figure 4-68: Specimen dimensions and strain gauges location

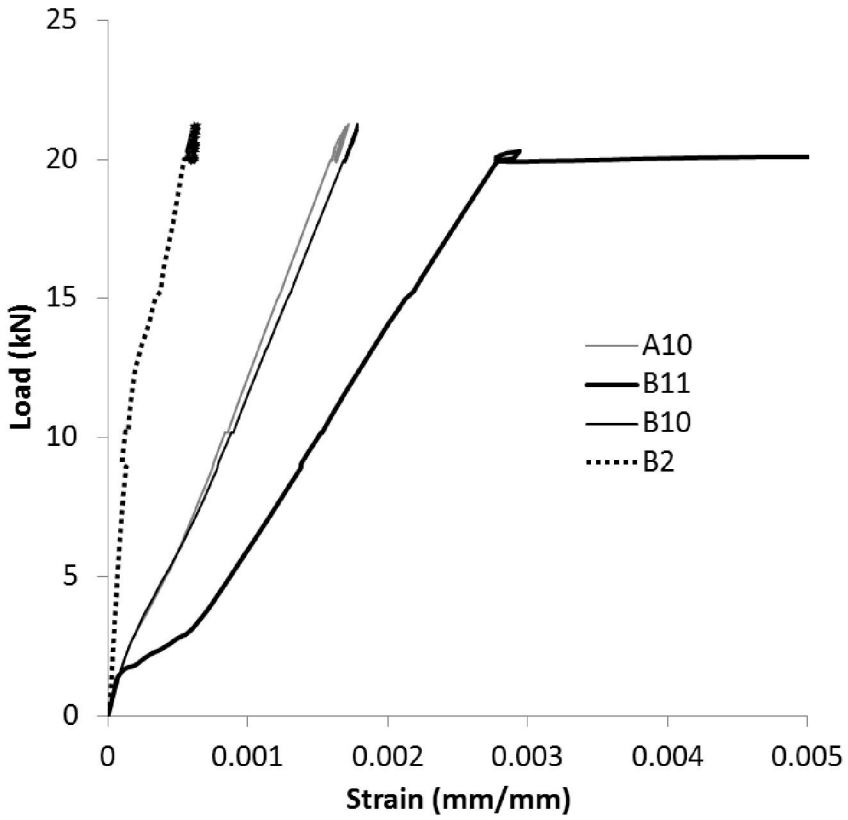

Figure 4-69: Load-strain diagram for specimen 10

4.2.11 Specimen 11

Specimen 11 was 2100 mm in length and was reinforced with two 10M bars at the bottom. Each side of this beam had de-bonded areas of 360 mm in total: 35% of the length of the beam. The 360 mm of de-bonded area on either side the beam was divided into nine 32 mm spans of de-bonded areas. The two de-bonded areas at either extremity of the beam were in the anchorage zone.

The maximum strength in the elastic range was recorded at 19.7 kN and a bending displacement of 12.9 mm. The yield strength was the same.

The cracks spread throughout the entire beam, with more visible concrete spalling in comparison to other specimen. The cracks formed under the point load in this specimen are less intense in comparison to other specimen, seeing as the force is more distributed along the length of the beam. Furthermore, some cracks formed as a result of the pull-out force, as illustrated in Figure 4-74.

The maximum deflection of this beam was recorded at 62.7 mm, and there was no significant increase in strength after the initial failure.

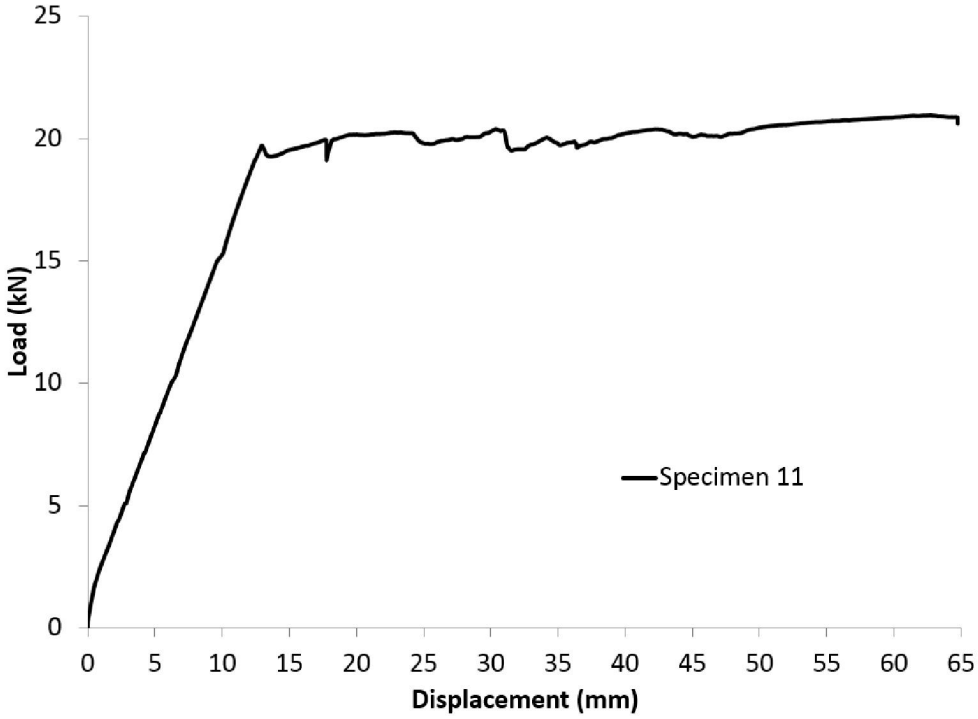

Figure 4-70: Load-displacement for specimen 11

Figure 4-71: Crack pattern in mid span specimen 11

Figure 4-72: Bottom crack in specimen 11

Figure 4-73: Corner crack propagation

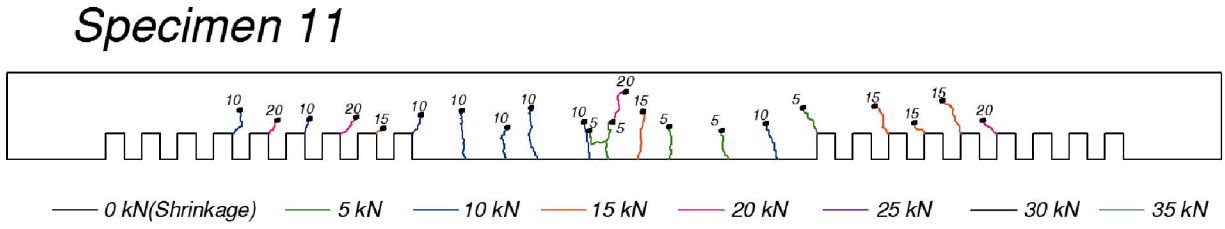

Figure 4-74: Details of Crack pattern for specimen 11

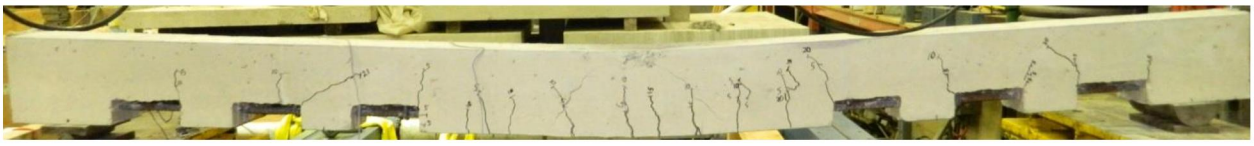

Figure 4-75: Crack pattern for specimen 11

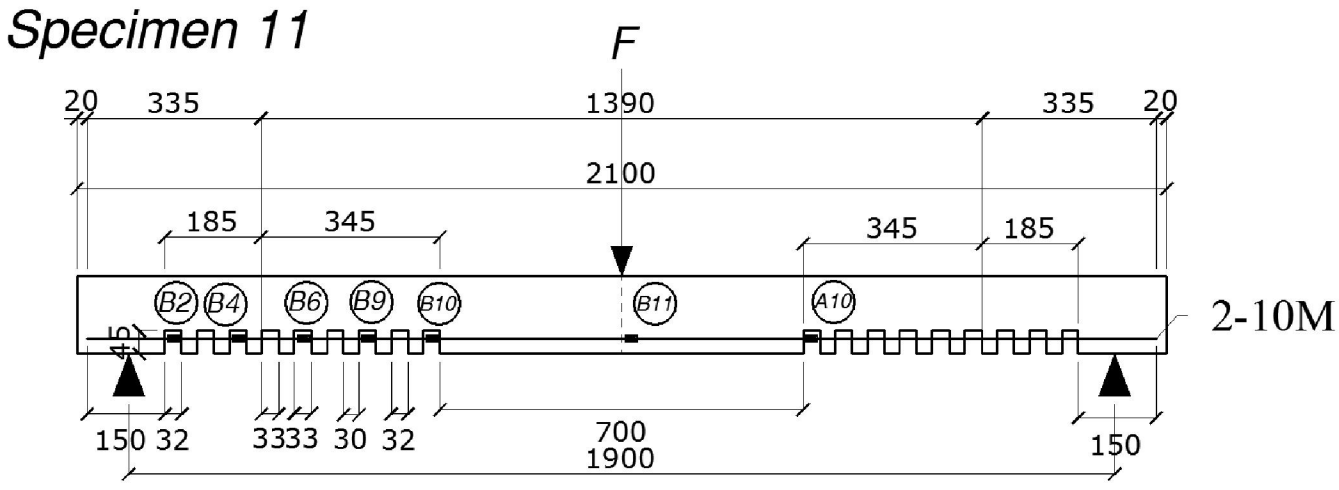

Figure 4-76: Specimen dimensions and strain gauges location

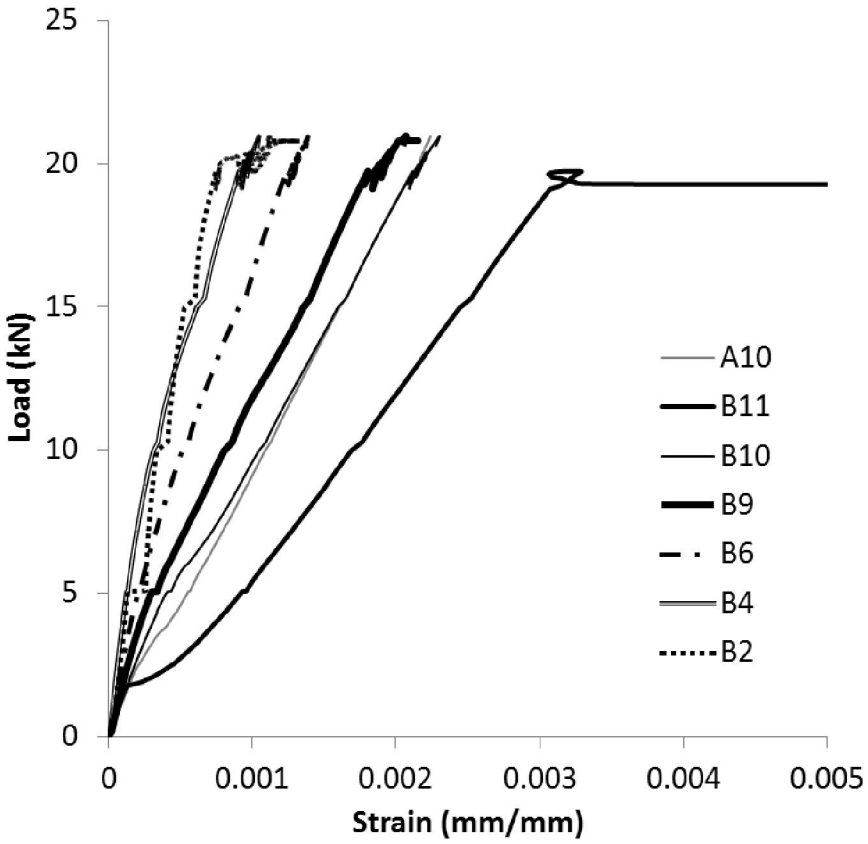

Figure 4-77: Load-strain diagram for specimen 11

4.2.12 Specimen 12

The total length of this specimen was 2100 mm and was reinforced with two fully-bonded 15M bars at the bottom.

A stronger control beam was tested with a steel ratio of 2.6%. This specimen had no exposed reinforcement.

The maximum load recorded in the elastic range was 33.93 kN and a displacement of 13 mm. The bottom reinforcements began to yield at a load of 31.7 kN.

Like specimen 1, the majority of the cracks were concentrated in proximity to the mid-span of the beam. These cracks formed a concave shape in which the peak reached the top centre of the beam (beneath the point load). There were no cracks when loading was under 10 kN. After increasing the load, the flexural cracks propagated to stretch from the bottom of the beam to the

top. There were also some cracks around the support area of the beam before the last stages of failure.

Moreover, additional damage was observed in the form of crashing on the top surface of the beam (Fig4-79). These damages were generated as a result of the compression stress of the bending acting at this beam.

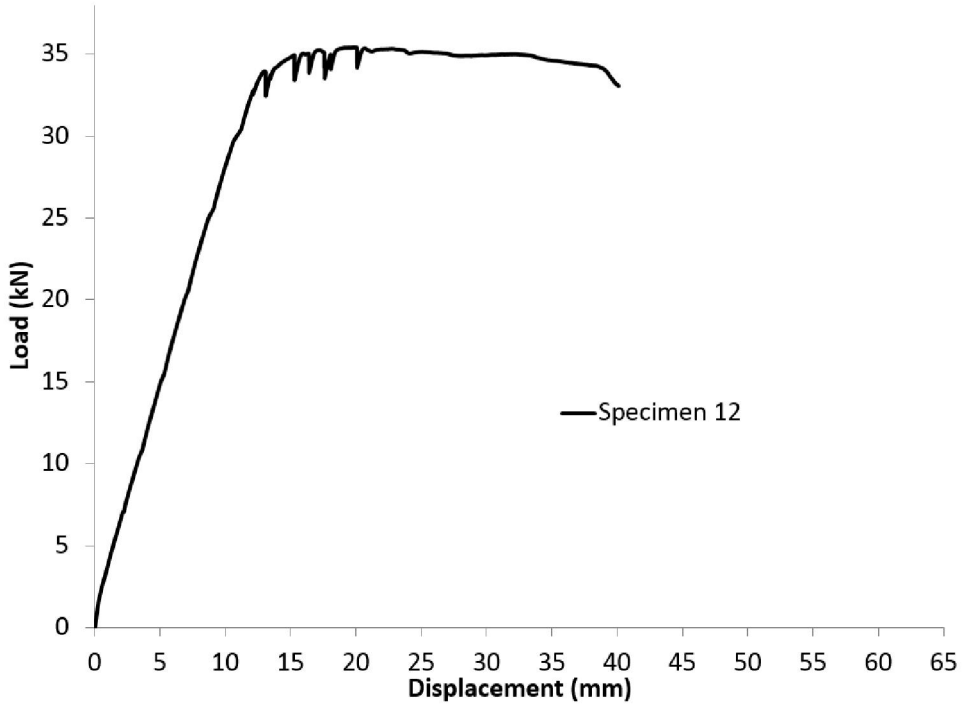

Figure 4-78: Load-displacement for specimen 12

Figure 4-79: Concrete spalling in compression zone

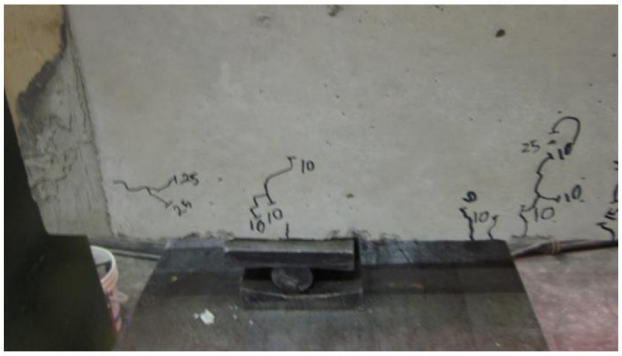

Figure 4-80: Cracks on the support

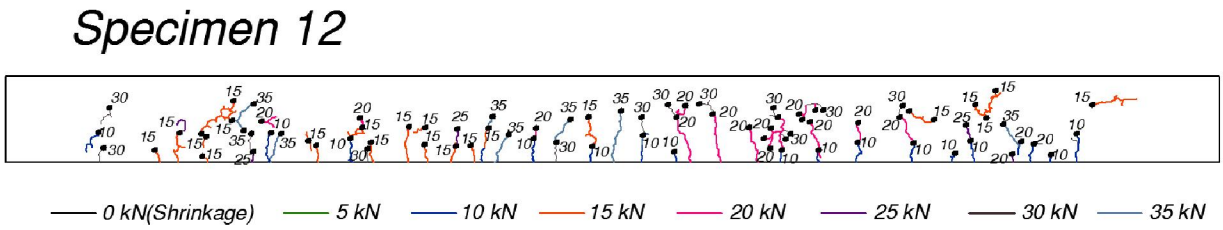

Figure 4-81: Details of crack pattern in specimen 12

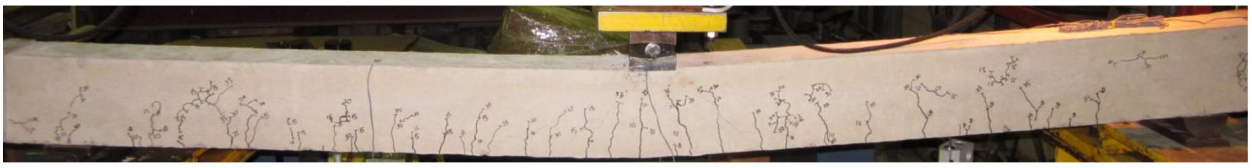

Figure 4-82: Crack pattern in specimen 12

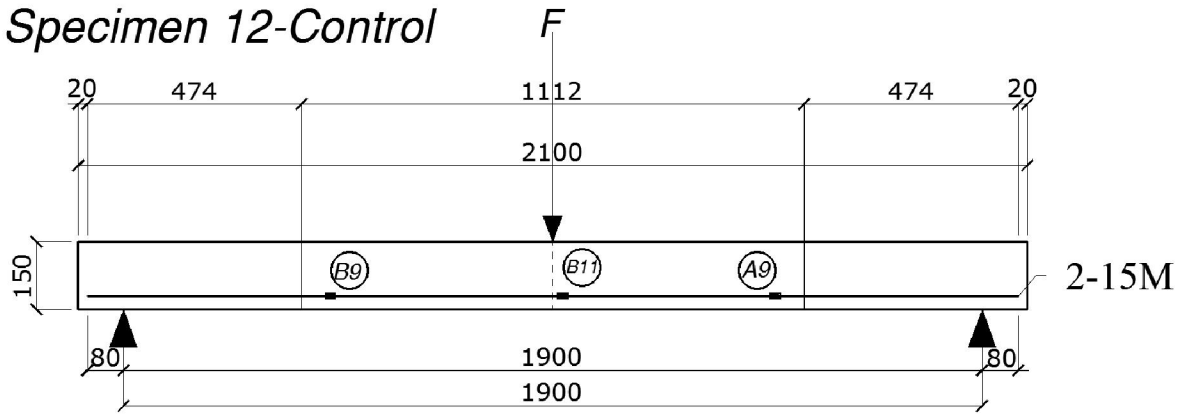

Figure 4-83: Specimen dimensions and strain gauges location

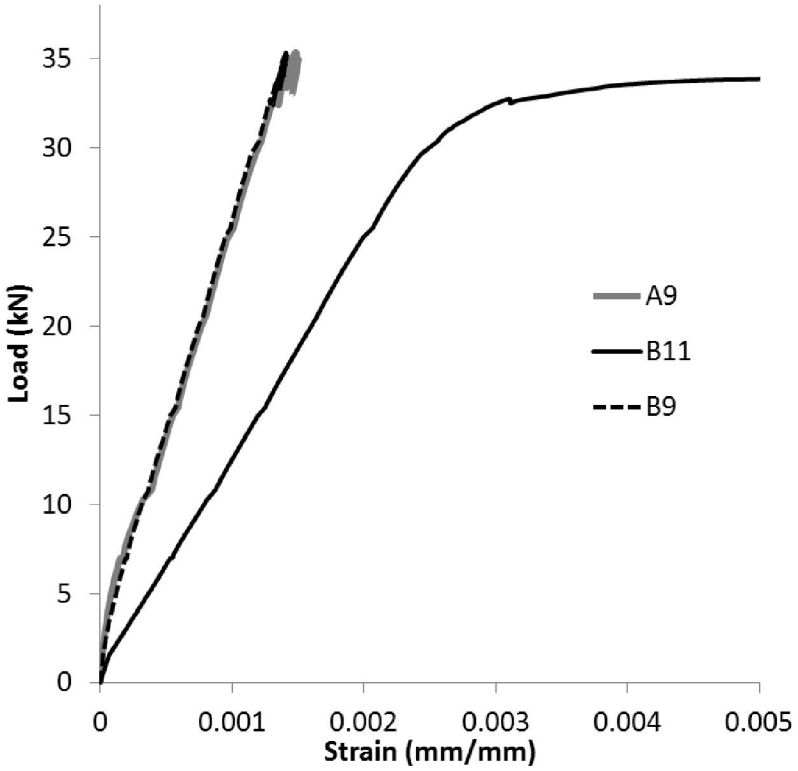

Figure 4-84: Load-strain diagram for specimen 12

4.2.13 Specimen 13

Specimen 13 was 2100 mm in length and was reinforced with two 15M bars at the bottom, each with a 700 mm exposed segment in the middle of the beam; almost 34% the total length.

As seen in Figure 4-85, the maximum load of this beam was 33 kN at a displacement of 21.1 mm; 94% the strength of the specimen 12. The yield load was the same.

The majority of the cracks formed are suggestive of the potential for pull-out failure. There was a crack situated in the middle of the beam (as shown in Figure 4-89), which deformed the de-bonded area of the beam, allowing the concrete to rest on the reinforcement. This caused the load force to transfer from the concrete to the reinforcement. There were also cracks on the bottom face of the beam near the mid-span with widths of 5 mm.

After the initial elastic failure, this specimen withheld a load of 33.23 kN with a 28 mm deflection. Following this stage, the strength reduced gradually in the beam, ultimately causing a failure at a displacement of 37 mm.

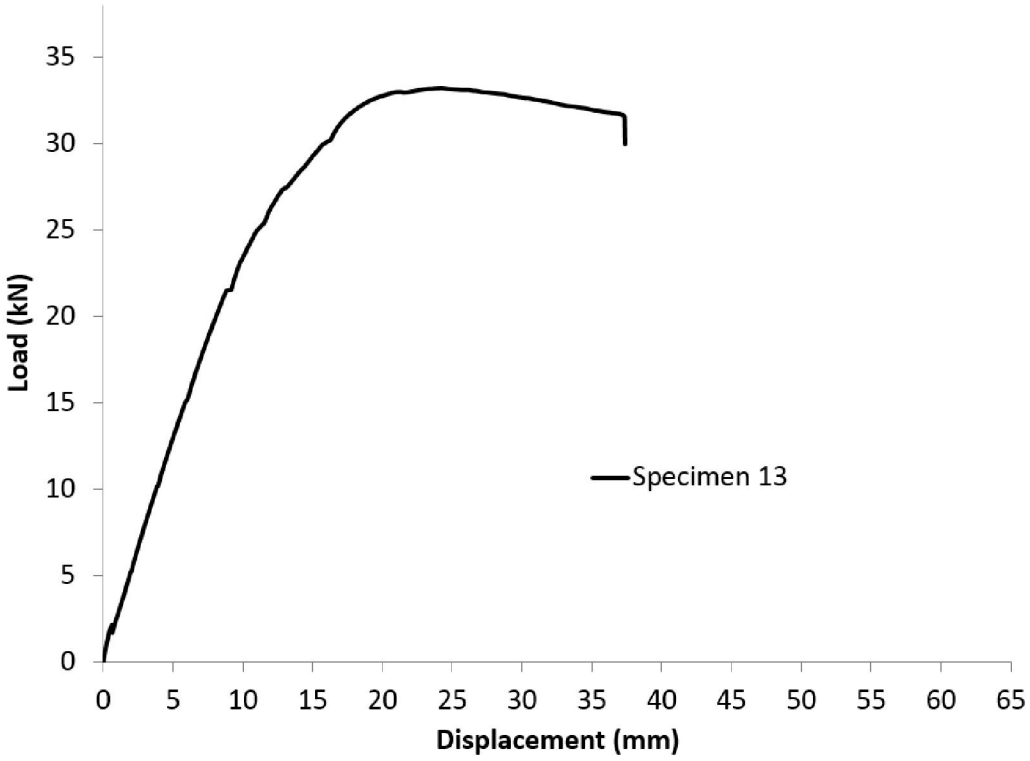

Figure 4-85: Load-displacement for specimen 13

Figure 4-86: Pull out crack for specimen 13

Figure 4-87: Bottom view of specimen 13

Figure 4-88: Mid-span crack

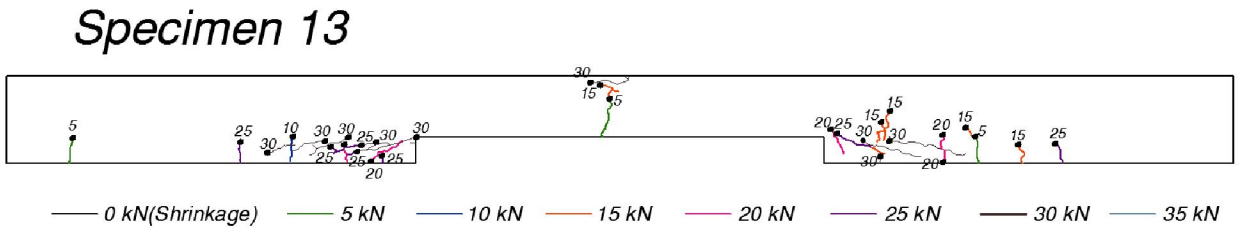

Figure 4-89: Details of crack pattern specimen 13

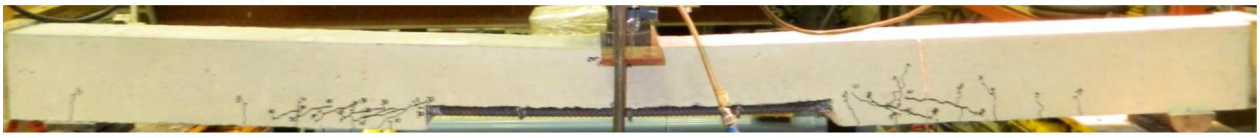

Figure 4-90: Crack pattern specimen 13

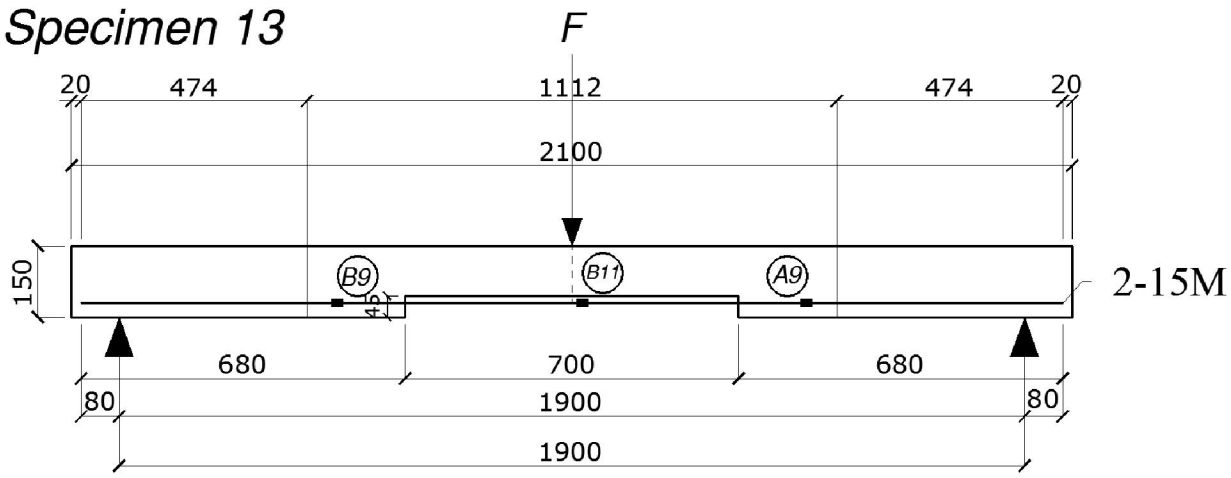

Figure 4-91: Specimen dimensions and strain gauges location

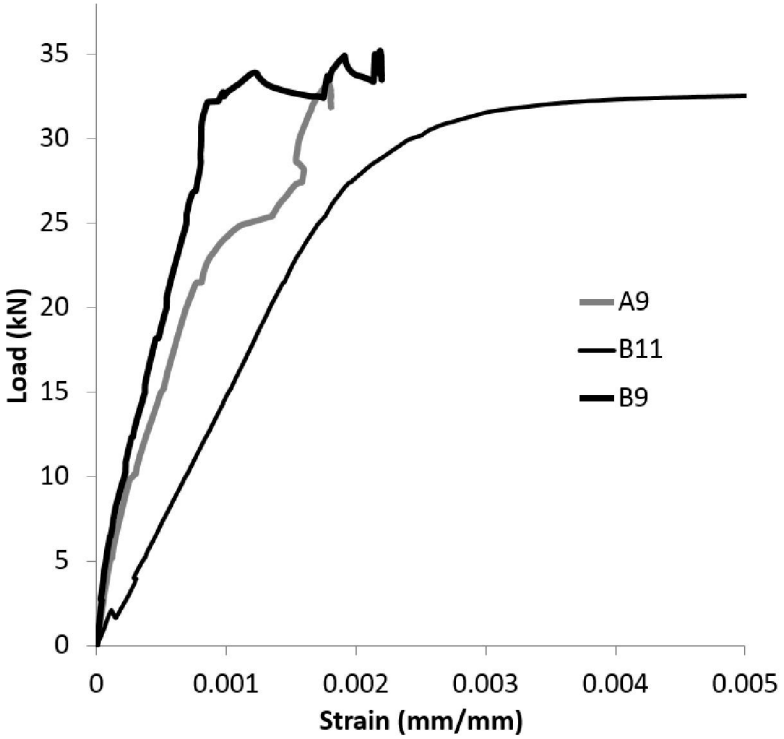

Figure 4-92: Load-strain diagram for specimen 13

4.2.14 Discussion of Experimental results

The increase in exposure lengths in cross-sections causes the reduction of compression block and alters the transfer of force, which results in the reduction of strength in the beam. Theoretically, the absence of concrete cover in the bottom side of the beam causes the non-uniform distribution of force in the concrete that result in steel elongation.

It is also important to note that exposed areas under the middle of the beam threats beam strength more than exposure areas on sides of the beam.

For comparison purposes, the cracks diagnosis and the control specimen response are also reproduced, in each series of de-bonded specimen response.

Chapter 5 : Analysis of Test Results

5.1 Overview

This chapter presents an analysis of the results of the tests on beams with exposed flexural reinforcing described in Chapter 4. The response of the beams observed from the flexural tests, including the load-displacement and load-strain behaviour, is analyzed. The cracking behaviour is also discussed, along with the development of the flexural reinforcing steel. Various failure modes were observed in the tests, including: pull-out/bond failures and yielding of the reinforcement. In this chapter, the capacities of the beams and their failure modes are predicted using structural resistance models employing the modified area concept, and the appropriateness of these models is discussed.

5.2 Summary of Main Test Results

A summary of the important results from the two series of tests are presented in Table 5-1:

Table 5-1: Summary of main test results.

Specimen	% Spalled	% Development	Yield Load, P_y (kN)	Ultimate Strength, P_{ult} (kN)	Displacement Δ_{ult} at P_{ult} (mm)	Stiffness (kN/mm)	P_{ult} / $P_{control}$	M_{ult} kN·m	Bar Size
01	00.0	100.0	22.80	23.30	12.5	1.7895	1.00	11.06	10
02	16.9	100.0	21.29	21.29	12.9	1.7612	0.91	10.11	10
03	33.9	100.0	20.00	20.03	16.9	1.1985	0.86	09.51	10
04	85.4	044.7	10.40	10.48	15.7	0.7838	0.45	04.97	10
05	28.1	100.0	21.85	22.44	16.6	1.4766	0.96	10.65	10
06	46.6	059.7	20.92	22.10	20.9	1.3240	0.95	10.49	10
07	51.4	044.7	14.80	14.80	15.6	1.0793	0.63	07.03	10
08	38.8	038.8	21.90	21.90	13.7	1.6136	0.94	10.40	10
09	34.9	064.1	22.11	22.83	18.4	1.5091	0.98	10.84	10
10	28.1	065.3	20.30	21.27	14.0	1.4509	0.91	10.10	10
11	28.1	71.3	19.73	20.96	12.9	1.4635	0.90	9.95	10
12	0.0	100.0	33.92	35.38	13.0	2.7619	1.00	16.80	15
13	33.9	100.0	33.00	33.23	21.2	2.3747	0.94	15.78	15

5.3 Load-Displacement Behaviour and Cracking Analysis

In the following sections, the load-displacement curves for various groups of specimens are compared.

5.3.1 Specimens 1, 2, 3, and 4

The load versus midspan displacement curves for Specimens 1-4 are presented in Figure 5-1. For Specimens 1, 2, and 3 the failure loads, P_{ult}, were 22.80 kN, 21.30 kN, and 20.00 kN respectively; while Specimen 4 failed at 10.48 kN (see Table 5-1). Looking at Figure 5-1, it can be seen that little separates the load-displacement curves for Specimens 1-3. However, a significant reduction in the initial stiffness and maximum load achieved by Specimen 4 can be seen. The maximum displacement prior to total loss of beam capacity is significantly lower for Specimen 4 than for the other specimens.

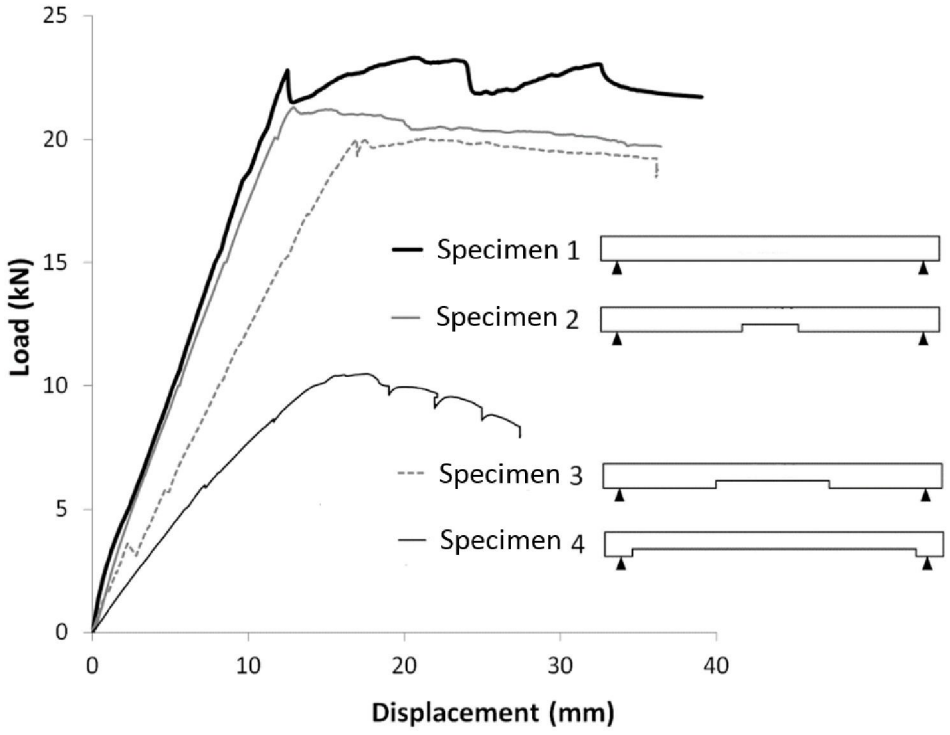

Figure 5-1: Load-displacement curves for Specimens 1, 2, 3, and 4.

The cracking patterns for these four specimens are shown in chapter 4. Looking at these cracking patterns, significant flexural cracking can be seen for Specimen 1. The crack spacing is roughly uniform within the cracked region and the crack depths closely follow the moment distribution,

with the deepest cracks occurring at the midspan. For Specimens 2 and 3, the crack spacing is less uniform. In the de-bonded region, there is a large gap between the vertical cracks outside the de-bonded region and the vertical crack or cracks at the beam midspan. This suggests a change in the load carrying mechanism from flexure to arch action in the de-bonded regions, with the uncracked concrete segments behaving primarily as compressive "struts". In general, the number of transverse (flexural) cracks decreases as the length of the exposed area increases. For Specimen 4, there are essentially three vertical cracks, indicating that the load was carried primarily by arch action. While the cracks are all on the bottom (flexural tension) side of the beam for Specimens 1 and 2, in Specimens 3 and 4, the cracks at the ends of the de-bonded region can be seen at the top of the beam, indicating that the top side was in tension at these locations. Such top cracks were observed previously by Luckai, (2011).

5.3.2 Specimens 1, 5, 6, and 7

The load versus midspan displacement curves for Specimens 1, 5, 6, and 7 are presented in Figure 5-2. Similar trends can be seen for this group of specimens as were seen for the first group. For Specimens 1, 5, and 6 the failure loads, P_{ult}, were 22.80 kN, 21.85 kN, and 20.92 kN respectively; while Specimen 7 failed at 14.80 kN (see Table 5-1). Looking at Figure 5-2, it can again be seen that little separates the load-displacement curves for Specimens 1, 5, and 6. However, a significant reduction in the initial stiffness and maximum load achieved by Specimen 7 can be seen. The maximum displacement prior to total loss of beam capacity is significantly lower for Specimen 7 than for the other specimens.

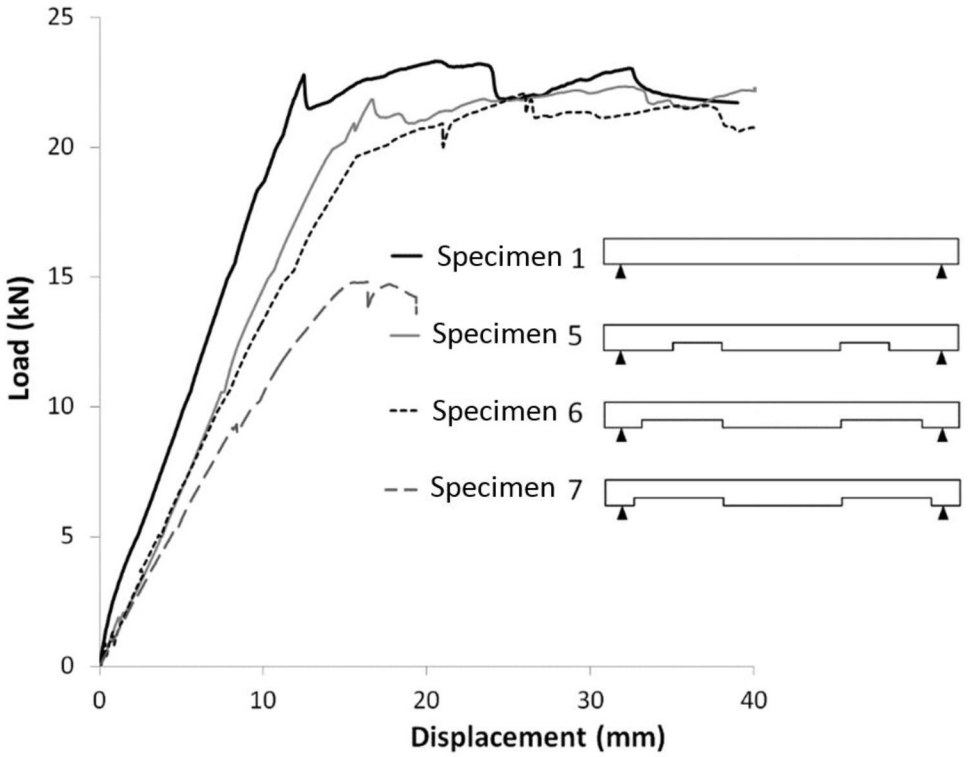

Figure 5-2: Load-displacement curves for Specimens 1, 5, 6, and 7.

Again, the cracking patterns for these four specimens are shown in chapter 4. Looking at these cracking patterns, a similar trend is seen of uniform vertical, flexural cracks in the bonded regions and large uncracked segments of the beam in the de-bonded regions, again suggesting that the load carrying mechanism is classic beam behaviour in the bonded regions and arch action in the de-bonded regions. In general, the number of transverse (flexural) cracks decreases as the length of the exposed area increases. For Specimens 6 and 7, vertical cracks on the top side of the beam are apparent at the edges of the de-bonded regions, indicating that the top side was in tension at these locations.

5.3.3 Specimens 7, 8, 9, 10, and 11

The load versus midspan displacement curves for Specimens 7, 8, 9, 10, and 11 are presented in Figure 5-3. The failure loads, P_{ult}, for these specimens were: 14.80 kN, 21.90 kN, 22.11 kN, 20.30 kN, and 19.73 kN respectively (see Table 5-1). Comparing the spalling patterns for these specimens, it can be seen that they all have spalled regions between the load point and the supports. However, while Specimen 7 has a single, large spalled region on each side of the load point, Specimens 8-11 have short bonded regions or "teeth" of concrete engaged with the

flexural reinforcing along the same length. Looking at Figure 5-3, it can be seen that these teeth are highly effective, in all cases resulting in a load-displacement behaviour not unlike that of the control specimen (Specimen 1) in terms of the peak load and maximum displacement achieved. However, a significant reduction in the initial stiffness and maximum load achieved is seen for Specimen 7. The maximum displacement prior to total loss of beam capacity is again significantly lower for Specimen 7 than for the other specimens.

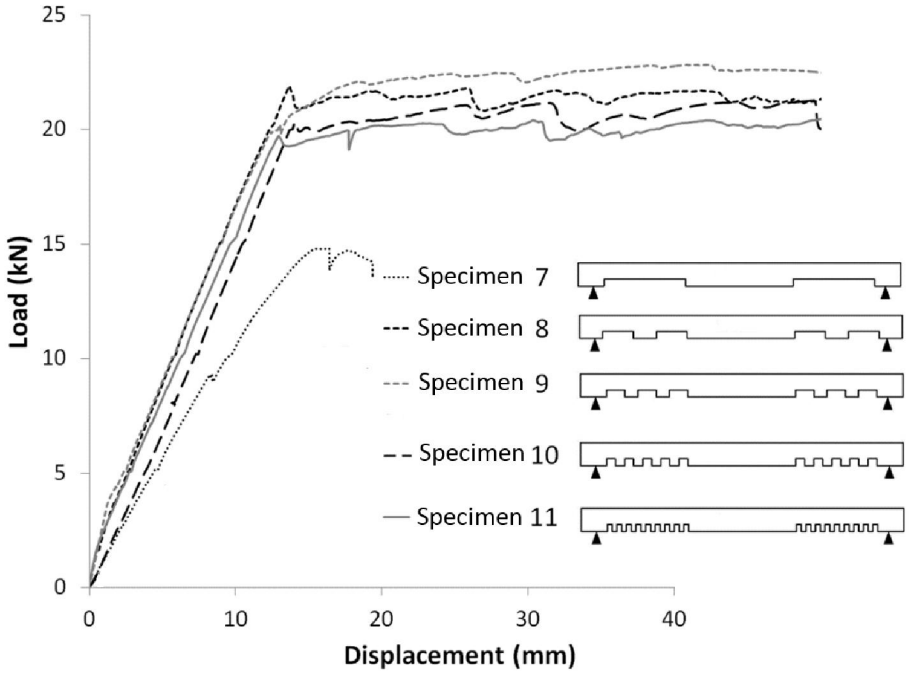

Figure 5-3: Load-displacement curves for Specimens 7, 8, 9, 10, and 11.

The cracking patterns for these specimens are shown in chapter 4. Looking at these cracking patterns for the specimens with larger de-bonded regions (i.e. Specimens 7-9), a similar trend is seen of uniform vertical, flexural cracks in the bonded regions and large uncracked segments of the beam in the de-bonded regions, again suggesting that the load carrying mechanism is classic beam behaviour in the bonded regions and arch action in the de-bonded regions. However, only in the case of Specimen 7 are cracks on the top side of the beam apparent. This suggests that the teeth in each case are having an influence on the load carrying mechanism, and thus reducing or eliminating the tensile stresses on the top side of the beam. In the case of Specimens 10 and 11, due to the small distance between the teeth, it is difficult to comment on a difference in the vertical crack spacing in the bonded and de-bonded regions. In the case of Specimens 8-11, the vertical cracks in the de-bonded regions tend to start at the outside corner of each "tooth". This

suggests that load transfer between the concrete teeth and the flexural reinforcing is occurring, and the end result is tension in the concrete at this corner, which is what might be expected if each of the teeth behaves as a cantilever beam.

5.3.4 Specimens 12 and 13

The load versus midspan displacement curves for Specimens 12 and 13 are presented in Figure 5-4.

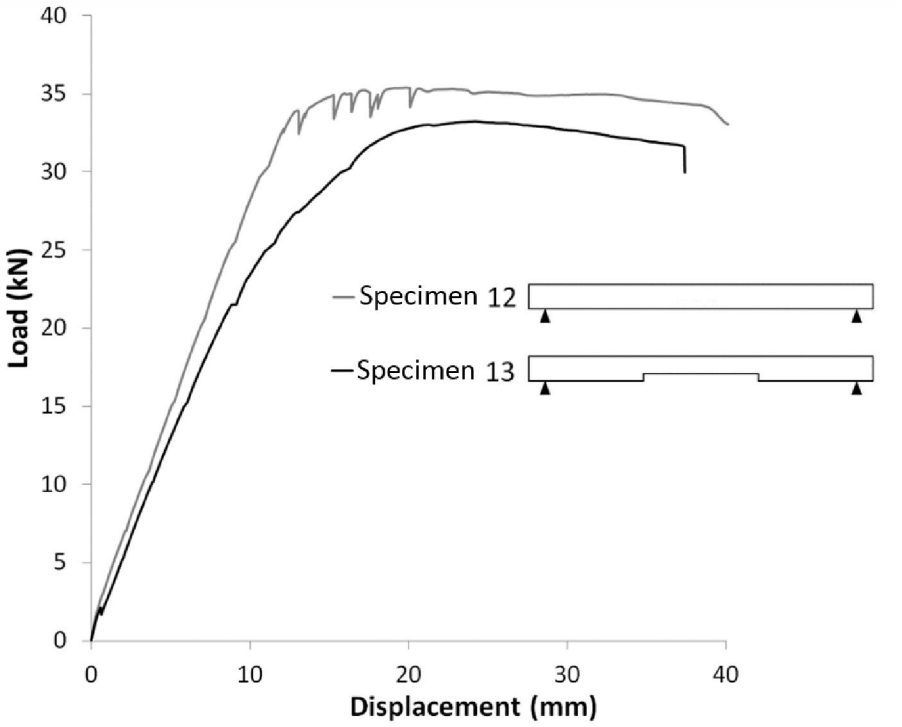

Figure 5-4: Load-displacement for Specimens 12 and 13.

The failure loads, P_{ult}, for these specimens were: 33.92kN and 33.00kN respectively (see Table 5-1). These two specimens were included in the test program to show the effect of steel ratio in the cross section. As mentioned earlier, Specimens 12 and 13 are reinforced with a larger bar size (15M).

Specimens 12 and 13 exhibited exactly the same pattern in their reduction of strength as did Specimens 1 and 2. In other words, the small de-bonded region at the midspan of Specimen 13 resulted in a slight decrease in initial stiffness and ultimate capacity. Specimens 12 and 13 have a higher capacity overall than Specimens 1 and 2, due to the larger flexural reinforcing bar size used.

The cracking patterns for both specimens are shown in chapter 4. The crack pattern trends follow closely those observed for Specimens 1 and 2. Significant flexural cracking can be seen for Specimen 12. The crack spacing is roughly uniform along the span. The crack spacing for Specimen 12 is smaller than for Specimen 1 due to the increased quantity of flexural reinforcing. For Specimen 13, the crack spacing is less uniform than for Specimen 12. In the de-bonded region, there is a large gap between the vertical cracks outside the de-bonded region and the vertical crack at the beam midspan.

5.4 Effect of Exposure Length on Ultimate Strength

In Figure 5-5, the ultimate load, P_{ult}, achieved for each specimen is plotted versus the length of the de-bonded or exposed area, L_{exp}. In order to simplify the interpretation of data, the variables on each axis were non-dimensionalized by dividing with respect to the ultimate capacity of the appropriate control specimen (Specimen 1 or 12), $P_{control}$, and the total beam length, L_{total}.

In Figure 5-5, it can be seen that if the flexural reinforcement is exposed for up to 35% of the beam length, then at least 80% of the control specimen capacity is always achieved. Specimens 1, 2, 3, and 4 were fabricated with reinforcement exposed at the midspan with increasing exposure length up to 85%. Figure 5-5 shows a reduction in strength down to 45% of the control beam capacity for Specimen 4. Specimens 1, 5, 6, and 7 have reinforcement exposed between the load point and the support. Specimen 7 has the largest strength reduction down to 63% of the control beam capacity.

Specimens 7, 8, 9, 10 and 11 are also grouped in Figure 5-5 to examine the effect of the de-bonded length for the specimens with "teeth" of bonded concrete within the de-bonded region. While the data points for these specimens fall near those for the other specimens, the general trend of decreasing strength with increasing exposed length is not followed. Rather, it can be seen that the strength decreases slightly with a decrease in the tooth size for Specimens 9, 10, and 11.

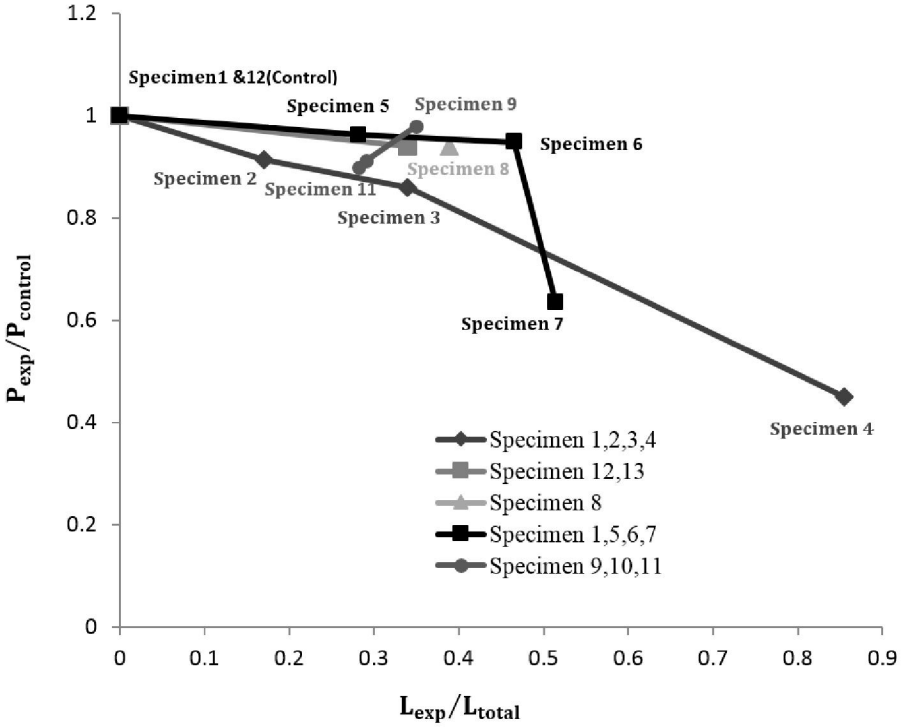

Figure 5-5: Effect of exposure length on ultimate strength.

Specimens 12 and 13, which are heavy reinforced, did not have a significant difference in strength.

5.5 Effect of Exposure Length on Initial Stiffness

In Figure 5-6, the initial stiffness, S, achieved for each specimen is plotted versus the length of the de-bonded or exposed area, L_{exp}. Again, the variables on each axis were non-dimensionalized by dividing with respect to the initial stiffness of the appropriate control specimen (Specimen 1 or 12), $S_{control}$, and the total beam length, L_{total}. In Figure 5-6, stiffness was calculated using the load-displacement data. The displacement at 80% of the yield load, P_y, was the basis for this calculation.

As seen in Figure 5-6, the stiffness of the beams was not affected significantly when the length of exposure is limited to less than 20% of the total length. Generally, by increasing the exposure length, the stiffness will reduce. There was an exception to this rule, however, for Specimens 8, 9, and 10, which had small "teeth" between the exposed regions. For example, Specimen 8 had a higher stiffness, even though it had a larger exposed length, since the "teeth" were larger.

The specimen with the lowest stiffness was Specimen 4, which had an exposure length equal to 85.4% of the total span, resulting in an initial stiffness that was only 44% of the control beam (Specimen 1). In general, a rough estimate of the initial stiffness can be obtained by assuming a straight line relationship between the results for Specimen 4 and the control specimens.

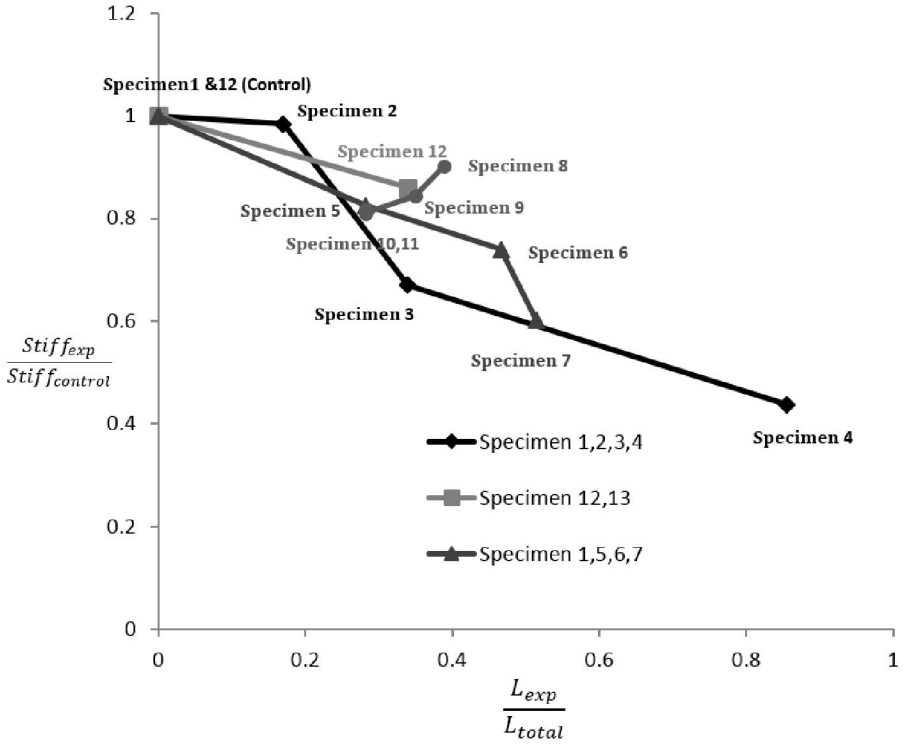

Figure 5-6: Effect of exposure length on initial stiffness.

5.6 Load versus Rebar Strain Behaviour

In the following sub-sections, the rebar strain results are compared for various specimens. A complete set of load versus rebar strain plots for each specimen can be found in chapter 4.

5.6.1 Strain Gauge B11: Specimens 2, 3, 4, and 13

In Figure 5-7, the rebar strains at the midspan (Strain Gauge B11) are plotted for Specimens 2, 3, 4, and 13. Comparing the load strain results, it can be seen that higher load levels and a clear yield plateau are reached for Specimens 2, 3, and 13. For Specimen 4 on the other hand, the peak load level is lower (10 kN versus 21.3 kN for Specimens 2 and 3) and the behaviour is linear, indicating that no yielding has taken place. This result, in addition to the observed behaviour of the specimens during the tests indicate that the failure mode for Specimens 2, 3, and 11 was yielding of the flexural reinforcing, whereas Specimen 4 experienced a pull-out/bond failure of the reinforcing near the support.

Comparing the results for Specimens 3 and 13, the flexural reinforcing ratio is double for Specimen 13 versus Specimen 3 (2-15M bars instead of 2-10M bars), and the strain at the midspan for Specimen 13 is almost half that for Specimen 3 for a given load level.

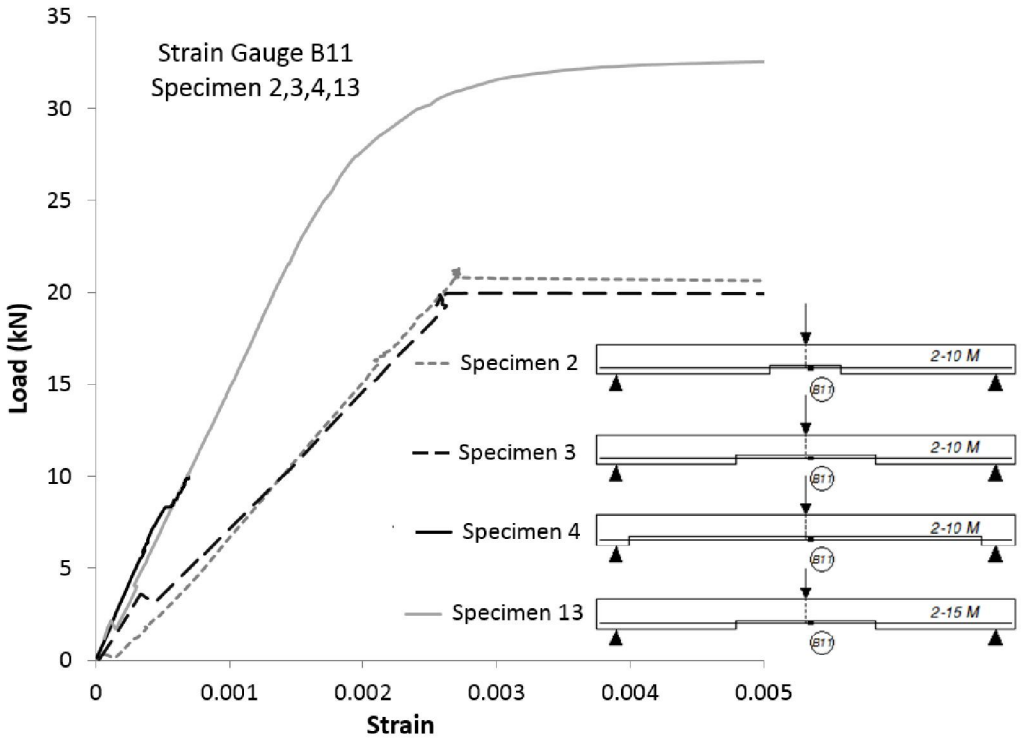

Figure 5-7: Load-strain results for Strain Gauge B11: Specimens 2, 3, 4 and 13.

5.6.2 4, 9, 10, and 11

In Figure 5-8, the rebar strains near the support (Strain Gauge B2) are plotted for Specimens 10, and 11. The comparison of these three specimens shows the effect of the concrete "teeth" on the

rebar strain. Given that the #2 strain gauge in sample 7 was crushed, we cannot conclusively compare the results from sample 7 with the remaining samples. As such, we were forced to omit the results obtained from sample 7.

Specimens 10 and 11 are relatively similar, however the difference in the length of teeth result in a small difference in strain. Comparing the strain data for these specimens, it can be seen that the strains are lower for Specimen 10 at a given load level. This suggests that the larger teeth on Specimen 10 are somewhat more effective at transferring load between the rebar and the concrete.

In Figure 5-9, the rebar strains near the support (Strain Gauge B3) are plotted for Specimens 6 and 9. Again in this figure, the effect of the concrete teeth in the de-bonded region can be seen as reducing the rebar strain at the gauge location for a given load level, indicating that load is being transferred between the rebar and the concrete by the teeth.

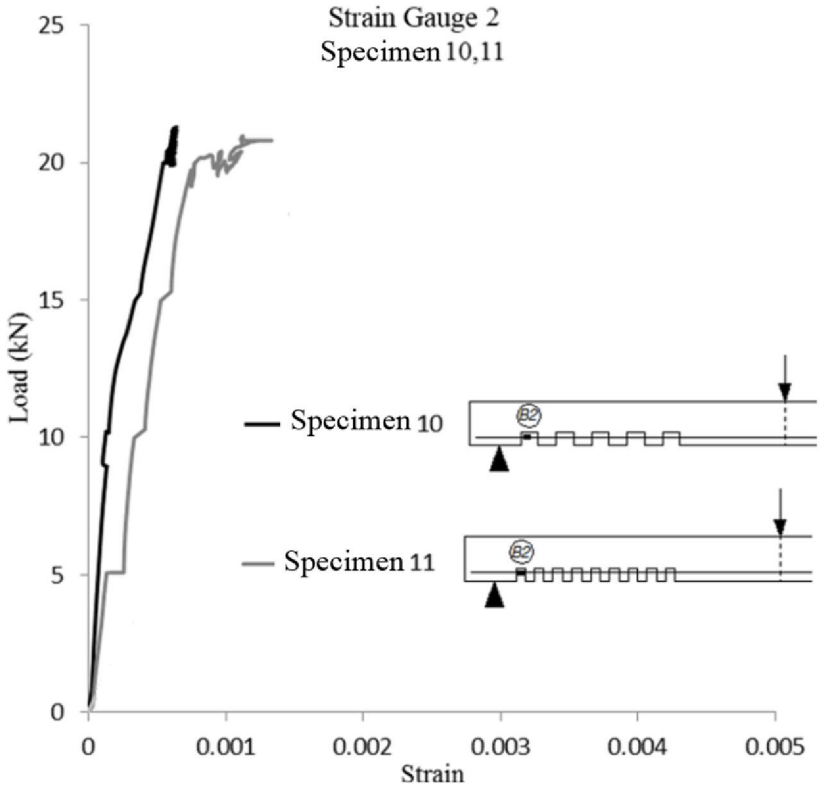

Figure 5-8: Load-strain results for Strain Gauge B2: Specimens 10, and 11.

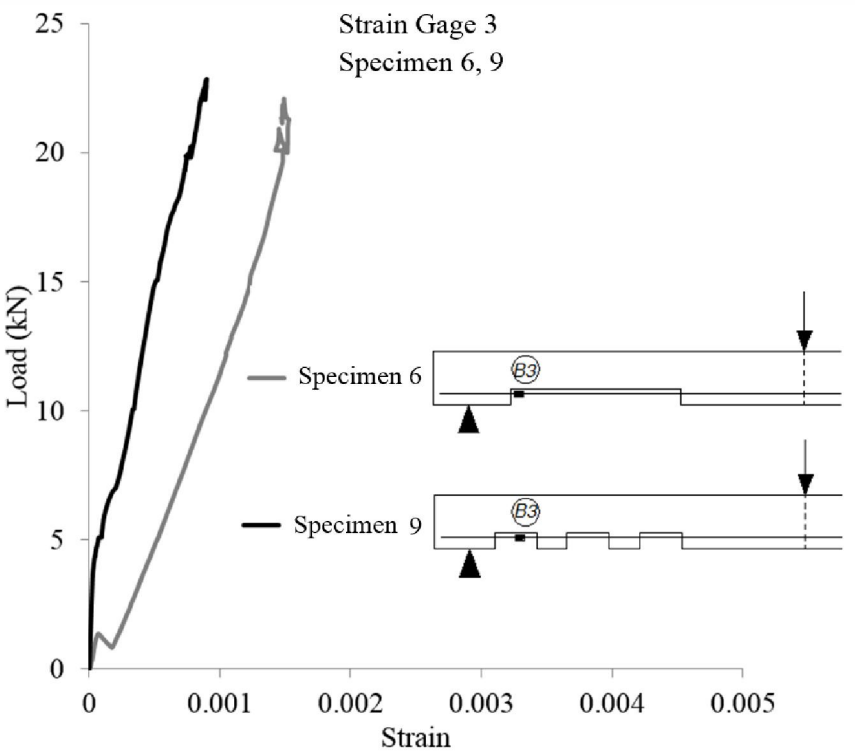

Figure 5-9: Load-strain results for Strain Gauge B3: Specimens 6 and 9.

5.6.3 Strain Gauge B6: Specimens 9 and 11

In Figure 5-10, the rebar strains near the quarter points (Strain Gauge B6) are plotted for Specimens 9 and 11. Both of these specimens had strain gauges at this location and both of them show almost the same behaviour, regardless of the difference in the tooth length. Based on the results in this Figure and those in Figure 5-8, it can be concluded that the length of the teeth has limited or no effect on steel strain. In other words, when spalling/exposure area is present on the surface of concrete, the size of the teeth has little effect on the steel strain, as long as the total de-bonded length is equal.

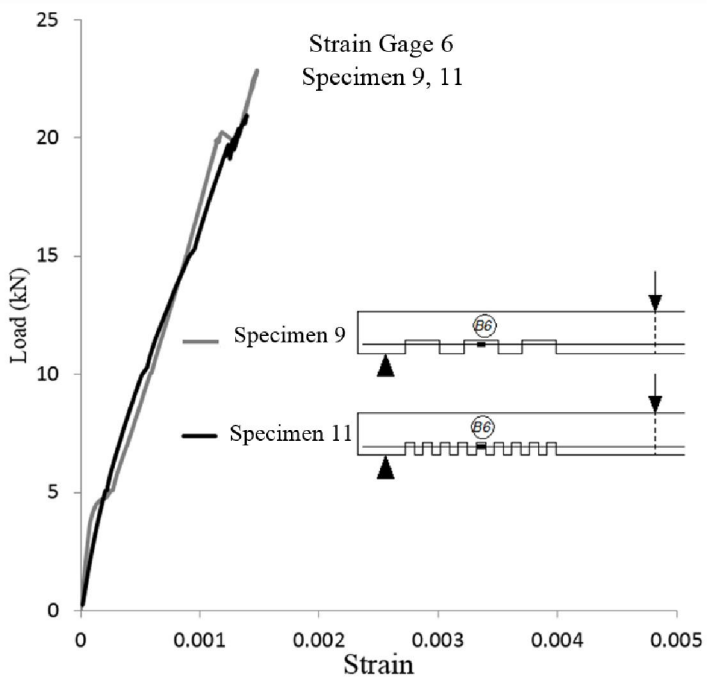

Figure 5-10: Load-strain results for Strain Gauge B6: Specimens 9 and 11.

5.7 Strain Profiles along Beam Span

When the flexural reinforcement is exposed, the strain is vary proportionally to the moment, as it would in a beam with fully bonded reinforcing. Measured reinforcing steel strains for Specimen 11 are plotted in Figure 5-11. This figure shows the strain profile along the beam span for the same reinforcing bar at 80% of the yield load. As seen in this figure, a trend line is well fitted, following an linear distribution, where x is the horizontal position. As seen in Figure 5-11, theoretical strains for the control beam (Specimen 1), calculated using the Response 2000 Software (Bentz, 2000), differ from the measured ones.

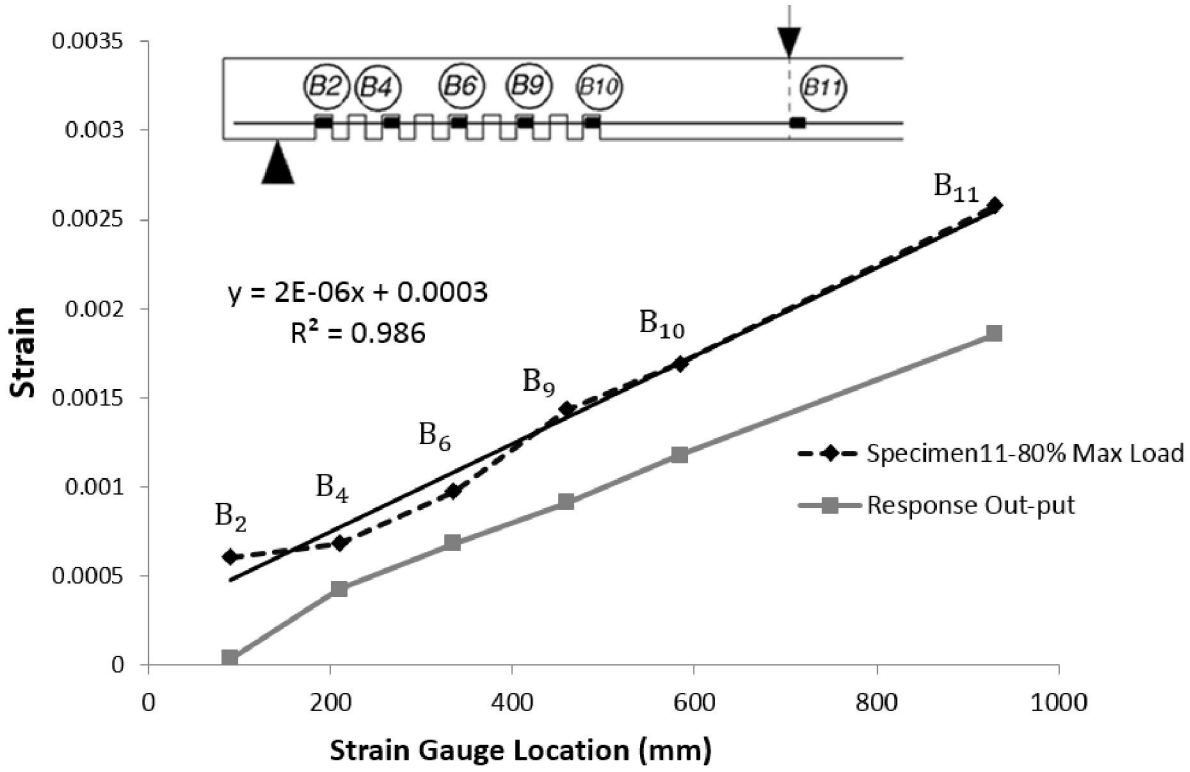

Figure 5-11: Comparison of rebar strains for Specimen 11with Response 2000 predictions for Specimen 1.

It is apparent from Figure 5-11 that significant load is transferred by the small "teeth" (bonded portions) in Specimen 11. If this weren't the case, then the strains recorded by Gauges B2 and B10 would be the same for a given load level. Therefore it is concluded that the concrete in the bonded or unspalled regions can have a significant effect on the beam behaviour after partial spalling.

In Figure 5-12, a similar comparison is presented for Specimen 9, and a similar trend is seen. The observed trend is that Response 2000 predicts lower strains than were measured near the supports. Since Response 2000 assumes that the reinforcement is fully bonded (as expected for the control beam), this suggests that the rebar near the supports was not fully developed at the gauge locations for the Specimens 9 and 11, which had de-bonded regions in close proximity to the supports.

For Specimens 1, 2, 3, and 4, which had a single de-bonded region at the midspan with no bonded "teeth", a different comparison was performed, wherein the midspan strain for a given

load level (P = 10 kN) was plotted versus the non-dimensionalized length of the de-bonded area (L_{exp} / L_{total}). The results of this comparison are plotted in Figure 5-13. Looking at this figure, it can be seen that as the exposed length at the midspan increases, the reinforcement strain decreases. For example, at P = 10 kN, the strain in Specimens 3 with 34% exposed is equal to $1.395 \cdot 10^{-3}$, and in Specimen 4 with 85% exposed the strain is $6.929 \cdot 10^{-4}$ (almost half). This trend can be explained by the shift in the load carrying mechanism from beam to arch action as the exposed length increases.

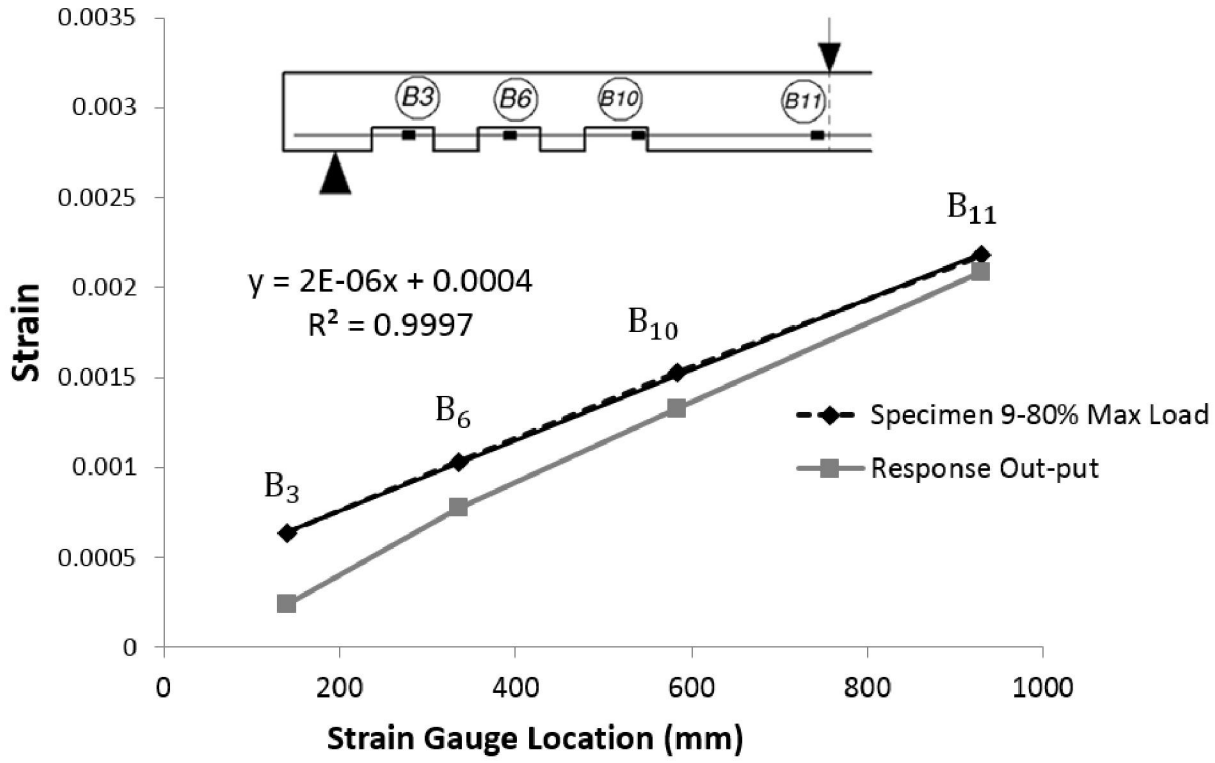

Figure 5-12: Comparison of rebar strains for Specimen 9with Response 2000 predictions for Specimen 1.

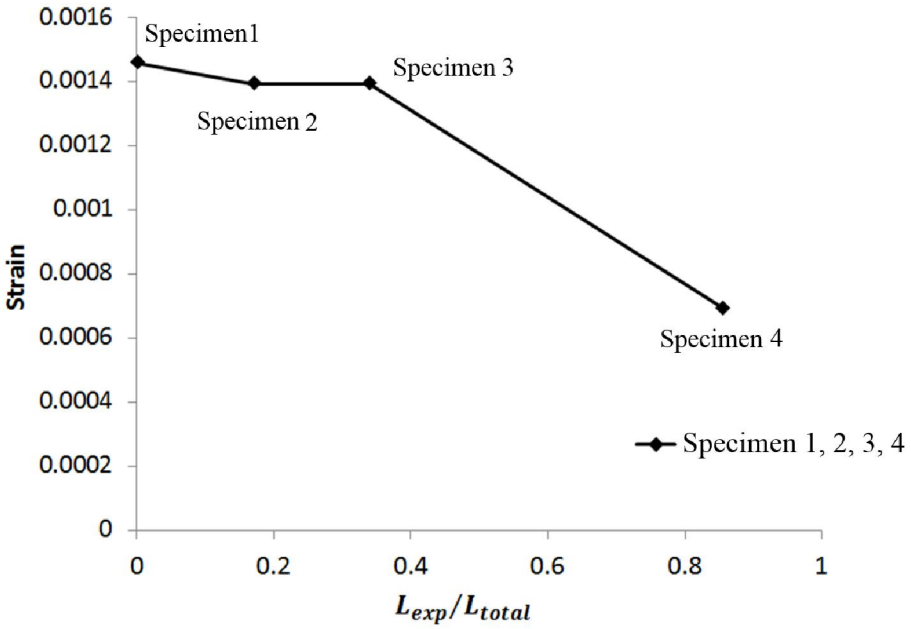

Figure 5-13: Mid-span strain at P = 10 kN versus exposure length.

5.8 Analysis with Resistance Models Employing the Modified Area Concept

A computer program developed based on Luckai, (2011) method with the use of Excel; minimum proposed bond value by CAN/CSA A23.3-04 (2006), absolute minimum bond requirement, and experimental bond values were compared. In cases where experimental specimens followed the code of concrete, results were as expected and no pull-out failure occurred (specimen 1,2,3,5).

By analyzing all data and representational diagrams, a method for assessing spalled beams by modifying cross-sectional areas is offered. The model proposes adding all discrete areas in which concrete is present, within the allotted minimum anchorage length recommended by the CAN/CSA A23.3-04 (2006).

$$l_i = \sum_{i=1}^{n} B_i \tag{5-1}$$

Figure 5-14: Bond and exposure length/labels

Where B_i is the bonding length and E_i represent the exposed length, as shown in Fig 5-14.

In any point of the cross section which $l_i < l_d$ (minimum anchorage length), the bond ratio will be assessed by the formula below:

$$A_d^{'} = A_d \left(\frac{I_i}{I_d}\right) \tag{5-2}$$

Where:

A_d' = equivalent cross section (modified)

A_d = actual steel cross section area

Analytical studies were carried out to predict the bond behaviour of a bar embedded in a concrete. However, some details were not considered in this model. i.e. the bond length along anchored bars is directly affected by the development of internal cracking in the concrete boundary layer around the rebar.

5.8.1 Specimens 1,2,3,5

Figure 5-15 displays the specimens which had sufficient anchorage lengths. As seen in Figure 5-15 the anchorage length is much greater than what the beam needs, so having bond failure (pull out failure or spalling concrete cover) in these four specimens is not possible. Failure in these specimens was entirely caused by yielding of the bottom reinforcement.

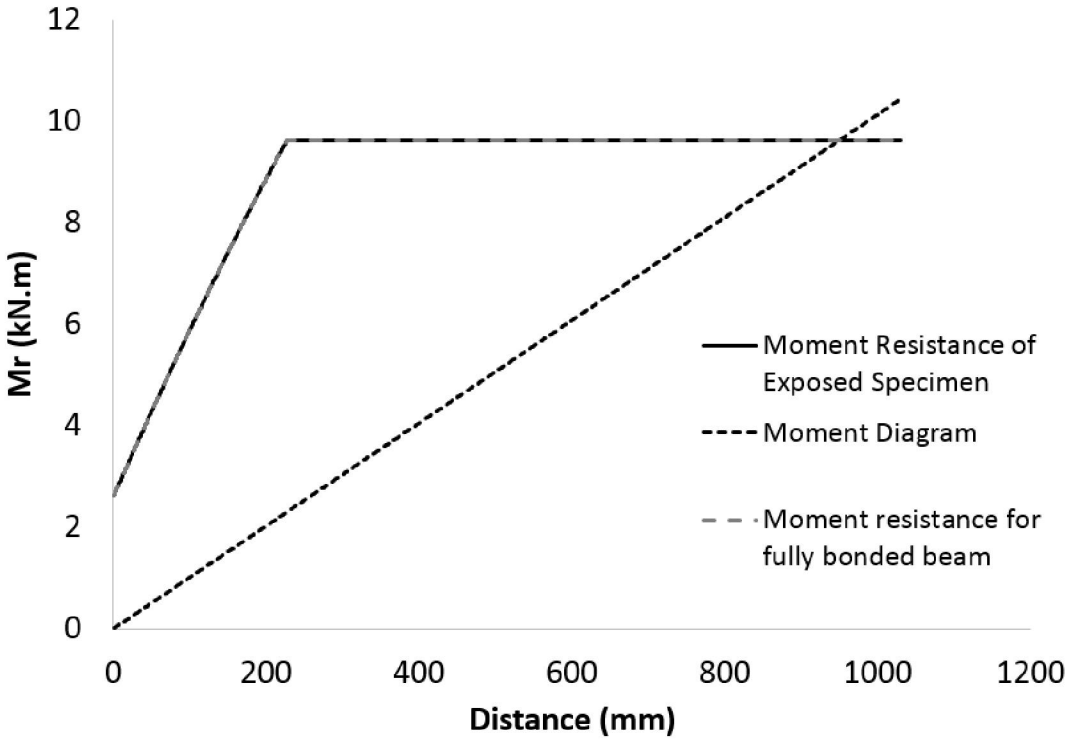

Figure 5-15: Moment diagram for specimen 1,2,3,4.

5.8.2 Specimen 4

Based on the model proposed earlier (Luckai, 2011), this specimen should fail by almost half of the bottom reinforcement capacity, which it did. As it appears, lack of anchorage length makes the beam not able to resist the maximum load, so it will eventually fail by bond failure (pull out).

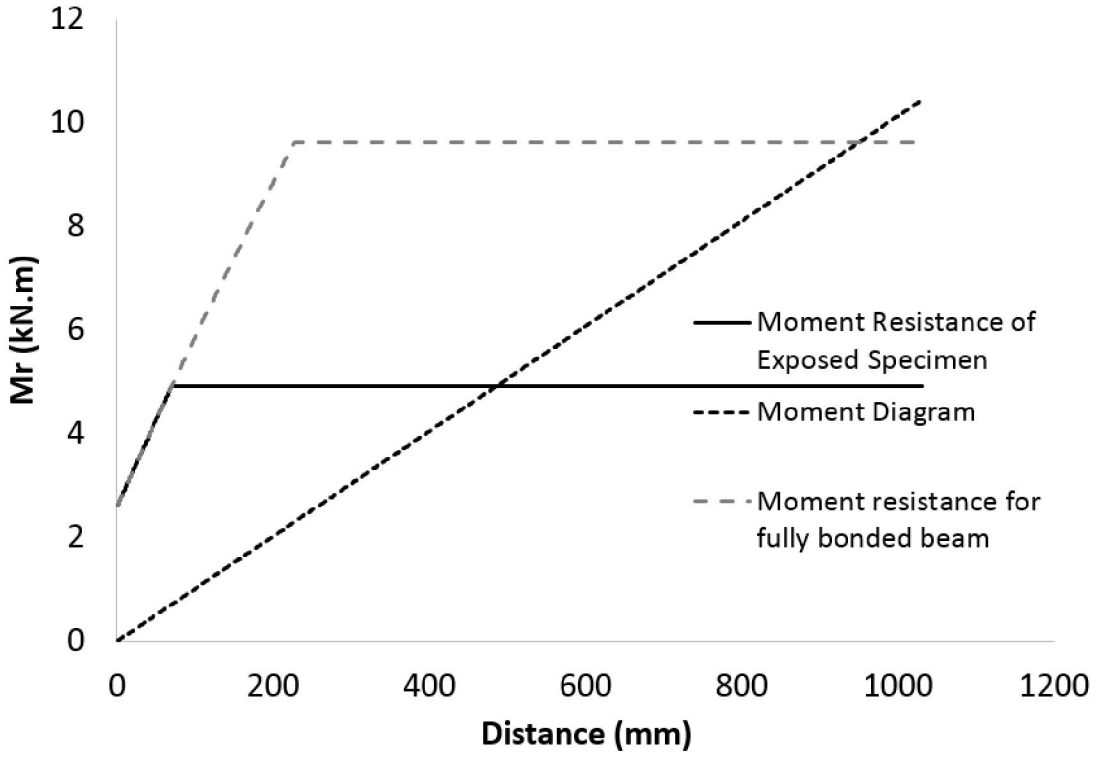

Figure 5-16: Moment diagram for specimen 4.

The maximum flexural strength for the fully bonded beam is equal to M=9.63 kN.m (yielding of bottom reinforcement). By using Excel spreadsheet was calculated the maximum flexural strength which beams could tolerate based on the proposed model; the results are presented in Table 5-2. The maximum moment is equal M=4.45 kN.m which is equal to F= 9.36 kN point load.

5.8.3 Specimen 6

Based on the concrete theoretical model, this specimen is close to bond failure in the location 600mm from support. The bonding capacity is a slightly greater than the actual tension in reinforcement, however the specimen did not fail due to pull-out and it under went the flexural failure, as shown in Figure 5-17.

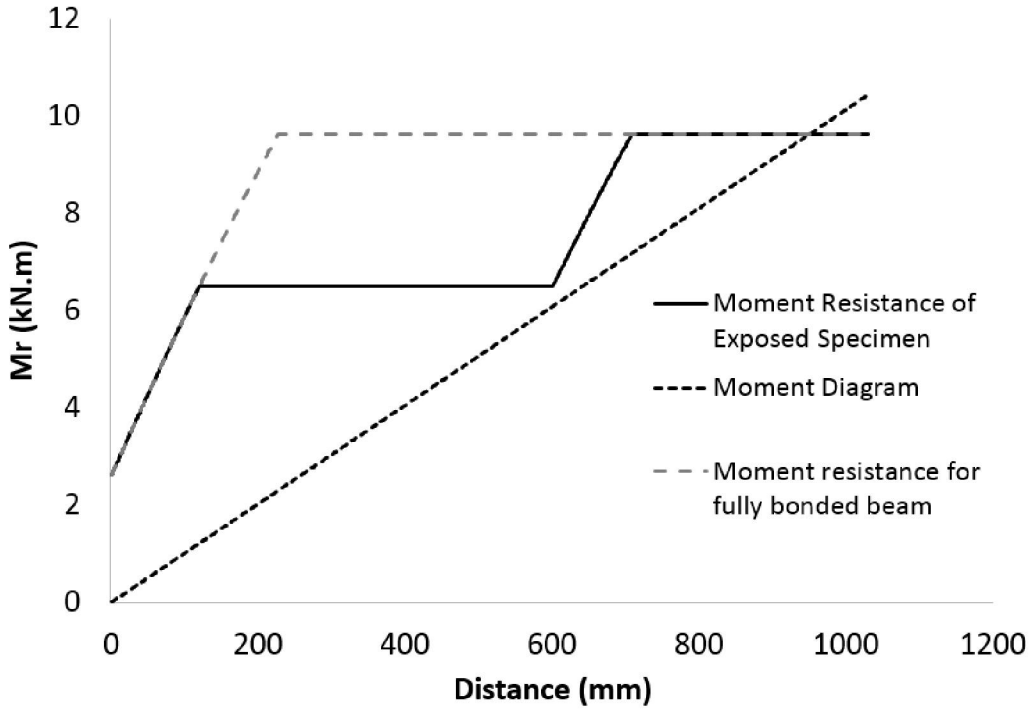

Figure 5-17 Moment diagram for specimen 6.

5.8.4 Specimen 7

This calculated moment resistance curve, crossed the moment diagram line in the graph somewhere around 6000mm from the support. Because of the large amount of exposure area, there is a large reduction in strength resulting in pull-out failure, as shown in Figure 5-18.

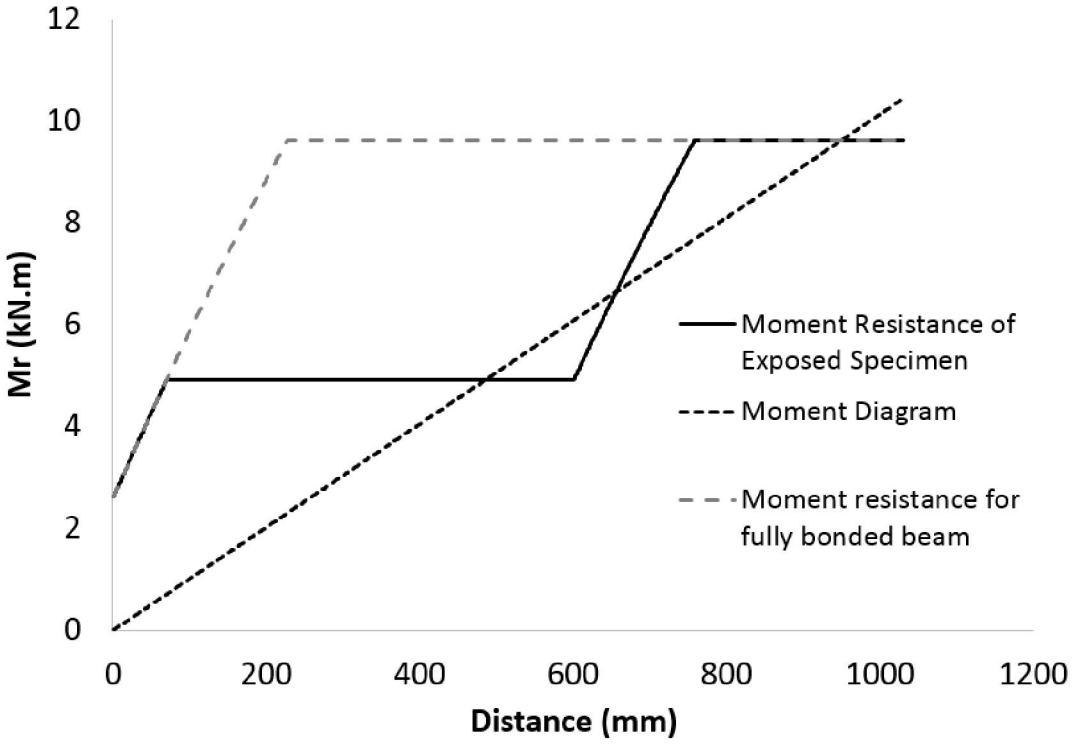

Figure 5-18 Moment diagram for specimen 7.

As calculated by Excel sheet the failure moment is M=6.35 kN.m (F=13.4 kN) which compares well with the experimental failure load 14.82 kN.

5.8.5 Specimen 8, 9, 10, 11

In all of the specimens below, the numerical model and real experiments both express the same concept, which is: only flexural failure occurred because the de-bonded areas were located at positions away from the actual moment line. i.e. for specimen 8 by losing 39% of the total bond , the specimen still maintains the anchorage length that provides sufficient resistance, as shown in Figure 5-19, 5-20, 5-21, 5-22.

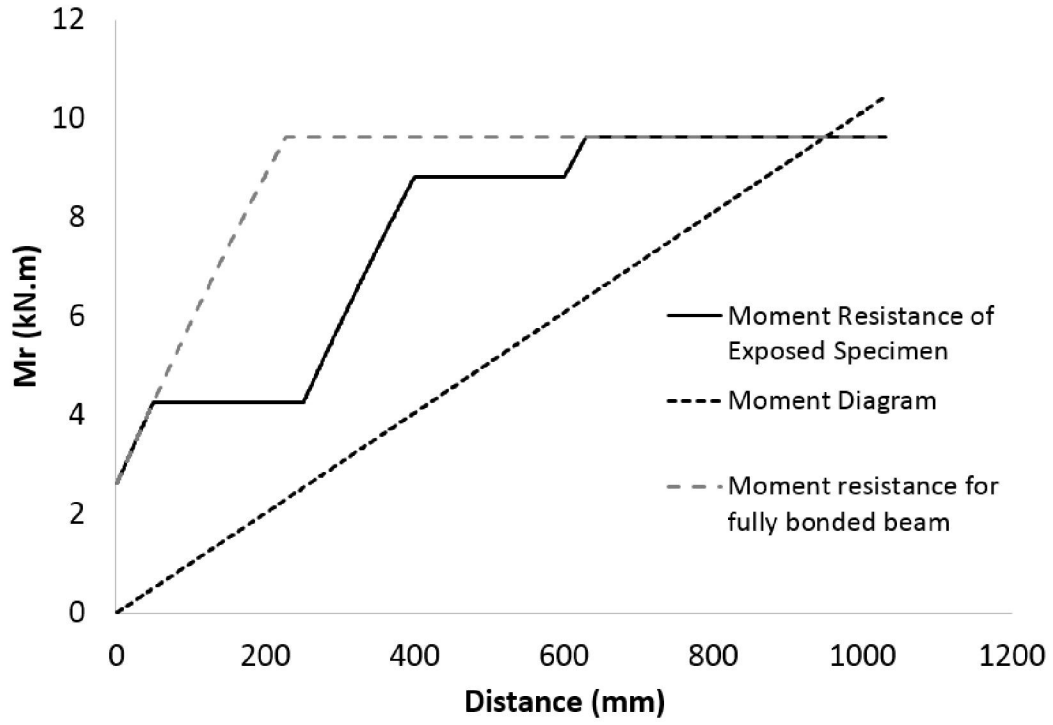

Figure 5-19 Moment diagram for specimen 8.

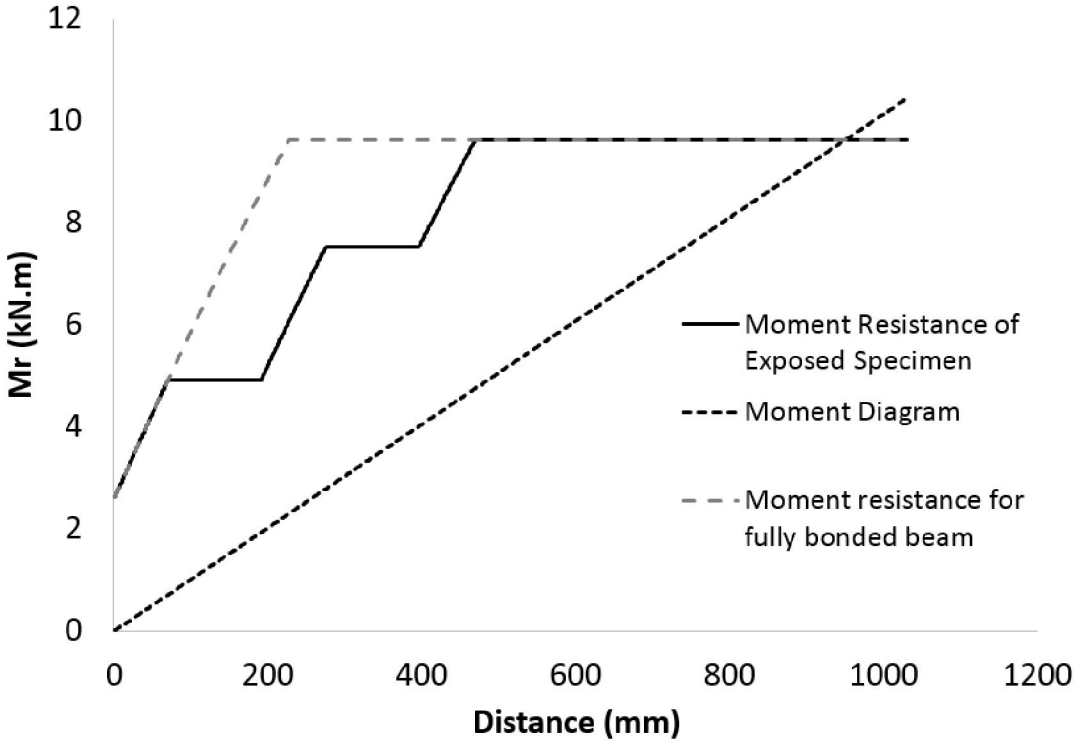

Figure 5-20 Moment diagram for specimen 9.

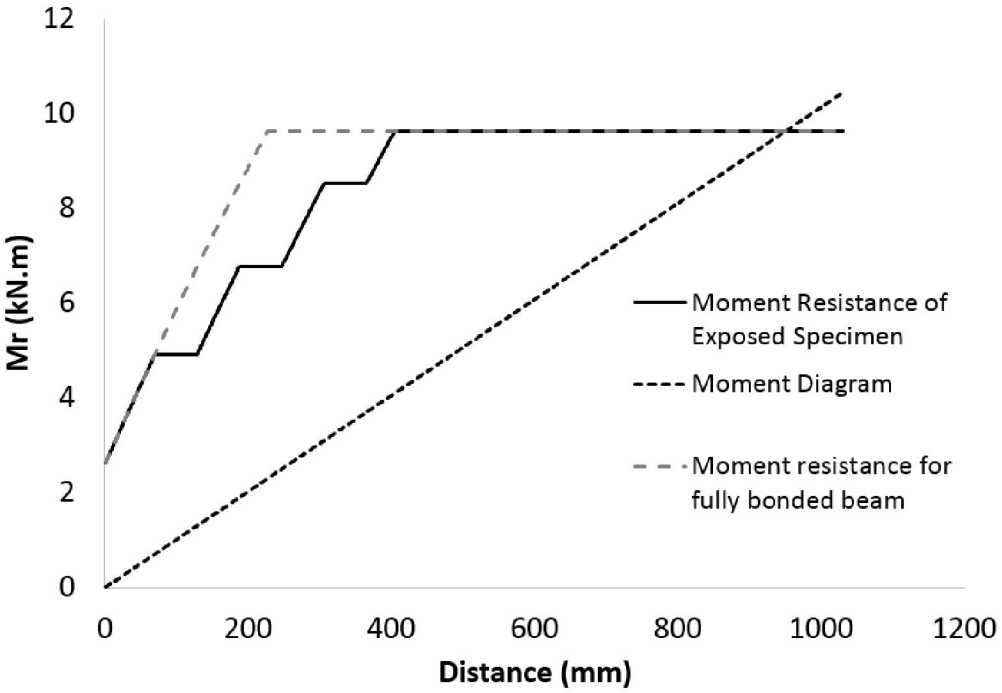

Figure 5-21 Moment diagram for specimen 10.

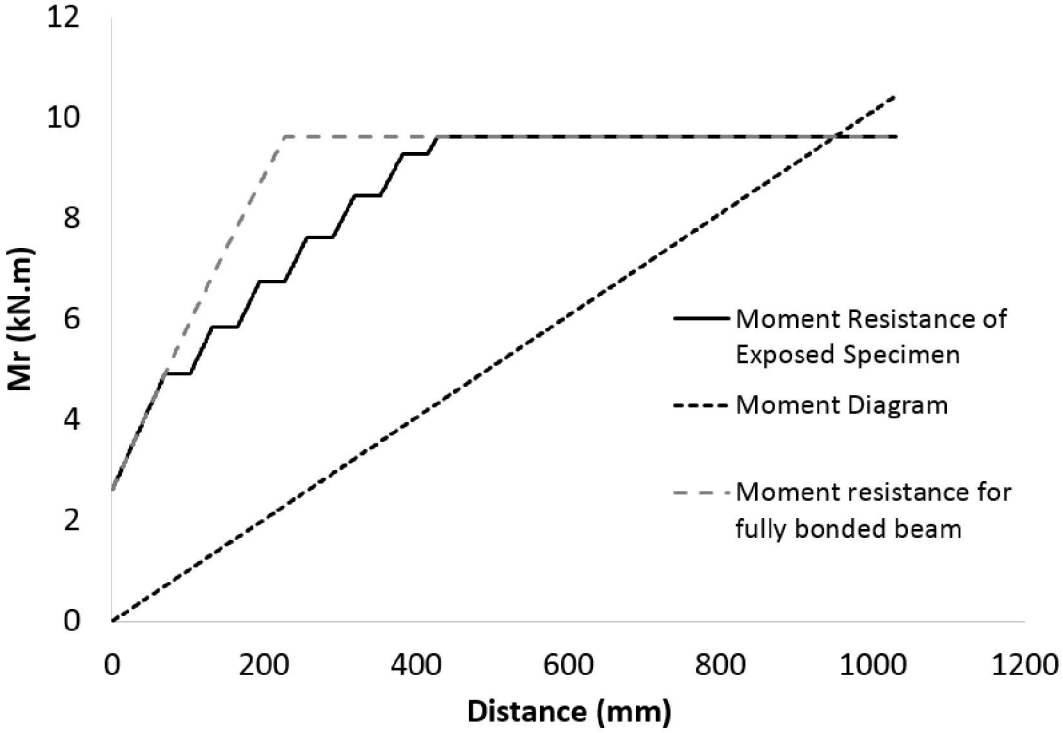

Figure 5-22 Moment diagram for specimen 11.

5.8.6 Specimen 12 and 13

In both of these specimens the anchorage length is enough to keep the beams safe from different bonding failures. The only key concept here is, that by comparing these two specimens with specimen 1 and 3, which have same geometrical shapes, it is discovered that as much as the bottom steel area increases, the angel between two lines "Moment diagram" and "Moment Resistance of fully bonded" on the graph will reduced. This means that, for specimens which are heavily reinforced, having exposure areas outside of anchorage zones can prove more critical than those with lesser steel ratio. In other words, the heavily reinforced cross sections are more sensitive to de-bonding when compared to regular sections, and any significant de-bonding in heavy reinforced section could lead to bond failure. These two specimens are identical in terms of Moment-Distance relationship.

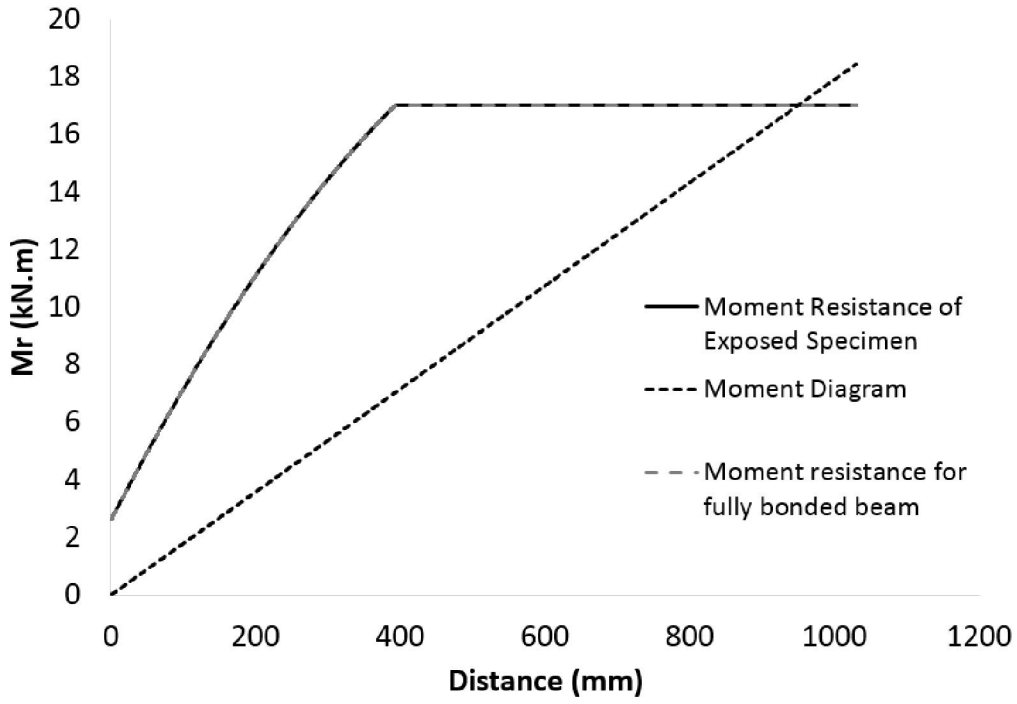

Figure 5-23 Moment diagram for specimen 12 and 13.

From these studies, the following observation can be made:

The mathematical model developed for the bond element offers a reasonably good prediction of the bond force-deformation, of pull-out experiments with slightly accurate calculations. The computer based approach for formulating the bond strength can be modified for any type of loading.

5.8.7 Summary Table

A summary of comparison between lab tests and predicted model are presented in Table 5-2:

Table 5-2 Comparisson between test and predicted strength

Specimen	Predicted M_{ult} kN.m	M_{ult} kN.m	$M_{ult} / M_{predict}$	Predicted mode of failure	Failure Mode
1	9.63	11.06	1.14	Flexural / Steel yield	Flexural / Steel yield
2	9.63	10.11	1.05	Flexural / Steel yield	Flexural / Steel yield
3	9.63	9.51	0.98	Flexural / Steel yield	Flexural/ Steel yield
4	4.45	4.97	1.11	Pull-out/Bond Failure	Pull-out/Bond Failure
5	9.63	1.65	1.10	Flexural / Steel yield	Flexural / Steel yield
6	9.63	10.49	1.08	Flexural/ Steel yield	Flexural/ Steel yield
7	6.35	7.03	1.10	Pull-out/Bond Failure	Pull-out/Bond Failure
8	9.63	10.40	1.08	Flexural / Steel yield	Flexural / Steel yield
9	9.63	10.84	1.12	Flexural / Steel yield	Flexural / Steel yield
10	9.63	10.10	1.04	Flexural / Steel yield	Flexural / Steel yield
11	9.63	9.95	1.03	Flexural / Steel yield	Flexural / Steel yield
12	17.03	16.80	0.98	Flexural / Steel yield	Flexural / Steel yield
13	17.03	15.78	0.92	Flexural / Steel yield	Flexural / Steel yield

Chapter 6 : Conclusions and Recommendations

This chapter presents the conclusions of the experimental study and analyses presented in this thesis and provides recommendations for future study in this general subject area.

6.1 Conclusions

Based on the work presented in this thesis, the following conclusions are made:

- Reinforced concrete beams can carry a significant portion of their original capacity after losing cover over a significant portion of their flexural reinforcing.
- The beams tested in this study with flexural reinforcing exposed in various patterns and amounts all achieved at least 80% of the capacity of the control specimens (with no reinforcing exposed), if the exposed length was less than 40% of the total length, and sufficient development length was provided.
- The specimens that failed at loads less than 80% of the capacity of the control specimens all had their flexural reinforcement exposed in such a way that a "pull-out" failure resulted.
- In general, the flexural stiffness of the beams was seen to decrease with an increase in the length of the exposed area. One exception to this was in the specimens with many "teeth" between the exposed regions near the supports such as specimens 10 and 11. For these specimens, it was found that the flexural stiffness increased with an increase in the length of these "teeth", in comparison with specimens 8 and 9.
- For the beams with flexural reinforced exposure at the midspan, the stresses in the flexural reinforcing were seen to decrease with an increase in the exposed length, suggesting a shift in the load carrying mechanism from flexural to arch action.
- The number of transverse (flexural) cracks decreases as the length of the exposed area increases, suggesting a shift in the load carrying mechanism from beam to arch action.
- Predictions of the beam specimen capacities and failure modes using structural resistance models employing the modified area concept are reasonably accurate and conservative in

most cases. The test-to-predicted ratio obtained with these models ranged from 0.92 to 1.23, with an average of 1.07, and the failure mode was correctly predicted in all but one of the tests.

Recommendations for Future Study

Based on the work presented in this thesis, the following areas of future study are identified:

- Although the results of the experimental study and analyses presented in this thesis are encouraging, it should be recognized that the models employing modified area concept are still in the development stage and require further validation through an expanded experimental study, investigating a broader range of specimen geometries and loading conditions. Specifically, it is recommended that further tests be conducted to cover a broader range of loading conditions and beams with splices in the flexural reinforcing along the span.
- A major difficulty in applying the modified area concept to real structures involves the estimation of the development length of the reinforcing steel in the unspalled regions. For this reason, it is recommended that a field investigation be performed of the concrete strength in regions of the soffit immediately adjacent to the spalled regions.
- One potentially unconservative assumption made in using the structural resistance models employing the modified area concept is that the plane sections assumption commonly used in beam analysis can be retained with little impact on the strength estimation for many practical cases. The safety implications of this assumption could be addressed and the limitations on the proposed methodology extended with the development of a correction factor or some other simple way to account for the effects of violating the plane sections assumption.
- Future experiments to supply results for developing a generalized bond model are needed, covering a broad range of bar sizes, beam geometries, and concrete strengths.
- It is recommended that future tests be conducted with actual corroded specimens, so that the effects of rebar section loss and the effects of the corrosion product on the bond strength can be verified experimentally and interactions between the various effects can be studied.

- The effects of transverse reinforcing steel (i.e. stirrups) on the bond strength were not considered in this current study, but could be investigated in future tests.
- The development of finite element models for predicting the load transfer between steel and rebar in the specimens with "teeth" between multiple spalled regions would be useful for understanding this phenomenon and developing simple predictive models.

References

ACI Committee 408, 1966, Bond and Development of Straight Reinforcing Bars in Tension. American Concrete Institute. 03: 408R-1, 408R-49.

Amleh, L. 2000.Bond Deterioration of Reinforcing Steel Concrete Due to Corrosion. McGill University, Montreal, Canada, 411.

Andrade,C. And Alonso, C. And Molina F.J. 1993. Cover cracking as a function of bar corrosion. Materials and Structures, 26: 453-464.

Al_Sulaimani, G. J., Kaleemullah, M., Basunbul, I.A. and Rasheeduzzafar. 1990. Influence of Corrosion and Cracking on Bond Behavior and Strength of Reinforced Concrete Members. ACI Structural Journal, 87: 220-231.

Basheer, L., Kropp, J. and Cleland, D. J. 2001. Assessment of the durability of concrete from its permeation properties: a review, Construction and Building Materials , 15.2:93-103.

Bresler, B and Bertero, V. 1968. Behavior of Reinforced Concrete under Repeated Load. Journal of the Structural Division. 94: 1567-1590.

Cairns, J. 1995. Strength in shear of concrete beams with exposed reinforcement. Proceedings of the ICE - Structures and Buildings, 110:176-185

Cairns, J. and Abdullah, R.1995.An Evaluation of Bond Pullout Tests and Their Relevance to Structural Performance. Structural Engineer, 5: 179-85.

Cairns, J. and Rafeeqi, FA. 1997. Behaviour of Reinforced Concrete Beams Strengthened By External Unbounded Reinforcement. Construction and Building Materials, 11: 309-317

Cairns, J. and Zhao, Z. 1993. Behaviour of concrete beams with exposed reinforcement. Proceedings of the ICE - Structures and Buildings, 99:141-154.

Darwin, D., Zuo, J., Tholen, M.L. and ldun, E.K. 1996. Development Length Criteria for Conventional and High Relative Rib Area Reinforcing Bars. ACI Structural Journal, 93: 347-359.

Eligehausen, R., Popov, E.P. and Bertero, V. V. 1982. Local bond stress-slip relationships of deformed bars under generalized excitations, Chamber of Greece, 4:69-80.

Evan Bentz, M. P. 2000. University of Toronto. Retrieved from http://www.ecf.utoronto.ca/~bentz/ r2k.htm

Gaetano, R. and Romano, F. 1992. Cracking Response of RC Members Subjected to Uniaxial Tension. Journal of Structural Engineering. 118: 1172–1190.

Gambarova, P.G. and C. Karakoc.1982. Shear-confinement interaction at the bar-to-concrete interface, Applied Science Publisher: 82-96.

Giuriani, E. and Plizzari, G.A. 1998. Interrelation of Splitting and Flexural Cracks in RC Beams. Journal of Structural Engineering, 124: 1032–104.

Highways Agency. 1995. Design Manual for Roads and Bridges. The assessment of concrete structures affected by steel corrosion, Vol3 Section 4. HMSO, London, Feb.

Jeppsson, J. and Thelandersson, S. 2002. Behavior of Reinforced Concrete Beams with Loss of Bond at Longitudinal Reinforcement. Journal of Structural Engineering, 129:1376-1383.

Laura Nicole Lowes 2000 , Finite Element Modeling of Reinforced Concrete Beam-Column Bridge Connections, University of California, Berkeley, chapter 4.

Luckai, J.2011. Evaluating the Effects of Spalling on the Capacity of Reinforced Concrete Bridge Girders, University of Waterloo. 427 Pages.

Maeda, M. 1995. Effect of Confinement on Bond Splitting Behavior in Reinforced Concrete Beams. International Association for Bridge and Structural Engineering, 5: 166-171.

Malvar, L.J. 1991. Bond of Reinforcement under Controlled Confinement. Naval civil Engineering lab port Hueneme, No NCL-TN-1833.

Mangat, P. S. and Elgarf, M. S. 1999. Flexural Strength of Concrete Beams with Corroding Reinforcement, ACI Structural Journal, 96: 149-158.

Maslehuddin, M., Allam, I.A., Al-Sulaimani, G. J., Al-Mana, A. and Abduljauwad, s. N. 1990. Effect of Rusting of Reinforcing Steel on its Mechanical Properties and Bond with Concrete. ACI Materials Journal, 87: 496-502.

Minkarah, I. and Ringo, B C. 1981. Behavior and Repair of Deteriorated Reinforced Concrete Beams. Transportation Research Board, 821:73-79.

Orangun, C. O., Jirsa, Jo. and Breen, J.E. 1977. A Reevaluation of Test data on development length and splices, ACI Journal, 74.3:114-122.

Phillips, D. V. and Binsheng, Z. 1993. Direct Tension Tests On Notched and Un-notched Plain Concrete Specimens. Magazine of Concrete Research, 45: 25 –35.

Rehm, G. and Eligehausen, R. 1979. Bond of ribbed bars under high cycle repeated loads. Journal of the American Concrete Institute, 76: 297-309.

Rodriguez, J., Ortega, LM. and Casal, J. 1997. Load carrying capacity of concrete structures with corroded reinforcement. Construction and Building Materials, 11: 239-248.

Task Group, 2000. Bond of Reinforcement in Concrete: State-of-art Report, FIB Béton, Lausanne, Switzerland. 427 Pages.

Tepfers, R. 1979. Cracking of Concrete Cover along Anchored Deformed Reinforcing Bars. Magazine of Concrete Research, 31: 3-12.

Untrauer, R.E. and Henry, R. L. 1965. Influence of Normal Pressure on Bond Strength. ACI Journal Proceedings, 62: 577-586.

Vecchio, J. and Collins, M.P. 1986. The modified compression-field theory for reinforced concrete elements subjected to shear. ACI Journal 82-32, 219-231.

Viwathanatepa, Suthipoul, Egor Paul Popov, and Vitelmo Victorio Bertero. 1979. Effects of generalized loadings on bond of reinforcing bars embedded in confined concrete blocks. University of California, Earthquake Engineering Research Center.

Warren, G.E. Anchorage Strength of Tensile Steel in Reinforced Concrete Beams. PhD thesis, low a State University, Ames, LA, USA 1969.

Zhang, S. and Raoof, M. 1995. Prediction of the behaviour of RC beams with exposed reinforcement. Magazine of Concrete Research, 47:335-344.

Zuo, J. and Darwin, D. 2000.Splice strength of conventional and high relative rib area bars in normal and high-strength concrete. ACI Structural Journal, 97.4: 630-641.